الجمـــــهوريـــــة الجـــزائريـــــة الديـــمقراطيـــــــــة الشـــعبيـــــــة
PEOPLE'S DEMOCRATIC REPUBLIC OF ALGERIA
وزارة التعـلـيـم الـعـالـي والـبـحـث الـعـلـمـي
MINISTRY OF HIGHER EDUCATION AND SCIENTIFIC RESEARCH
جـامـعـة عمّـار ثـلـيـجـي بالأغـــواط
AMAR TELIDJI UNIVERSITY- LAGHOUAT

كـلـيـــة الـتكنولوجيا
FACULTY OF TECHNOLOGY
ELECTRONICS DEPARTEMENT

Dissertation Master Degree in Microelectronic

Domain : Technology Sciences
Filiere : Electronics
Option : Microelectronic

Présented by

Mohammed Yacine BENYAHIA

THEME

Study and simulation of Photovoltaic Properties on the Performance of p-InGaN/n-InGaN Single Junction.

Thursday, 27th June 2024

Publicly supported in front of the jury composed of :

Dr. CHATTA Wahiba	*MCB University of Laghouat*	President
Mme. VILBOIS Leila.Amal	*MAA University of Laghouat*	Examiner
Dr. BELLAKHDAR Aissa	*MCA University of Laghouat*	Supervisor
Dr. BIRANE Mouhoub	*MCA University of Laghouat*	Co-Supervisor

Academic Year 2023/2024

بِسْمِ اللَّهِ الرَّحْمَٰنِ الرَّحِيمِ

الحمد لله الذى علم الإنسان ما لم يعلم ، والصلاة والسلام على سيّدنا مُحَمَّد الذي بعث معلّما وعلى آله وصحبه الذين اتّبعوه بإحسان وبعد ، نقدم لكم اليوم هذه المذكرة ونحن نأمل ونطمع أن تنال إعجابكم جميعاً ، ونتمنى من الله أن نكون قد وفقنا في

تقديمها وكتابتها

This thesis was carried out at the Faculty of Technology, Department of Electronics, Amar Taleghi University - Laghouat, this thesis was only possible thanks to the efforts and assistance of many people, to whom I would like to extend my sincere thanks.

First of all, I would like to thank my supervisor **Dr. *BELLAKHDAR Aissa*** from the University of Laghouat for suggesting this topic to me and for his advice, guidance, corrections and encouragement that enabled this thesis to proceed smoothly.

I would also like to thank **Dr. *CHATTA Wahiba***, a professor at the University of Agawat, who honored me by presiding the jury for this thesis.

I would also like to thank **Mme. VILBOIS Leila Amal**, a professor at the University of Laghouat, who honored me with the honor of examiner this thesis and participating in the jury.

I would also like to thank **Dr. *BIRANE Mouhoub*** of the University of Laghouat for assisting in this work as a supervisory assistant.

I would also like to thank all the professors of the Department of Technological Sciences who contributed to my training from the first session of the study until the end of the semester, without neglecting to thank everyone who contributed from near or far to the completion of this work.

I would like to express my sincere thanks and appreciation to **Mr. Marc BERGMAN**, the developer of the **Scapes software**. Your dedication and creativity in developing this software have had a significant impact on improving our experience, making it easier and more efficient.

Thank you, Marc Bergman, for your dedication and valuable contribution to the field of software development.

Mohammed Yacine BENYAHIA

"Ultra-low-mass solar cell technology could lead to the creation of large, low-cost solar power plants deployed in space, bringing clean energy to Earth."

Professor Craig Underwood, Emeritus Professor of Spacecraft Engineering at the Space Research Center at the University of Surrey

I dedicate this humble work in memory of my father, may he rest in peace, to whom I owe a lot in my life and who will remain a symbol of love for work and the remedy of knowledge, and who never hesitated in his life. I am not happy to not share this event with him, but he is present and will remain in my heart forever. I hope to live up to your good opinion and live according to the values he instilled in us.

Thank you very much to him and may all my good deeds be in his balance of good deeds in memory of my grandmother

To all those who have lost their loved ones.

To my beloved mother, to whom I owe everything, even my life. She is and will remain a symbol of courage that accompanied me not only in all stages of my life, but also gifted me, encouraged me, and did not withhold anything from anyone.

To all the small and large family.

To all my friends.

To all the teachers who contributed to my training, in all integrated courses, I will be grateful forever, especially Dr.Rachid Zerdoum, Dr.Aissa BELLAKHDAR

and Dr.Naceur SELMANE.

«Family, health, and friends are all that matters in life; everything else is just an addition that we may or may not care about».

Coralie Thévenet

TABLE OF CONTENTS

Acknowledgements .... ………………………………………………………….. i
Dedications ....…………………..…………………………………………….. ii
Table of Contents ....………..……………………………………………….. iii
List of figures ……………………………………………………………….. vii
List of tables ………………………………………………………………….. viii
Abbreviations And Notations……………………………………………………………… ix
General conclusion ……… ………………………………………………………... 2

Chapter I Generalities on solar energy and photovoltaics 4

I - Introduction 5
I.1 Solar Energy 5
I.1.1 The source of solar energy 5
I.1.2 Solar Radiation 5
I.1.3 The spectrum of solar radiation 6
I.1.4 Number of air masses 8
I.2 Photovoltaic Solar Cells 9
I.2.1 Definition of Photovoltaic Energy 9
I.2.3 Definition of the Photovoltaic Cell 9
I.2.3 Principle of Operation of the Solar Cell 11
I.3 Semiconductor 12
I.3.1 Band structure 12
I.3.2 Fermi level 13
I.3.3 Types of Semiconductors 14
I.3.4 Intrinsic Semiconductor 15
I.3.5 Extrinsic semiconductor 16
I.3.6 P-type semiconductors 17
I.3.7 N-type semiconductors 17
I.3.8 Bipolar PN Junction 18
I.3.9 Characteristics of a photovoltaic cell 19

I.3.10 Equivalent circuit of a photovoltaic cell 19
I.3.11 I-V characteristic of a photovoltaic cell 20
I.3.12 Solar cell parameters 21
I.3.13 Short circuit current of I_{sc} 21
I.3.14 Open circuit voltage of V_{oc} 22
I.3.15 The fill factor and Energy conversion efficiency of FF and η 22
I.4 Conclusion 23
Références chapitre I ……………….………………………………….... 24

Chapter II The properties of InGaN material 26

II . Study of InGaN Material 27
II.1 Introduction 27
II.2 Definition of InGaN 27
II.3 InGaN material properties 28
II.3.1 Optical and Optoelectronics Properties 28
II.3.2 Structural properties of group-III nitrides 30
II.3.2.1 Zinc Blende (GaN and InN structural parameters) 30
II.3.2.2 Wurtzite (GaN and InN structural parameters) 31
II3.3 Effect of polarization 32
II.3.3.1 Spontaneous Polarization 32
II.3.3.2 Piezoelectric Polarization 33
II.3.4 Thermal properties 35
II.3.5 Electronic properties 35
II.3.5.1 Band Gap 35
II.3.5.2Carrier mobility 36
II-3-5-3 Dielectric rigidity 36
II.4 State-of-the-art of InGaN-based solar cells 37
II.4.1 Homojunctions 37
II.4.2 Heterojunctions or Multi-junction cells 38

II.4.3 Generation of solar cells 39

II.4.4 Advantages, challenges, and strategies of InGaN-based solar cells 39

II.4.4.1 Advantages of InGaN-based Solar Cells 39

II.4.4.2 Challenges of InGaN-based Solar Cells 40

II.4.4.3 Strategies for Enhancing InGaN-based Solar Cells 40

II.5 conclusion 42

Références Chapitre II 43

Chapter III: Simulation of a p-InGaN/n-InGaN single junction (Results and Discussion) 45

III. Simulation of a p-InGaN/n-InGaN Single Junction (Results and Discussion) 46

III.1. Introduction 46

III.2 Description of the SCAPS 1D Simulator 46

a). Main menu « Action panel » 46

b) Structure selection 46

c). Layer properties 48

d). Simulation results « Characteristic I(V) » 49

III.3 Structure of a PN and PPN-junction 49

III.3.1 Solar cell structure 51

III.3.2 The bandgap strucure of PN and PPN junction InGaN solar cells 52

III.3.3 Structure of PN junction p-In0.7Ga0.3N/ n-In0.7Ga0.3N 54

III.3.3.1 Influence of the thickness in the p-In0.70Ga0.30N and n-In0.70Ga0.30N regions. 56

III.3.3.2 Influence of the doping concentration in the p-In0.70Ga0.30N and n-In0.70Ga0.30N regions. 57

III.3.4 Structure of PPN junction p-In0.6Ga0.4N/p-In0.7Ga0.3N/n-In0.7Ga0.3N 57

III.3.4.1 Influence of the thickness in PPN junction 60

III.3.4.1.1 Influence of the thickness of top p-In0.6Ga0.4N region (dp1) 60

III.3.4.1.2 Influence of the thickness of the middle p-In0.7Ga0.3N region (dp2) 62

III.3.4.2 Influence of the doping concentration in the PPN junction 63

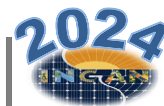

III.3.4.2.1 Influence of the doping concentration in the top p-In0.60Ga0.40N region (Na1) 46
III.3.5 Conparaison between PN and PPN junction of InGaN solar cell 48
III. Conclusion Générale 66
Références Chapitre III 67
Abstract

List of Figures

Figure I-1 :	Types of solar radiation distribution	6
Figure I -2 :	Types of solar radiation distribution	7
Figure I -3:	Condition of measurement of rayonnement AM_x	8
Figure I -4 :	Transform solar energy into electric energy by the photovoltaic (PV)	9
Figure I -5 :	photovoltaic solar cells	10
Figure I -6 :	Components of photovoltaic solar cells	10
Figure I -7 :	(a) working principle of solar cell with p-n junction structure and (b) loss mechanism in standard p-n junction solar cells.	11
Figure I -8 :	Band structure of the three categories of materials	13
Figure I -9 :	Classification of materials by resistivity and conductivity values	13
Figure I -10 :	Difference Types of Semiconductors	14
Figure I -11 :	Type Groupe Semi-Conductor	14
Figure I -12 :	Conduction Mechanism in Case of Intrinsic Semiconductors (a) In the absence of an electric field (b) In the presence of an electric field	15
Figure I -13 :	(a) Intrinsic Semiconductor at T = 0 Kelvin, behaves like an insulator (b) At t>0, four thermally generated electron pairs	16
Figure I -14 :	Classification of Extrinsic Semiconductor	17
Figure I -15 :	p type semiconductor	17
Figure I -16 :	n type semiconductor	18
Figure I -17 :	P-N junction are of two types – diffusion and drift	19
Figure I -18 :	Equivalent circuit of a photovoltaic cell	20
Figure I -19 :	Characteristic of a photovoltaic cell	20
Figure I -20 :	The short circuit current	21
Figure I -21 :	The open circuit voltage	22
Figure I -22 :	The fill factor FF	22

Figure II -1 :	particular semiconductor compounds (III-V) indium gallium-nitride (InGaN)	27
Figure II -2 :	Band gap and the corresponding wavelength as a function of the lattice hexagonal and Cobic	28
Figure II -3 :	Correspondence between the solar spectrum AMx and the In(x)Ga(1-x)N gap	29
Figure II -4 :	(a) Refractive index dispersion relations and (b) absorption coefficient spectra of GaN substrate and InxGa1-xN films used in the simulations, as extracted from the ellispometric data analysis.	30
Figure II -5 :	Schematic wurtzite lattice of InGaN material and ((c) Crystal structure of wurtzite. (d) Unit cell of the wurtzite structure.	31
Figure II -6 :	polarisation spontanée dans le GaN	32
Figure II -7 :	Piezoelectric polarization in GaN	34
Figure II -8 :	Band structure of wurtzite phase a) GaN; b) InN and c) InGaN	35
Figure II -9 :	Generation of solar cells InGaN	39
Figure II -10 :	Advantages, challenges, and strategies of InGaN-based solar cells	41

Figure III-1 :	SCAPS startup panel, the action or main panel	47
Figure III-2 :	Definition of a solar cell structure.	48
Figure III-3 :	Parameters of a p-In0.60Ga0.40N cell layer.	48
Figure III-4 :	Display panel for I-V curves	49
Figure III-5 :	Structure of a PN-junction (left) and a PPN-junction (right) InGaN solar cell.	**51**
Figure III-6 :	(a) Diagram of band energy levels of the PPN structure	53
	(b) Diagram of band energy levels of the PN structure	53
Figure III-7 :	(a) IV curves of the PN-junction InGaN solar cell structure.	54
	(b) Quantum efficiency curves of the PN-junction InGaN solar cell structure.	54
	(c) Effect of thickness of top layer on Jsc and Voc	55
	(d) Effect of thickness of top layer on FF and eta	55
Figure III-8 :	(a) IV curves of the PN-junction InGaN solar cell structure.	56
	(b) Quantum efficiency curves of the PN-junction InGaN solar cell structure.	56
	(c) Effect of thickness of bottom layer on Jsc and Voc	56
	(d) Effect of thickness of bottom layer on FF and eta	56
Figure III-9 :	(a) Effect of the doping concentration of top layer on Jsc and Voc	57

	(b) Effect of the doping concentration of top layer on FF and eta	**57**
Figure III-10 :	(a) Effect of the doping concentration of bottom layer on Jsc and Voc	**59**
	(b) Effect of the doping concentration of bottom layer on FF and eta	59
Figure III-11 :	(a) IV curves of the PPN-junction InGaN solar cell structure.	61
	(b) Quantum efficiency curves of the PPN-junction InGaN solar cell structure.	61
	(c) Effect of the thickness of top (dp1) layer on Jsc and Voc	61
	(d) Effect of the thickness of top (dp1) layer on FF and eta.	**61**
Figure III-12 :	(a) Effect of the thickness of bottom (dn2) layer on Jsc and Voc	62
	(b) Effect of the thickness of bottom (dn2) layer on FF and eta	62
Figure III-13 :	(a) Effect of the doping concentration of top (dp1) layer on Jsc and Voc	63
	(b) Effect of the doping concentration of top (dp1) layer on FF and eta	63
Figure III-14 :	Coparaison of IV curves between PPN-junction and PN-junction of InGaN solar cell structures.	65
Figure III-15 :	Comparaison of quantum efficiency curve between PPN-junction and PN-junction of InGaN solar cells structures.	65

List of tables

Table II-1:	**GaN and InN structural parameters**	**31**
Table II-2:	Difference Between Zinc Blende and Wurtzite	32
Table II-3:	Main properties of III-N compounds at room temperature (300K).	33
Table II-4:	Elastic and Piezoelectric Coefficients of the Main III-Nitrides Compared to GaN.	34
Table II-5:	Presents the electronic and thermal **properties** of several well-known semiconductors in comparison with GaNProperties at 300 K.	36
Table III.1	**Difference Parameters Between GaN and InN**	**50**
Table III.2	Simulation parameters for the InGaN materials in the PN and PPN junction InGaN solar cells	
Table III.3	Influence of the thickness of top p-InGaN region (dp)	54
Table III.4	Influence of the thickness of bottom n-InGaN region (dn)	56
Table III.5	Influence of the doping concentration in the top p-InGaN region	57
Table III.6	Influence of the doping concentration in top layer (dp = 0.01 um, dn = 1um, Na = 1.1020 cm-3)	58
Table III.7	Influence of the doping concentration in top layer (dp = 1 um, dn = 1um, Nd = 1.1020 cm-3)	58
Table III.8	Influence of the doping concentration in the bottom n-InGaN region	**59**
Table III.9	Influence of the doping concentration in the bottom n-InGaN of PN junction (dn=0.01um)	60
Table III.10	Influence of the doping concentration in the bottom n-InGaN of PN junction (dn = 1um)	**60**
Table III.11	Table III.11 : Influence of the thickness layer in the top p-InGaN of PPN junction	61
Table III.12	Table III.12 : Influence of the thickness layer in the middle p-InGaN of PPN junction	62
Table III.13	Table III.13 : Influence of the doping concentration in the top p-InGaN of PPN junction (Nd2 = 1.1018 cm-3)	63
Table III.14	Table III.14 : Influence of the doping concentration in the top p-InGaN of PPN junction (Nd2 = 1.1020 cm-3)	64
Table III.15	Comparaison of an optimized values of the photovoltaics parameters between the PPN and the PN structures	64

List of notations

Symbol	Unit	Description
C	Meters per second (m/s)	**Light speed**
E_g	Electronvolts (eV)	**Energy gap of a material**
h	Joule-seconds (J·s) or Energy per photon (eV)	**Planck's constant**
I	Amperes (A)	**Total current**
I_0	Amperes (A)	**Saturation current**
I-V	Volts (V) as it represents a voltage in an IV curve	**Current-voltage**
J_{MPP}	Amperes per square meter (A/m²)	**Maximum- power current**
Jsc	Amperes per square meter (A/m²)	**Short circuit current-density**
J-V	Amperes per square meter (A/m²) as it represents a current density in an IV curve	**Current-density vs. Voltage**
K	Kelvin (K)	**Boltzmann's constant**
λ	meters (m)	**wavelength of light**
L	(meters, m)	**Length**
P_{MPP}	Watts	**Maximum power**
PMPP	Watts per square meter (W/m²)	**Maximum power point power**
q	Coulombs (C)	**Electronic charge**
R_s	Ohms (Ω)	**Series resistance**
T	Temperature (Kelvin, K)	**Environment temperature**
V	Volts (V)	**Applied potential**
VMPP	Volts (V)	**Maximum-power voltage**
Voc	Volts (V)	**Open circuit voltage**
a b c	(A°)	**Crystal lattice parameter in the plane**
B	Pascals (Pa) or Megapascals (MPa)	**Elastic modulus**
C11,C12,C13,C33	Pascals (Pa)	**Elastic constant**
E	Pascals (Pa) or Gigapascals (GPa)	**Young's modulus**
e31,,e33	Coulombs per newton (C/N), or picoCoulombs per newton (pC/N) in some cases	**Piezoelectric coefficients**

List of Abbreviations

AM 1.5	**Standard terrestrial solar spectrum 'Air Mass 1.5'**
CdTe	Cadmium Telluride
CFOA	Current-Fed Operational Amplifier (a type of amplifier used in solar cells)
CIGS	Copper-Indium-Gallium-Selenide
DDSS	Dye-sensitized solar cells
DOP	Dopant (a chemical element added to a semiconductor to alter its electrical properties)
Eg	Energy gap of a material
EQE	External Quantum Efficiency
ETL	electron transport layer
ETM	Electron transport material
FF	Fill Factor, measuring the efficiency of a solar cell's energy conversion
HTL	Hole transport layer
IQE	Internal Quantum Efficiency
Isc	Short-Circuit Current, the maximum current a solar cell can produce
I-V	Current-Voltage
JMPP	Maximum power point current, the current at the maximum power point.
Jsc	Short circuit current
J-V	Current-density vs. voltage
LED	Light-Emitting Diode
MIS	Metal-Insulator-Semiconductor

OPV	Organic photovoltaic
PCE	Power conversion efficiency
PCE	Perovskite solar cell
PMPP	Maximum power point power, the maximum power output of the solar cell.
P-N	Positive-Negative (referring to a P-type and N-type semiconductor)
PNJ	P-N Junction (the interface between a P-type and N-type semiconductor)
PV	Photovoltaic
QD	Quantum dot
QE	Quantum Efficiency
Rs	Series resistance
SCAPS	Solar Cell Capacitance Simulator
SPV	Solar Photovoltaic (conversion of sunlight into electrical energy)
VMPP	Maximum power point voltage, the voltage at which the solar cell delivers maximum power
Voc	Open-Circuit Voltage, the maximum voltage a solar cell can produce
$\mu_{e,h,..}$	Electron, Hole mobility
GSC	global solar constant

GENERAL INTRODUCTION

Today, the production of electricity by converting light using photovoltaic cells is largely dominated by silicon, with 95% of installed photovoltaic panels (monocrystalline, polycrystalline and thin-film) [1]. However, these commercial panels suffer from low average efficiency, around 13% (between 12 and 18% for monocrystalline, between 12 and 15% for polycrystalline and between 6 and 9% for thin-film [2]). This is why a great deal of research is focusing on increasing the efficiency of silicon panels (nanostructures, thin films, plasmonics, etc.) and on alternative materials with higher efficiency (CdTe, CIGS, GaAs, etc.). Generally speaking, these new materials are deposited in thin layers (a few hundred nanometers), but still offer attractive yields, there by reducing production costs.

Among the new thin-film materials being considered for photovoltaics is the InGaN alloy. InGaN currently appears to be the most promising material for photovoltaic applications, with the potential for high conversion efficiencies. InGaN materials have an attractive modulable gap energy ranging from 0.7 eV to 3.42 eV, and a high optical absorption coefficient of over 10^5 /cm, indicating better absorption of the solar spectrum [3.4]. Its gap energy can be modulated by varying the rate of Indium x in the $In_xGa_{1-x}N$ alloy, making it a very promising material for ultra-thin film solar cells in space applications.

The aim of our work is the « **Study and Simulation of Photovoltaic Properties on the Performance of p-InGaN/n-InGaN Single Junction. Numerical simulation** »

The manuscript is divided into three chapters. The first chapter explains how a solar cell works, its most important parameters and its various applications, as well as the PN junction.

The second chapter describes the InGaN material, its characteristics, its main structural, electrical, thermal and optical properties, and its growth. The third chapter consists of two main parts, the first part gives a detailed description of the Solar Cell Capacitance Simulator (SCAPS-1D) which is used to simulate the solar cell performances based on p-InGaN/n-InGaN Single Junction. The second part describes the simulation of PN and PPN junction solar cells structures, this part also presents and discusses some results obtained using the Scaps 1D program.

Finally, we draw a general conclusion.

REFERENCES

[1] **Les technologies de fabrication des modules. Photovoltaïque.info. [Online] 03 2011. [Cited: 12 21, 2011.] http://www.photovoltaique.info/Les-differentes technologies.html.**

[2] **ADEME**. Energies et matières renouvelables - Solaire photovoltaïque. Agence de l'environnement et de la maîtrise de l'énergie. [Online] 02 01, 2011. [Cited: 01 12, 2012.]**http://www2.ademe.fr/servlet/KBaseShow?sort=1&cid=96&m=3&catid=13924**

[3] **Yamaguchi, M**., “III-V compound multi-junction solar cells: present and future,”Sol. Energy Mater. Sol. Cells 75, 261-269 (2003).

[4] **Wu, J., Walukiewicz, W., Yu, K. M., Ager III, J. W., Haller, E. E., Lu, H., Schaff, W. J., Saito, Y. and Nanishi, Y.,** “Unusual properties of the fundamental band gap of InN,” Appl. Phys. Lett. 80, 3967-3969 (2002).

Chapter I

Generalities on solar energy and photovoltaics

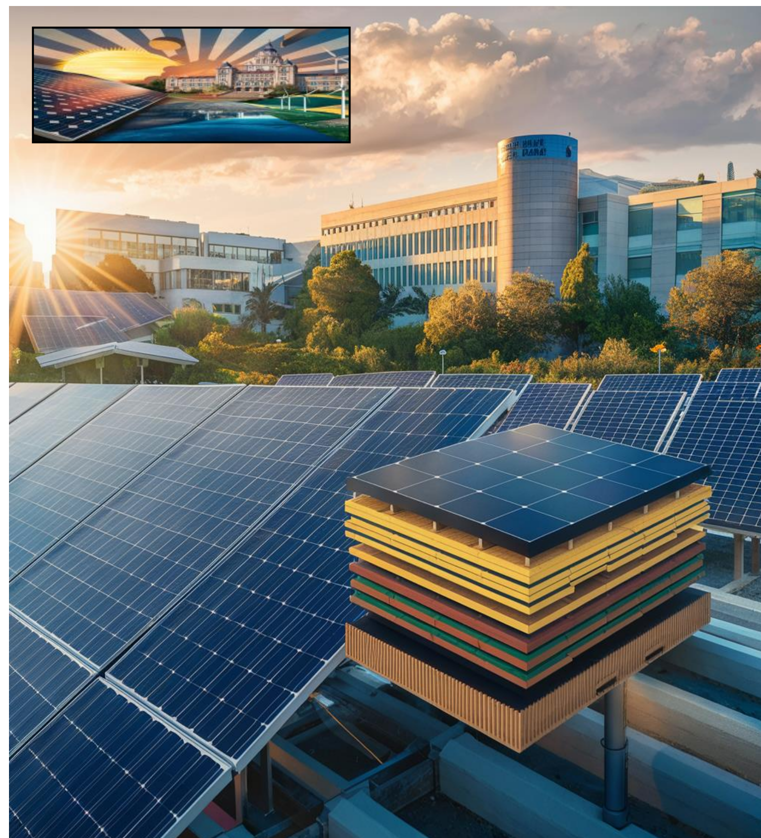

I- Introduction

There exist various types of renewable energy sources distributed across the Earth's surface, including kinetic wind energy and solar energy. Thermal energy undergoes conversion processes to generate usable energy forms like electricity, catering to human energy needs.

I.1 Solar Energy

Solar energy stands out among renewable energy sources due to its widespread availability, being hailed as a crucial energy form. Harnessing merely a fraction, even ten percent, of Earth's energy reserves could potentially meet global energy demands for numerous years.

The forthcoming section will delve into key aspects of solar energy and strategies for its effective utilization.[1].

I.1.1 The source of solar energy

Solar energy is primarily generated in the sun's nucleus through the fusion of two hydrogen atoms to form a helium atom, resulting in a release of tremendous energy[2] [3]. This energy is then emitted as solar radiation, reaching the Earth and serving as a vital source for various renewable energy technologies like solar photovoltaic systems. The sun's constant fusion reactions maintain its high temperature of 5777 K, sustaining the continuous generation of solar radiation that powers solar energy applications on Earth. Solar radiation consists of direct and diffuse components, with direct radiation being crucial for concentrating solar power technologies, highlighting the importance of harnessing this energy source for sustainable electricity generation. Understanding the solar radiation processes and variations is essential for maximizing the efficiency and deployment of solar energy systems [4].

I.1.3 Solar Radiation

Solar radiation or sunlight is a collection of electromagnetic waves, of which the human eye can see a field called visible light, while the remaining field is invisible to the naked eye. Mirror rays from the sun's spectrum are characterized by color rays from red to violet, which are the colors of the rainbow. Red waves have a wavelength of 700 nanometers and violet waves are short-wavelength and have a wavelength of about 400 nanometers. Two parts of the sun's spectrum are not visible to the naked eye: As in Figure I.1, the part with a wavelength longer than 700 nanometers (up to about 2700 nanometers) is the infrared band, and the other part with a wavelength shorter than 400 nanometers, which is called the ultraviolet band ultraviolet[5] [6].

Solar radiation can be divided into four types:

1. A direct ray that penetrates the atmosphere and reaches the earth's surface without trouble, without scattering, and remains intact without loss.
2. A reflected ray that is reflected on the ground or on objects on the earth's surface.
3. A diffuse ray that is scattered by the atmosphere and some of it may leak out depending on the weather.
4. The total radiation resulting from the sum of direct, reflected, and diffuse rays.

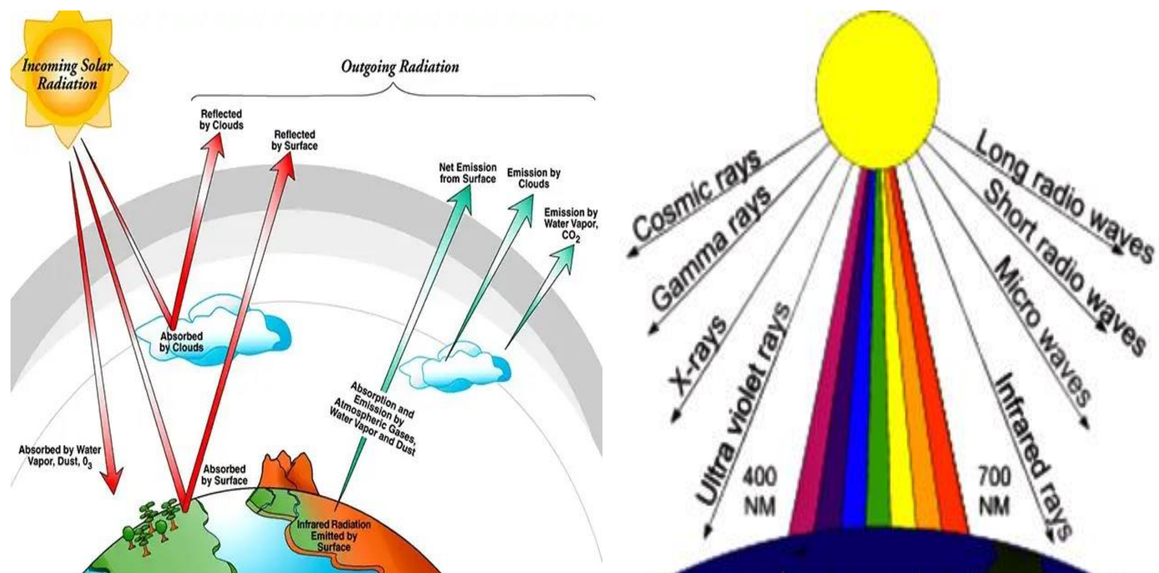

Figure I.1 : Types of solar radiation distribution[5] [6].

I.1.4The spectrum of solar radiation

Solar radiation carries energy and its energy varies with its wavelength. As the wavelength of light increases, its energy decreases. This means that ultraviolet radiation has a relatively high energy. Therefore, they are harmful to the skin of the human body if exposed for too long. The sun's rays fall to Earth after passing through the atmosphere. Some of them are absorbed by the atmosphere. Different gases in the atmosphere, such as nitrogen, oxygen, carbon dioxide, water vapor, and others, have different abilities to absorb sunlight.

The brightness of direct sunlight can reach (93 lumens) of radiation per watt of flux, including infrared, visible, and ultraviolet radiation. The average power of solar energy incident on a square meter of Earth's surface is

$$E_0 = 1367\ W/m^2 \quad (I.1)$$

This constant is called the global solar constant (GSC)

Scientists distinguish three types of rays that make up solar radiation:

Thermal or infrared radiation, which is inelastic and is estimated to account for about 50% percent of total solar radiation

Their wavelength ranges from (4.0-0.75) microns (1/1000th of a millimeter) and they play an important role in the entire activity.

As for the so-called visible light rays, they are actually invisible, as visible sunlight is like the sun's rays that penetrate the cosmic space without us seeing them, but are scattered by transparent physical media such as the atmosphere or reflected from it such as the surface of the moon. Scattering is the secret to illuminating the atmosphere with daylight, knowing that light can be analyzed with a glass prism into its basic components. The proportion of visible light rays is estimated at 37% of the total solar radiation, and their wavelengths range from (40.0-74.0 microns). The strength of visible light rays on the Earth's surface increases at noon during the day in summer.

Ultraviolet radiation (also called bioluminescence) is aspherical and accounts for about (3....) of the total solar radiation and its wavelength ranges from (5.40.17) microns [7] [8].

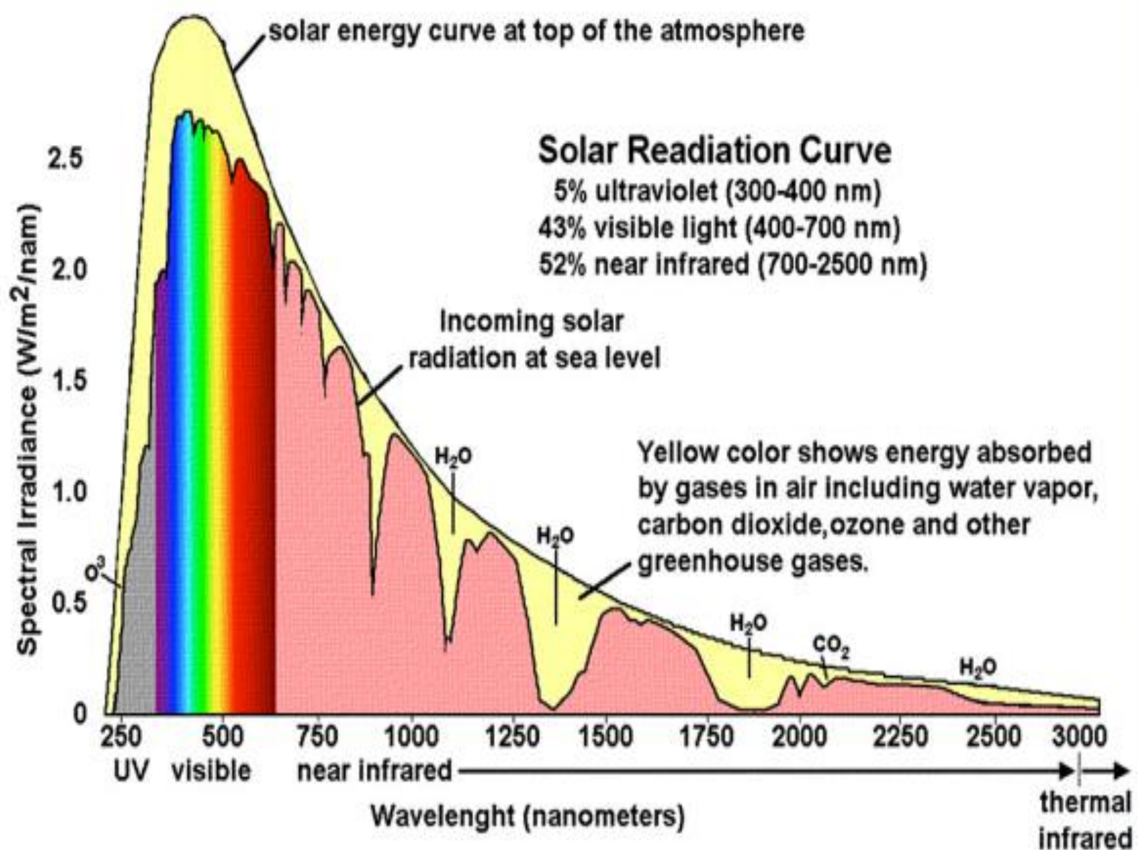

Figure I.2 : Types of solar radiation distribution[9].

I.1.5 Number of air masses

the evolution of the solar spectrum throughout the day and its variability based on geographical location are key characteristics. Reference spectra have been established to aid in evaluating the performance of photovoltaic devices from various manufacturers and research institutions. These standardized spectra underwent modifications in the early 2000s to improve resolution and conform to international standards. The previous solar spectrum, was phased out in 2005. In general, the differences among spectra have minimal effects on device efficiency [10], with newer spectra being more user- **Figure I.3** . The solar spectrum outside the Earth's atmosphere, characterized as a 5,800 K black body, is referred to as "AM0" or "zero atmospheres". Cells used in space power applications, such as on communication satellites, are commonly assessed using "AM0". The solar spectrum after passing through the atmosphere to sea level with the sun directly overhead is known as "AM1", representing "one atmosphere"[11]. A standard solar spectrum, depicted graphically as spectral irradiance versus wavelength, is shown in **Figure I.2** .

Air mass is a measure of how far light travels through the Earth's atmosphere. It is defined as the ratio of the actual path length of sunlight to the minimum path length, which occurs when the sun is directly overhead. This ratio indicates the amount of atmosphere that light must pass through before reaching an observer on the ground. The air mass is a function of the solar elevation angle, with higher angles corresponding to shorter path lengths and lower angles corresponding to longer path lengths [12] [13] :

$$AM_x = \frac{1}{\cos(\theta)} = \sqrt{\frac{h^2+s^2}{h^2}} = \sqrt{1+\frac{s^2}{h^2}} \quad \text{with the zenith angle } \theta \qquad (I.2)$$

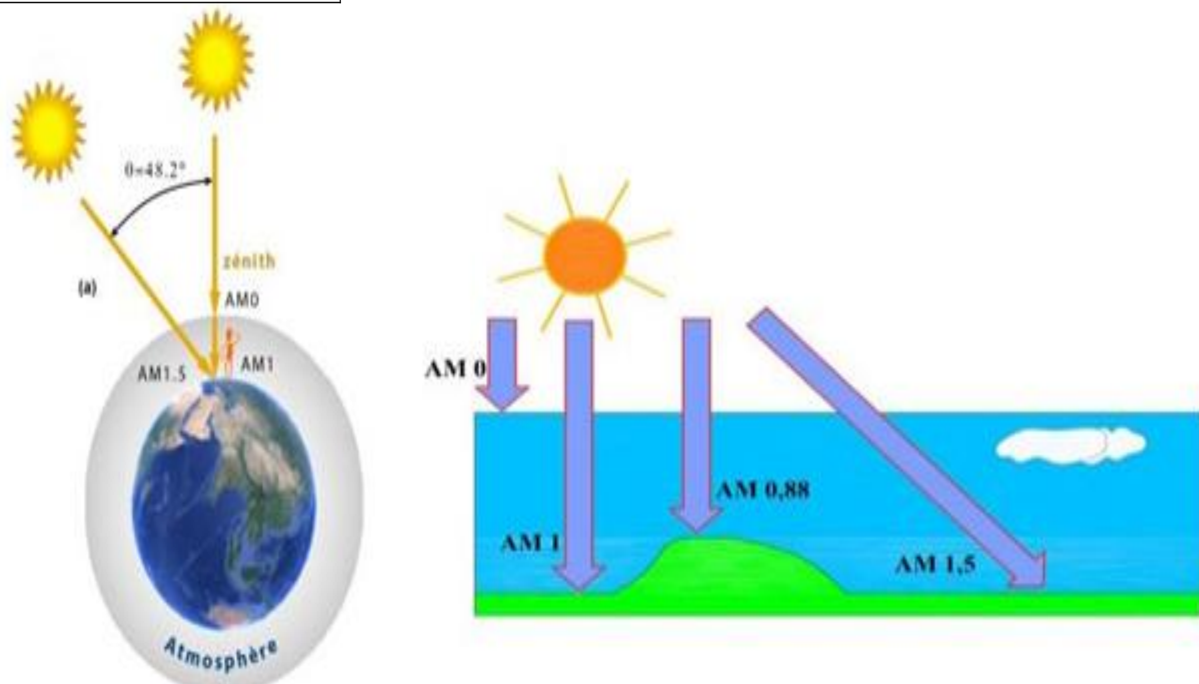

Figure I.3 : Condition of measurement of rayonnement AMx[13]

I.2 Photovoltaic Solar Cells

One of the alternative energy sources that is gaining popularity around the globe is photovoltaic (PV) electricity. It is pure, sustainable, and non-polluting energy. This energy is produced by using solar cells to transform solar radiation into electrical energy. Electrical devices in homes and businesses can be powered by it, By creating a semiconductor material that can transmit positive and negative electrical charges when exposed to light, these cells enable the direct conversion of solar energy into electricity. This electrical energy is known as photoelectric energy.

Among the most significant and extensively utilized forms of renewable energy in the world, photovoltaic energy is applied in numerous fields.

I.2.1 Definition of Photovoltaic Energy

Photovoltaic energy, derived from solar radiation through solar cells made of semiconductors like silicon, is a crucial form of renewable energy[14]. It stands out for its cleanliness, renewability, and eco-friendliness, offering numerous advantages such as zero emissions of harmful gases and independence from fossil fuels, known for causing pollution[15]. This energy type is particularly beneficial for remote areas without centralized grids, providing electricity to buildings and homes, and powering small devices like laptops and smartphones efficiently . The evolution of photovoltaic technology, driven by advancements in materials and manufacturing processes, has significantly enhanced its efficiency and applicability, making it a promising solution for sustainable energy needs [16].

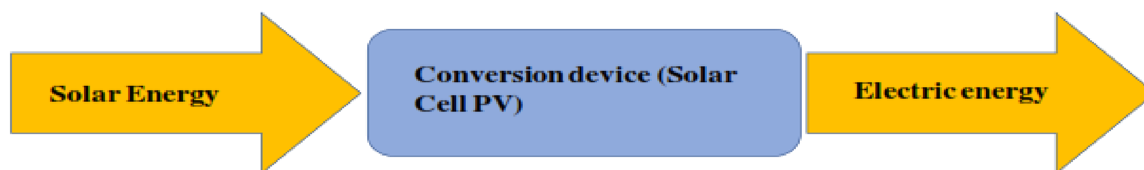

Figure I. 4: Transform solar energy into electric energy by the photovoltaic (PV) [17]

I.2.2 Definition of the Photovoltaic Cell

The photovoltaic cell, also known as a solar cell, is a semiconductor device that converts sunlight directly into electric current through the photovoltaic effect[18]. It typically comprises a semiconductor substrate with base regions, collecting electrodes, connecting electrodes, a passivation layer, and collecting electrodes stacked in a specific configuration [19] ,**Figure I.5** .

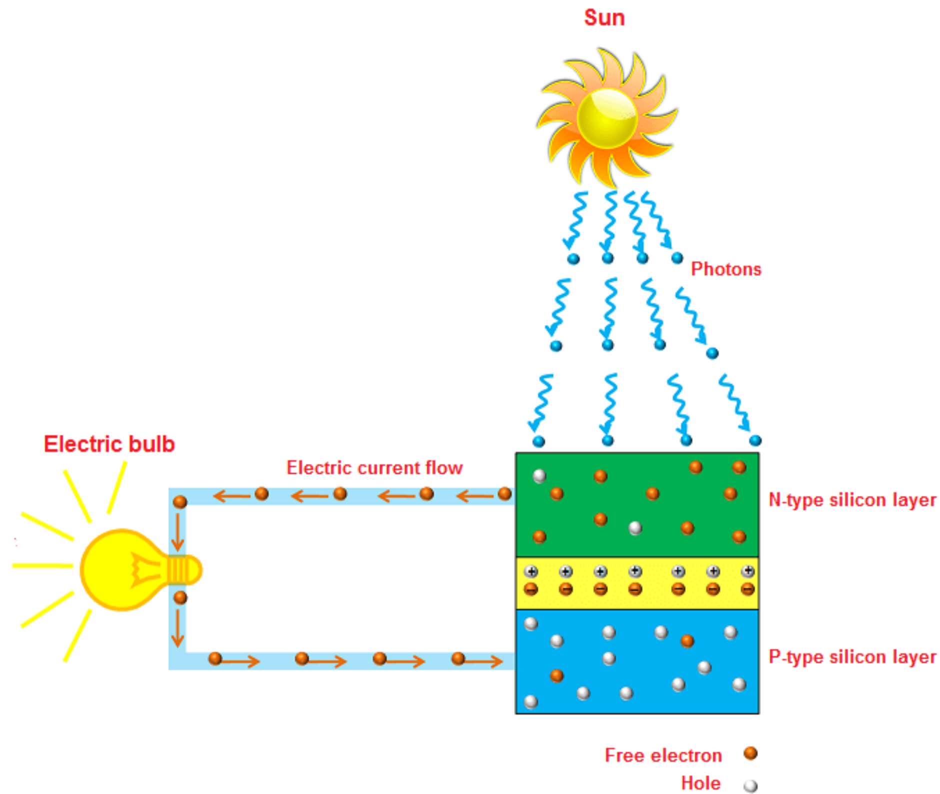

Figure I.5 : photovoltaic solar cells[20].

The cell's operation relies on the energy of incoming photons raising electrons from the valence band to the conduction band, with equilibrium carrier concentration and minority carrier concentration gradients playing crucial roles in determining current densities and material characteristics **Figure I.6** [21].

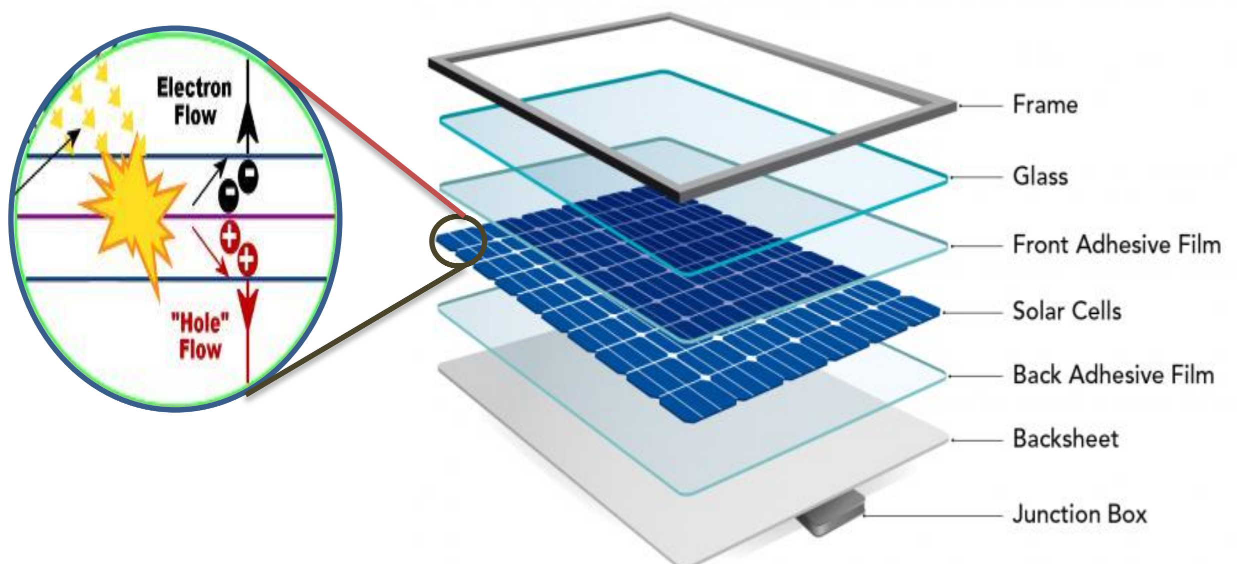

Figure I.6 : Components of photovoltaic solar cells [21].

I.2.3 Principle of Operation of the Solar Cell

The principle of operation of photovoltaic cells is based on the direct conversion of solar light energy into electrical energy using the photoelectric effect. The photovoltaic solar cell consists of a thin layer of semiconductor material sandwiched between two layers of oppositely charged materials.

When the solar cell is exposed to sunlight, electrons are released in the semiconductor material, and these electrons move towards the upper layer of the solar cell. The liberated electrons from the semiconductor material move to the upper layer due to the electrostatic effect that arises between the two different layers in the semiconductor material.

As the electrons reach the upper layer, they move through an external wire and head towards the lower layer of the solar cell, obtaining electrical energy during this process. Electrical energy is produced by multiple solar cells connected sequentially or in parallel.

These cells are connected to an electrical energy conversion device, where the direct current generated by the solar cell is converted into alternating current used in household electrical systems.

General Operation of the Photovoltaic Solar Cell is illustrated in **Figure I.7** . .[22].

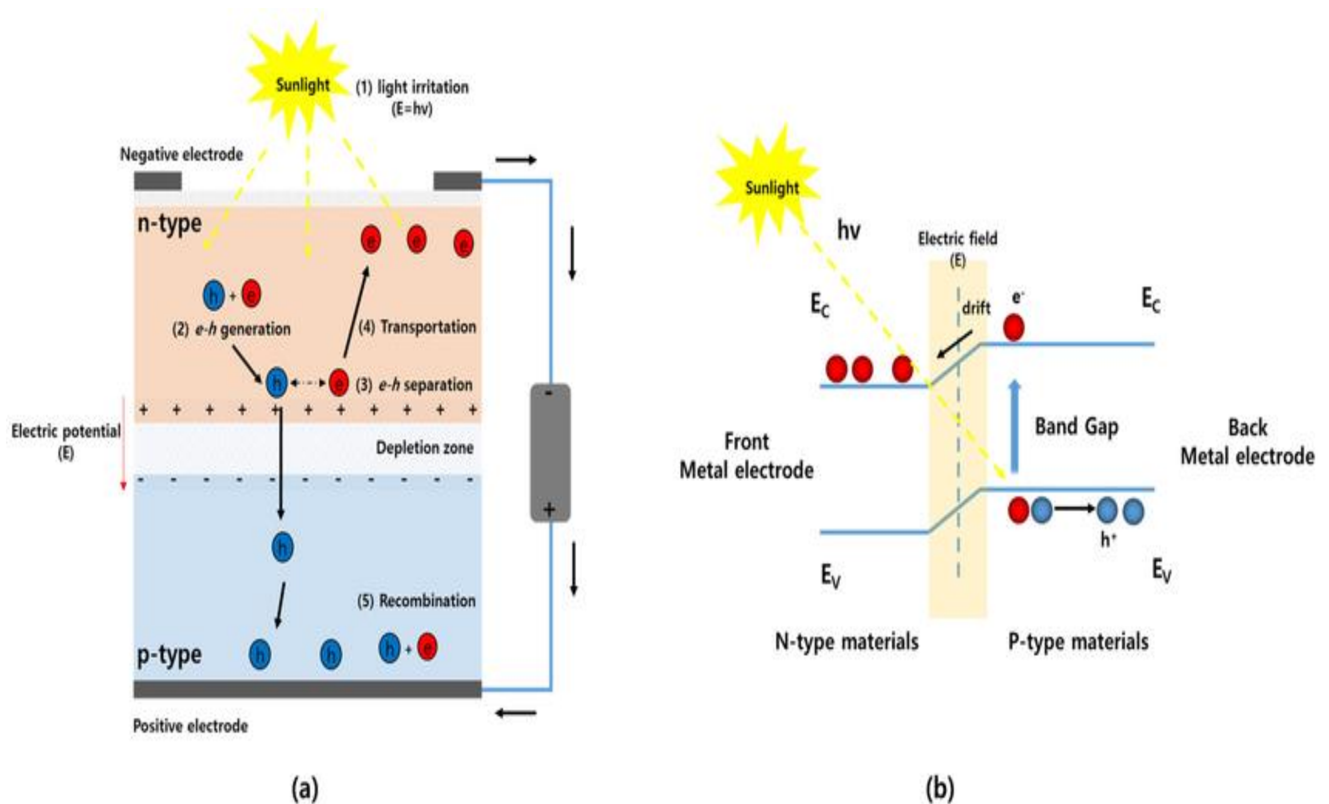

Figure I.7 : (a) working principle of solar cell with p-n junction structure and (b) loss mechanism in standard p-n junction solar cells. [23].

1. Light absorption and generation of carriers. Photons originating from sunlight arrive at the surface of the solar cell, which absorbs them. Many electron–hole pairs are produced by the photon-absorption mechanism.
2. Carrier separation and collection of the light-generated carriers to generate a current. The electrons are released into the negative layer, and the decomposed electrons flow through the positive layer.
3. Generation of a voltage across the solar cell. The electrons overcome the boundary energy at the n-type layer and flow through the negative electrode at the top of the cell, which is connected to an external load. This provides a path for the positive material layer; thus, electricity is generated. When the electric field is sufficiently strong to cease further diffusion of holes and electrons, the depleted region reaches equilibrium. Integrating the electric field across the depleted region determines what is called the built-in voltage (also called electric field or voltage). Electrons and holes diffuse into regions with lower concentrations of them.
4. Carrier collection and dissipation of power in the load. Electrons return to the cell after exiting the external load and repeatedly move from the positive to the negative side for continuous electricity generation [23].

I.3 Semiconductor

Semiconductors are materials whose conductivity is intermediate between that of conductors and insulators. This conductivity strongly depends on temperature. A semiconductor is a material in which the peripheral electrons are distributed between at least two energy bands separated by a relatively small energy gap of the order of 1 eV [24].

I.3.1 Band structure

In a crystal, a moving particle is subject to a potential that depends on the periodicities of the crystal lattice [25]. In a simple model of a material with two energy levels (**Figure I.8**), an electron with energy Ev belongs to the valence band and is bound to the atom. If it receives energy " in the form of a photon, for example " allowing it to reach the level Ec, which is the energy corresponding to the conduction band, the electron becomes free and can then participate in the creation of an electric current. The energy required for the electron to become free is denoted Eg, the energy associated with the band gap:

$$E_g = E_c - E_v \quad (I.3)$$

Unlike insulators (Eg> 5 eV), semiconductors have a gap of the order of 3eV, whereas for metals the gap is nonexistent .

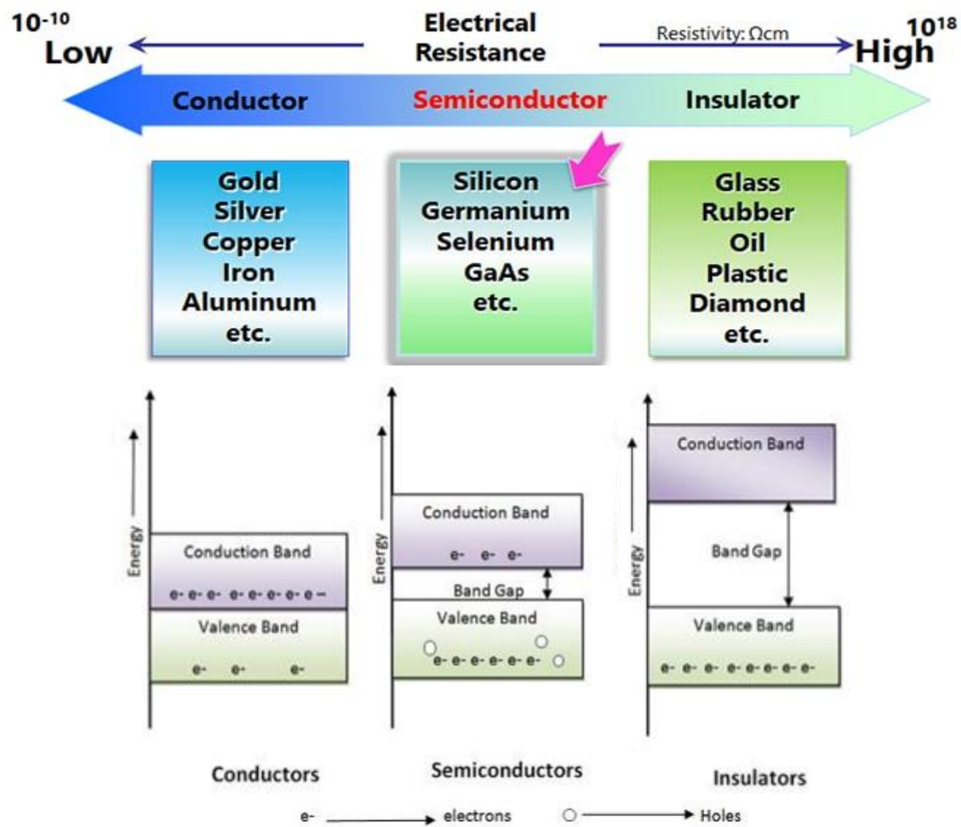

Figure I.8 : Band structure of the three categories of materials [26].

I.3.2 Fermi level :

materials heavily relies on the Fermi level. Symbolized by "E_F", the E_F is quantified in energy measures like electron volts (eV). An increased Fermi level usually leads to /heightened electronic conductivity rates. Techniques such as photoemission spectroscopy, scanning tunneling microscopy, and conductivity measurements can be employed to ascertain the Fermi level. [27],[28]

The Fermi function is a probability distribution function defined as follows:[28]

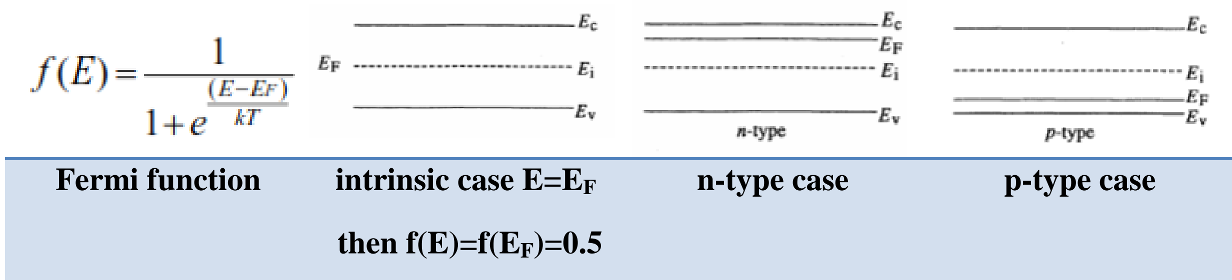

Fermi function	intrinsic case $E=E_F$ then $f(E)=f(E_F)=0.5$	n-type case	p-type case

Figure I.9 : Classification of materials by resistivity and conductivity values[29]

I.3.3 Types of Semiconductors

Semiconductors can be classified as follows[29]

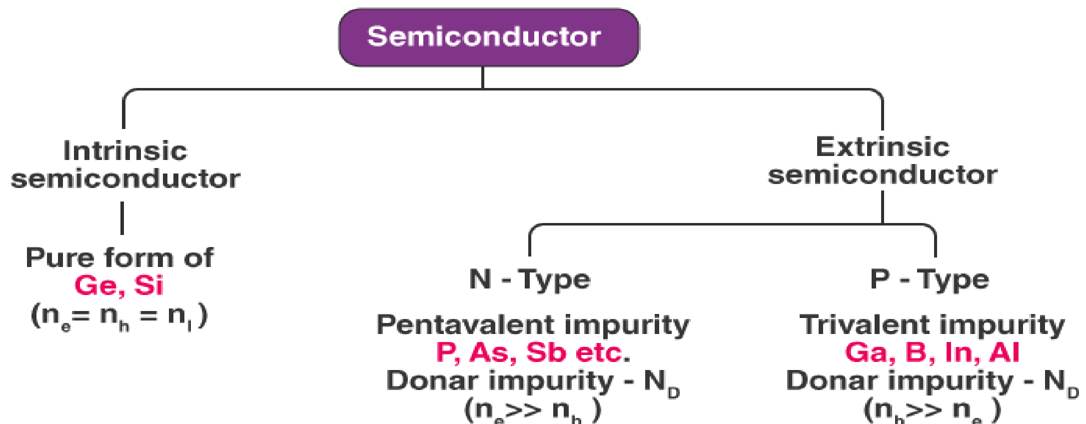

Figure I.10: Difference Types of Semiconductors [30].

Depending on the kind of dopant, n-type or p-type semiconductor can be made.

Semiconductors made of several elements are called compound semiconductors, as opposed to those made of a single element such as silicon semiconductors. There are combinations such as Group III and Group V of the periodic table, Group II and Group VI, Group IV, etc [30]

Element(s)	Material
Single	Si, Ge
Compound	Group II-VI ZnSe CdTe
	Group III-V GaAs InGaN InP
	Group IV-IV SiC

Group II	Group III	Group IV	Group V	Group VI
Be Beryllium	B Boron	C Carbon	N Nitrogen	O Oxygen
Mg Magnesium	Al Aluminum	Si Silicon	P Phosphorus	S Sulfur
Zn Zinc	Ga Gallium	Ge Germanium	As Arsenic	Se Selenium
Cd Cadmium	In Indium	Sn Tin	Sb Antimony	Te Tellurium
Hg Mercury	Tl Thallium	Pb Lead	Bi Bismuth	Po Polonium

Figure I.11 : Type Groupe Semi-Conductor[30]

Doping phosphorus (P) of Group V into silicon (Si) of Group IV makes n-type semiconductor**.**

Doping boron (B) of Group III into silicon (Si) of Group IV makes p-type semiconductor.

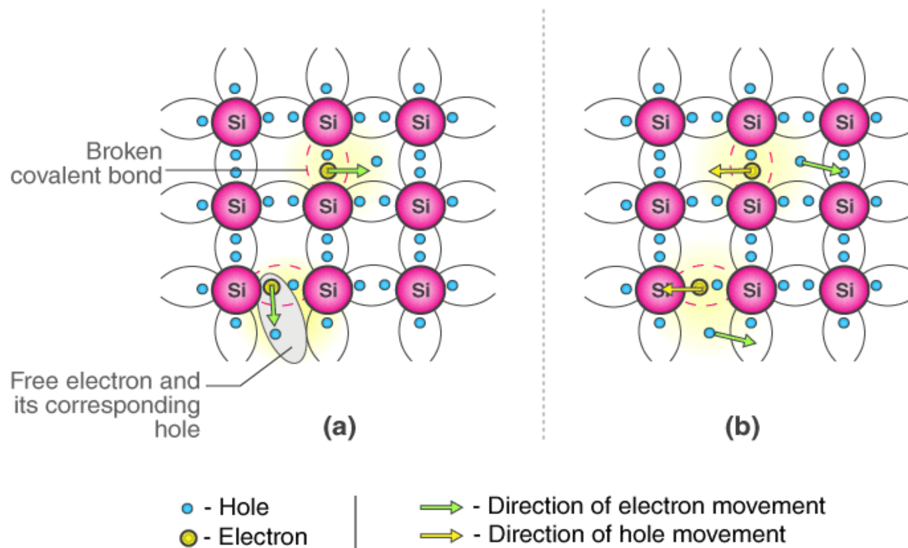

Figure I.12: Conduction Mechanism in Case of Intrinsic Semiconductors (a) In the absence of an electric field (b) In the presence of an electric field [30].

I.3.4 Intrinsic Semiconductor

An intrinsic type of semiconductor material is made to be very pure chemically. It is made up of only a single type of element. [30]

Germanium (Ge) and silicon (Si) are the most common types of intrinsic semiconductor elements. They have four valence electrons (tetravalent). They are bound to the atom by a covalent bond at absolute zero temperature.

When the temperature rises due to collisions, few electrons are unbounded and become free to move through the lattice, thus creating an absence in its original position (hole). These free electrons and holes contribute to the conduction of electricity in the semiconductor. The negative and positive charge carriers are equal in number.

The thermal energy is capable of ionising a few atoms in the lattice, and hence, their conductivity is less. [30]

The Lattice of Pure Silicon Semiconductor at Different Temperatures

- **At absolute zero Kelvin temperature:** At this temperature, the covalent bonds are very strong, there are no free electrons, and the semiconductor behaves as a perfect insulator.
- **Above absolute temperature:** With an increase in temperature, a few valence electrons jump into the conduction band, and hence, it behaves like a poor conductor.

Energy Band Diagram of Intrinsic Semiconductor : The energy band diagram of an intrinsic semiconductor is shown below. [30]

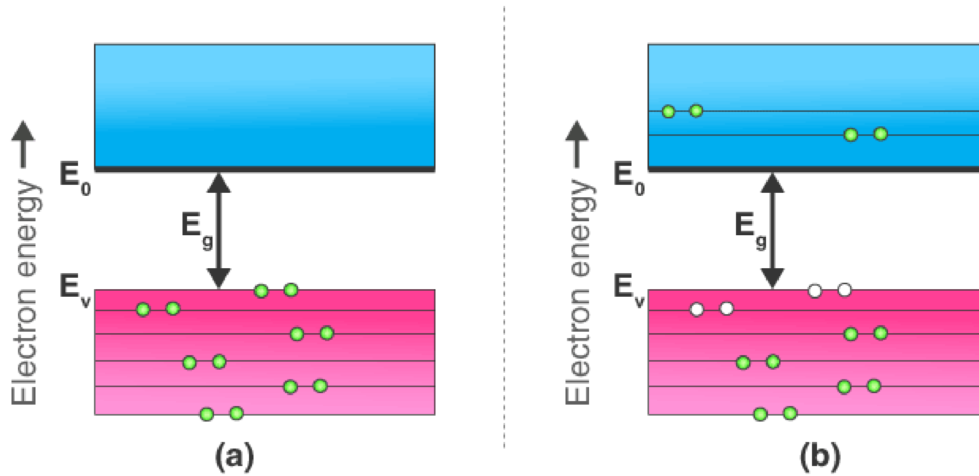

Figure I.13: (a) Intrinsic Semiconductor at T = 0 Kelvin, behaves like an insulator (b) At t>0, four thermally generated electron pairs[29].

In intrinsic semiconductors, current flows due to the motion of free electrons, as well as holes. The total current is the sum of the electron current Ie due to thermally generated electrons and the hole current I_h.

Total Current (I) = $I_e + I_h$ (I.4)

For an intrinsic semiconductor, at finite temperature, the probability of electrons existing in a conduction band decreases exponentially with an increasing band gap (Eg). [30]

$$n = n_0 e^{-Eg/2.Kb.T} \quad (I.5)$$

Where,

E_g = Energy band gap

K_b = Boltzmann's constants

I.3.5 Extrinsic semiconductor

Extrinsic semiconductors, created through controlled impurity introduction, play a crucial role in semiconductor device functionality[31]. The characteristics of n- and p-type dopants in various materials have been extensively studied, with group VII atoms being effective n-type carriers in SnS2 monolayer nanosheets[32], and P and O being preferable for

n-type doping in cubic silicon nitride, The charge redistribution between dopants and their neighbors is a key factor in n- and p-type effects in silicon, Practical doping protocols have been developed for Ge1−ySny semiconductors, enabling the creation of n- and p-type doped layers with controlled and efficient doping, These studies collectively highlight the importance of extrinsic semiconductors and the role of doping in their properties and applications. An extrinsic semiconductor can be further classified into types [30]

N-type Semiconductor and P-type Semiconductor.

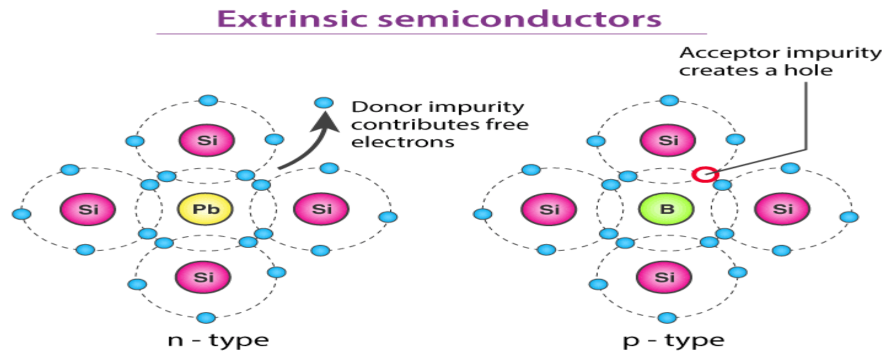

Figure I.14: Classification of Extrinsic Semiconductor [I.30]

I.3.6 P-type semiconductors

A p-type semiconductor is an intrinsic semiconductor doped with boron (B) or indium (In). Silicon of Group IV has four valence electrons and boron of Group III has three valence electrons. If a small amount of boron is doped to a single crystal of silicon, valence electrons will be insufficient at one position to bond silicon and boron, resulting in holes* that lack electrons. When a voltage is applied in this state, the neighboring electrons move to the hole, so that the place where an electron was present becomes a new hole, and the holes appear to move to the "–" electrode in sequence[30].

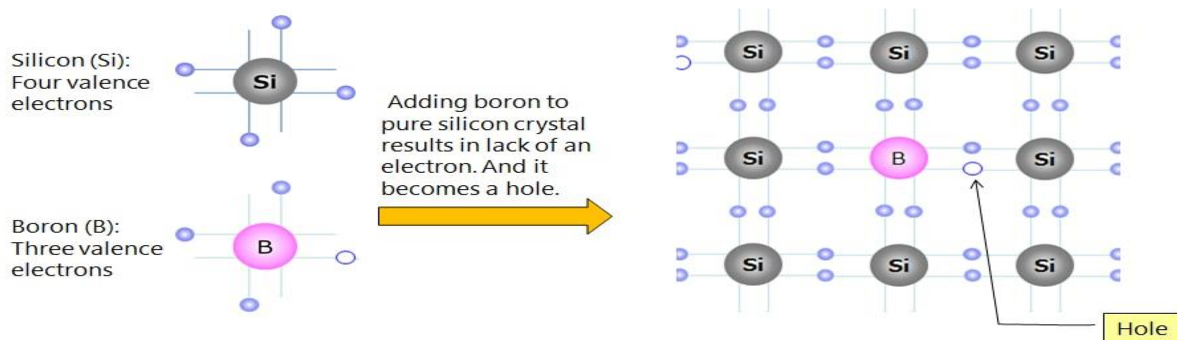

Figure I.15: p type semiconductor [30]

I.3.7 N-type semiconductors

An n-type semiconductor is an intrinsic semiconductor doped with phosphorus (P), arsenic (As), or antimony (Sb) as an impurity. Silicon of Group IV has four valence electrons and

phosphorus of Group V has five valence electrons. If a small amount of phosphorus is added to a pure silicon crystal, one of the valence electrons of phosphorus becomes free to move around (free electron*) as a surplus electron. When this free electron is attracted to the "+" electrode and moves, current flows[30]

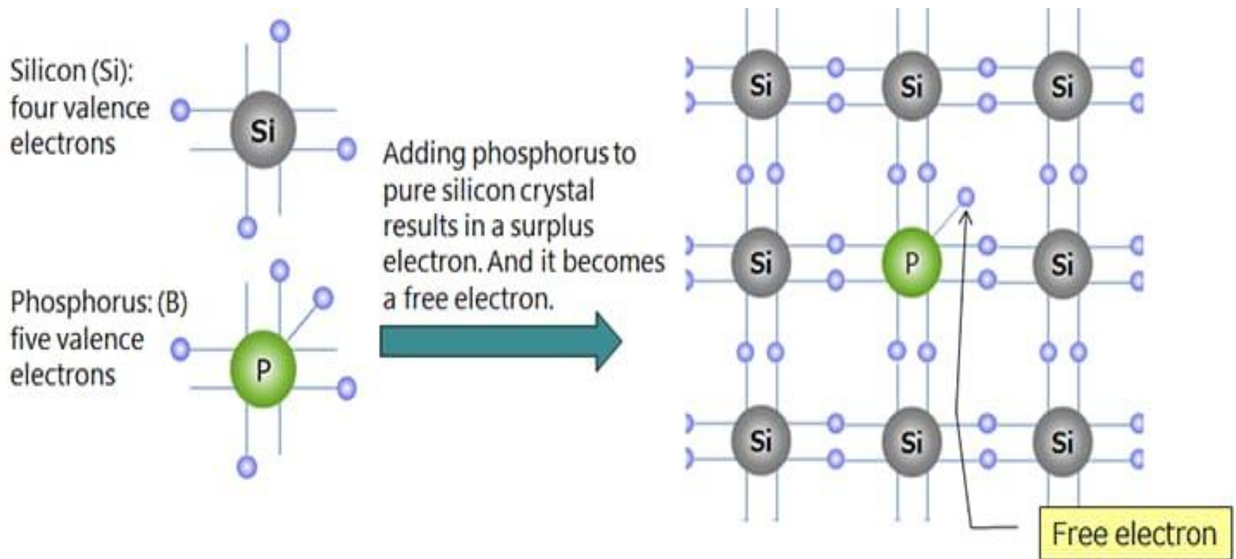

Figure I.16 : n type semiconductor [30].

I.3.8 Bipolar PN Junction

The bipolar PN junction is an electronic compound consisting of two semiconductor halves of type N and type P. The bipolar PN junction is the intersection of type N and type P materials to form an interface between the two regions. The type P region consists of a semiconductor type containing hole carriers, and the type N region consists of a semiconductor type containing excess electrons. The two regions are intentionally doped with different impurities to control the concentration of electric charges in the transitional region between the two halves.

The properties of the bipolar PN junction depend on its structure, shape, the degree of doping of the halves, and the strength of the electric field present in the transitional region between the halves. The bipolar PN junction is used in various electronic applications such as photovoltaic solar cells, electronic switches, LED lights, and sensors. [30]

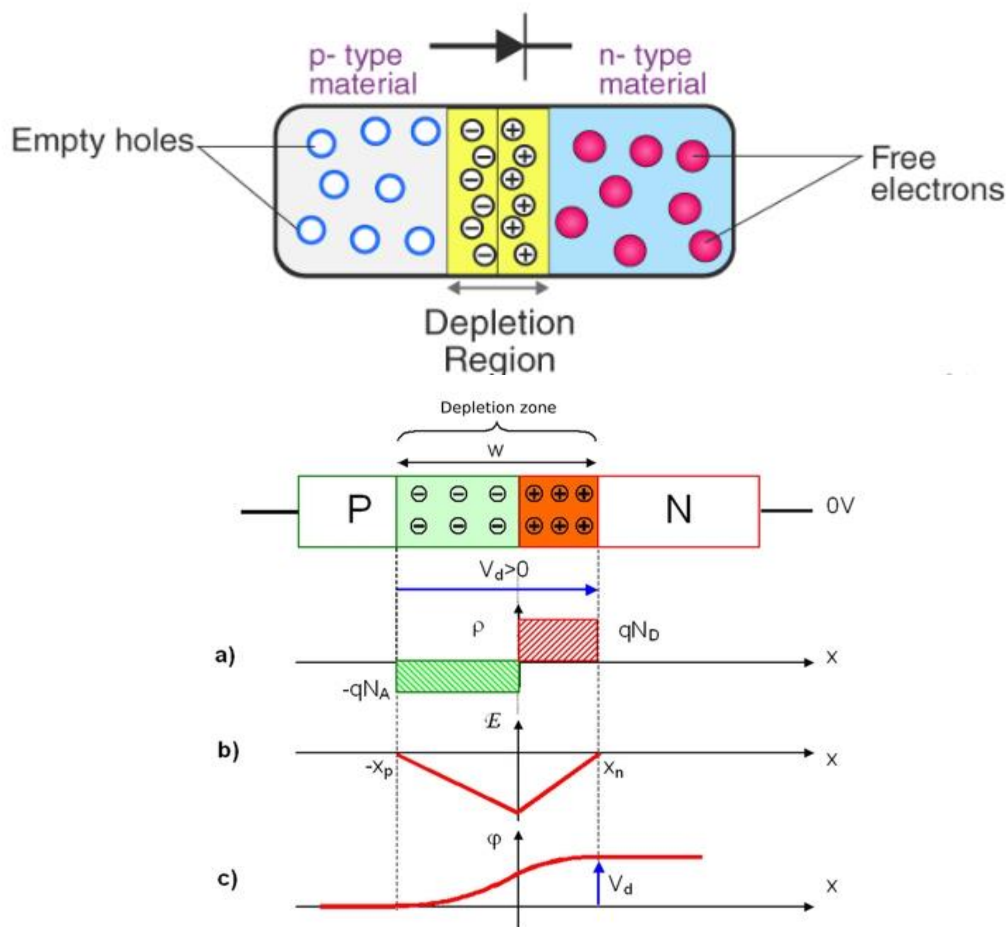

Figure I.17: P-N junction are of two types – diffusion and drift[29].

I.3.9 Characteristics of a photovoltaic cell

The basic characteristics of a solar cell are the short-circuit current (I_{SC}), the open-circuit voltage (V_{OC}), the fill factor (FF) and the solar energy conversion efficiency (η). The influence of both the diode saturation current density and of I_{SC} on V_{OC}, FF and η is analyzed for ideal solar cells [31] :

I.3.10 Equivalent circuit of a photovoltaic cell

A genuine solar cell is depicted in **Figure I.18**, illustrating an electrical model of the photovoltaic cell. The diagram highlights the current generator Iph, which corresponds to the photogenerated current Iobs = Id of the forward-biased diode, along with Rs and Rsh representing the shunt resistor and the series resistance, respectively. The series resistance is attributed to the resistivity of various layers of the cell such as emitter, base, and metal contacts, particularly their interface with the semiconductor. It is crucial for this resistance to be minimized to mitigate its impact on cell current. Achieving this entails reducing the

resistivity of the material utilized. On the other hand, Rsh, the shunt resistance, signifies the existence of a leakage current through the transmitter due to a malfunction, which may arise from high-temperature metal contacts diffusing into the transmitter or a short-circuit at the cell's edges. Ideally, this resistance should be maximized [33].

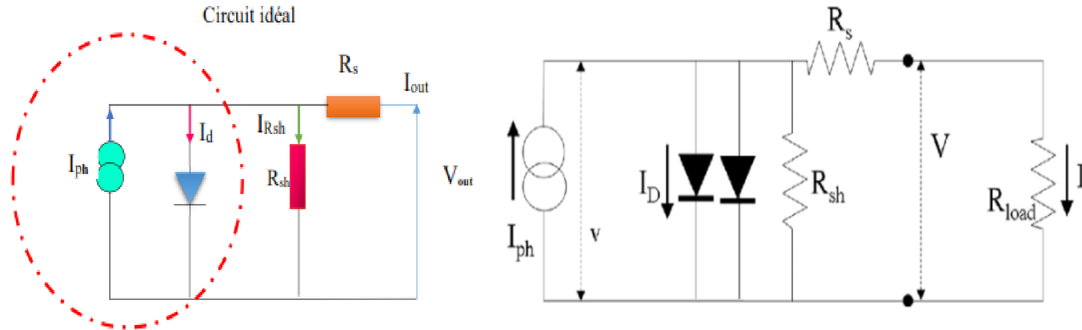

Figure I.18 : Equivalent circuit of a photovoltaic cell [34]

$$I = I_{ph} - I_D$$

$$\boxed{I = I_{PH} - I_D - I_{SH}}$$

$$V_{ideal} = V + (I \times R_S) \Rightarrow I_{SH} = \frac{V + (I \times R_S)}{R_{SH}}$$

$$\boxed{I = I_{ph} - I_0\left(\exp\left(\frac{q(V + (I \times R_S))}{k_b T}\right) - 1\right) - \frac{V + (I \times R_S)}{R_{SH}}} \text{ mode 1D} \quad (I.6)$$

$$\boxed{I = I_{ph} - I_{01}\left(\exp\left(\frac{q(V + (I \times R_S))}{k_b T}\right) - 1\right) - I_{02}\left(\exp\left(\frac{q(V + (I \times R_S))}{k_b T}\right) - 1\right) - \frac{V + (I \times R_S)}{R_{SH}}} \text{ mode 2D}^{[I.35]} \quad (I.7)$$

I.3.11 I-V characteristic of a photovoltaic cell

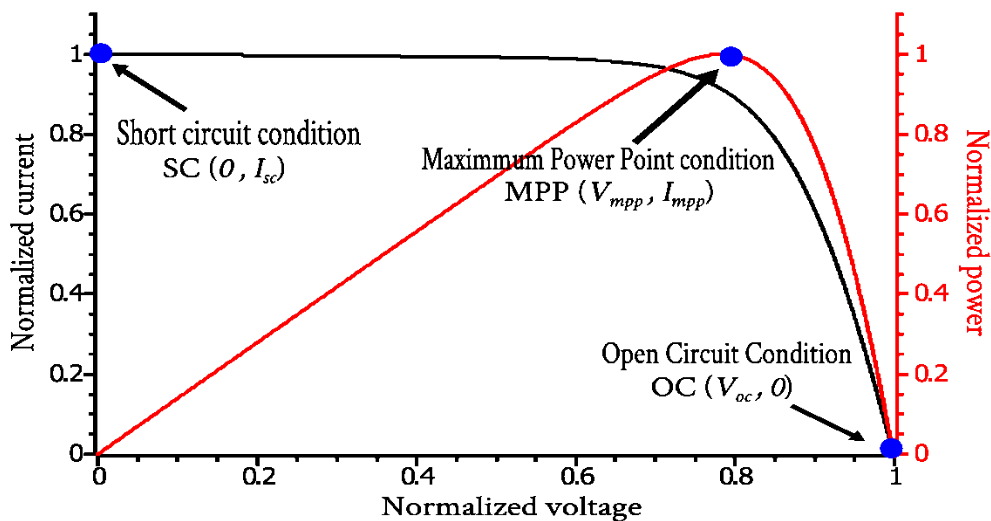

Figure I.19 : Characteristic of a photovoltaic cell [36].

The three physical quantities that define this curve are :

- **Vco**: Open-circuit voltage, this value represents the voltage generated by an illuminated, unconnected cell.
- **Isc**: Short-circuit current, representing the current generated by an illuminated cell connected to itself.
- **Pm**: Its maximum power point: MPP (maximum power point) obtained for an optimum optimal voltage and current: Vopt, Iopt (sometimes also called Vmpp, Impp).are defined by :

I.3.12 Solar cell parameters

The parameters of a photovoltaic cell are determined from the current-voltage current-voltage (I-V) characteristic curve (**Figure I.20** .), which describes the cell's operation.

The main characteristic quantities of solar cells are:

- Short circuit current I_{sc}
- Open circuit voltage V_{oc}
- The fill factor FF
- Energy conversion efficiency η
- The spectral response R_s

I.3.13 Short circuit current of I_{sc} :

The short-circuit current expressed in aý is the current flowing in the cell under illumination and by shorting the terminals of the cell. It grows linearly with the illumination intensity of the cell and it depends on the illuminated surface, the wavelength of the radiation, the mobility of the charge carriers and the temperature. It can also be said that the current is the current initiated by the cell under illumination in reduce output. Which means :

$I_{sc} = I(V = 0)$ and equations analytical $\boxed{I = I_{ph} - I_{sc}(e^{v/v_T} - 1)}$ (I.8)

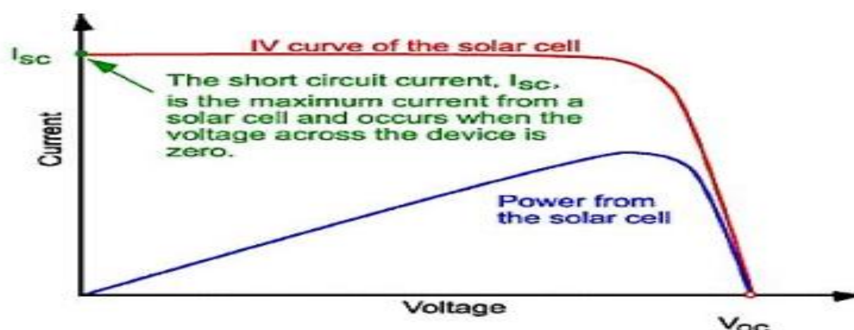

Figure I.20 : The short circuit current I_{sc} [37]

I.3.14 Open circuit voltage of V_{oc} :

The open circuit voltage Voc is the maximum voltage available from a solar cell, and this occurs at zero current. The open circuit voltage expresses the direct polarization of the resulting cell by polarizing the junction with the light -generated current. The schematic of the open circuit voltage on the I-V curve is in **Figure I.21 .**

$$I_0 = \left(e^{\frac{eV_{oc}}{\eta k_b T}} - 1 \right) - I_{sc} = 0 \quad \text{and} \quad V_{oc} = \frac{\eta . k_b . T}{e} \ln\left(\frac{I_{sc}}{I_0} - 1 \right) \qquad (I.9)$$

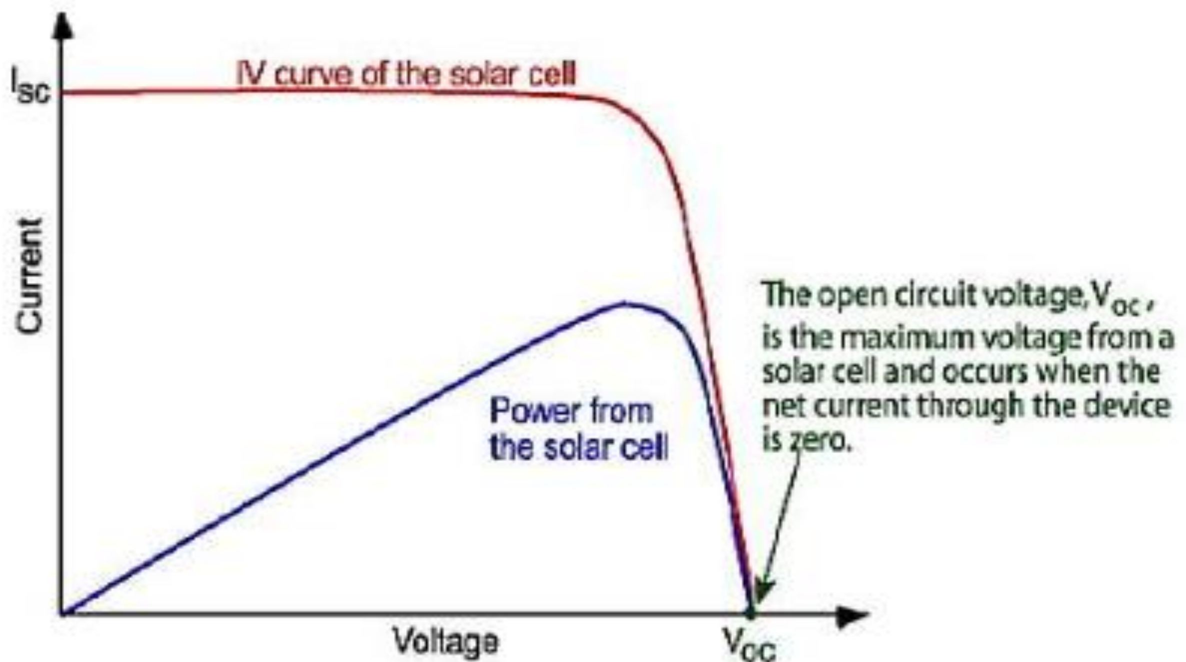

Figure I.21 : The open circuit voltage

I.3.15 The fill factor and Energy conversion efficiency of FF and η

The "fill factor" is the ratio of maximum power P_m, to the open-circuit V_{oc} voltage and short circuits current I_{sc}. It is known by the abbreviation "FF".² the FF is illustrated in **Figure I. 22**.

$$FF = \frac{I_m . V_m}{V_{oc} . I_m} = \frac{P_m}{V_{oc} . I_{sc}} \qquad (I.10)$$

In the ideal case, the fill factor (FF) is100 %. For a silicon solar cell, the AA typically ranges between77.0% and 82.0%.

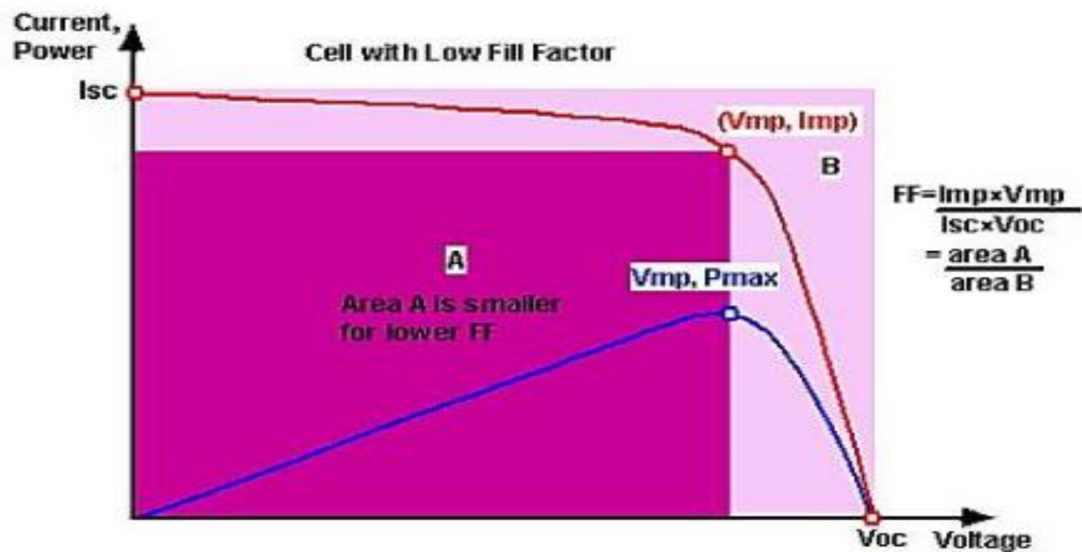

Figure I. 22 : The fill factor FF[38]

Conversion efficiency is the most commonly used medium or benchmark for comparing a solar cell to another. The efficiency represents the ratio between the electrical capacity generated by the cell and the photovoltaic power it receives. Therefore, it depends on the intensity of incoming light and the temperature of the solar cell. Therefore, the conditions under which cell efficiency is measured to compare a cell to another must be controlled. In general, solar cell efficiencies are measured at 25 ° C and AM1.5 light. In space, light AM0[38].

$$\eta = \frac{FF.I_{sc}.V_{oc}}{P_{inc}} = \frac{P_{out}^{max}}{P_{inc}} \quad (I.11)$$

I.4 Conclusion :

In this chapter, we presented some of the general concepts related to the solar cells in terms of their definition, operation mode and a comparison between some of the solar cell examples based on Si ,CIGS, GaAs, and InGaN, respectively. These concepts allow and facilitate us to understand and grasp the second chapter, which will be paired around the InGaN-based solar cells.

REFERENCES

[1] **Emma, Jones. (2022).** Rapid Adaptation of Renewable Energy – A Review on Solar Energy, Types and Overview. doi: 10.36548/rrrj.2022.1.002

[2] Hashruf Hanifa - Study of the effect of front junction barrier height and operating temperature on the performance of solar cells, University of M'sila - Master's Thesis 2020. ZnO/CdS/CZTS

[3] **GAYL, D., NESS. (2023)**. Solar Energy. doi: 10.5772/intechopen.106155

[4] **Jorge, Morales, Pedraza. (2022).** Solar energy for electricity generation. doi: 10.1016/b978-0-12-823440-2.00006-8

[5] **C.Julian.Chen**,PhysicsofSolarEnergy .pdf https://www.hindawi.org/books/79392975/2/

[6] https://www.notstory.com/2015/07/blog-post.html , https://www.nrel.gov/research/re-photovoltaics.html

[7] **Laurie Emmanuelle André**, these docteur Soutenue le 29 novembre **2017**

[8] https://bonsaimontreal.com/wpcontent/uploads/2020/09/Diffe%CC%81rence-Types-Lumie%CC%80res.pdf

[9] **Definitions of the AM0, AM1.5** and many others from the National Department of **Energy**: http://rredc.nrel.gov/solar/spectra/ - U.S. Department of Energy: Description of Air-Mass

[10] http://www.greenrhinoenergy.com/solar/radiation/spectra.php

[11] https://pvpmc.sandia.gov/modeling-guide/1-weather-design-inputs/irradiance-insolation/air-mass/

[12] https://www.pveducation.org/pvcdrom/properties-of-sunlight/air-mass

[13] **(2023). Solar Photovoltaic Energy System**. doi: 10.5772/intechopen.108958

[14] **Siti, Aminah, Mohammad. (2023**). Performance evaluation of electrical energy produced by polycrystalline silicon cells. doi: 10.24191/ba/v7i1/79426

[15] **(2022). Introduction to photovoltaics**. doi: 10.1016/b978-0-12-823483-9.00012-7

[16] **A. BENMIR,** "Simulation d'une cellule solaire photovoltaïque en couche mince à hétérojonction: CdS/CIGS et CdS/CZTS."

[17] **(2022). Solar Light Energy:** A Photovoltaic Cell. Green energy and technology, doi: 10.1007/978-981-19-2099-8_5

[18] **(2022). Solar Cells.** doi: 10.1002/9781119686040.ch7

[19] **Yoshikawa, Kunta. (2021).** Photovoltaic cell, photovoltaic cell module, and method for manufacturing photovoltaic cell.

[20] https://www.physics-and-radio-electronics.com/blog/solar-panels-solar-panels-work/

[21] https://www.ossila.com/pages/history-of-solar-cells

[22] **Swati, Sharma., Anwarul, M, Haque., Balram, Singh., Jaykishan, Jayantkumar, Gandhi. (2022).** Photovoltaic Cell in the Nutshell of Manufacturing Process. International Journal For Science Technology And Engineering, doi: 10.22214/ijraset.2022.47320

[23] **Kim S, Hoang VQ, Bark CW**. Silicon-Based Technologies for Flexible Photovoltaic (PV) Devices: From Basic Mechanism to Manufacturing Technologies. Nanomaterials. 2021; 11(11):2944. https://doi.org/10.3390/nano11112944

[24] **Charles Kittel :** Physique de l'état solide. Edition Dunod, (1998).

[25] **Henry Mathieu** : Physique des semiconducteurs et des composants électroniques. Edition Masson,(1998).

[26] **Lasladj, M. (2015).** Simulation numérique des cellules solaires de troisième génération pour des applications spatiales (Doctoral dissertation),
Erdoğan, E., Kundakçi, M., & Mantarci, A. (2016). InGaN thin film deposition on Si(100) and glass substrates by termionic vacuum arc. Journal of Physics: Conference Series, 707.

[27] **R. F. Pierret,** Semiconductor Device Fundamentals**, Addison-Wesley Publishing, Reading, Massachusetts, 1996.** https://byjus.com/jee/semiconductors/

[28] https://byjus.com/jee/semiconductors/

[29] https://toshiba.semicon-storage.com/ap-en/semiconductor/knowledge/e-learning/discrete/chap1/chap1-1.html

[30] **C. Xia, Yuting Peng, Heng Zhang, Tianxing Wang, S. Wei, Yu** JiaPhysical Chemistry, Chemical Physics – PCCP Dio 10.1039/c4cp02214a

[31] **XuZhao, Peng Chen, C. Xia, Tianxing Wang, X. Dai DIO** https://doi.org/10.1039/C5RA27540G

[32] **P-N Junction," Electronics Hub website**, https://www.electronicshub.org/pnjunction/

[33] **Usman, H., Lawal, S.M., & Shehu, R.S. (2014).** Behavioral Characteristics of Photovoltaic Cell with Different Irradiation in Matlab/Simuling/Simscape Environment. *International Letters of Chemistry, Physics and Astronomy*.

[34] **AMARA Makhloufia & NIA Ibtissam** Mémoire de Master 2020-2021 Département d'Électronique Simulation et optimisation d'une cellule solaire à base du matériau InGaN

[35] **Mme MEZIANI Zahra**, Mémoire de Magister Option : Microélectronique 2012 MODELISATION DE MODULES PHOTOVOLTAIQUES

[36] https://www.pveducation.org/pvcdrom/welcome-to-pvcdrom/solar-cell-operation.

[37] **N. Oleksiy**, "Simulation, fabrication et analyse de cellules photovoltaïques à contacts arrières interdigités," Institut national des sciences appliquée de Lyon, 2005

[38] **A. Blakers, N. Zin, K. R. McIntosh, and K. Fong**, "High efficiency silicon solar cells," Energy Procedia, vol. 33, pp. 1-10, 2013.

Chapter II

The properties of InGaN material

Study of InGaN Material

II.1 Introduction

Nitride-based materials have been studied intensively in recent years for their application in photovoltaics (PV) [1]. These alloys have a direct bandgap that can be modified over a wide range of wavelengths covering the majority of the solar spectrum [2], making it possible to manufacture a multijunction solar cell based on the same material.

This chapter focuses on ternary InGaN compounds. They are interesting semiconductors for solar energy applications because of their wide gap potential, almost the entire solar spectrum can be covered, making them good candidates for single- and multi-junction solar cells by changing the indium content in the mixed material. This chapter presents the structural and electrical properties of indium gallium nitride (InGaN), and solar cells using these materials [3].

II.2 Definition of InGaN

This substance is categorized as a semiconductor within the nitrides group (III), consisting of nitrogen and elements sourced from group (V) of Mendeleev's periodic table, specifically gallium and indium, as illustrated in **Figure II.1** . Gallium-indium nitride represents a blend of gallium nitride (GaN) and indium nitride (InN). Consequently, the ensuing discussion in this section will primarily focus on the structural, electrical, and optical characteristics of InGaN [4] [5] .

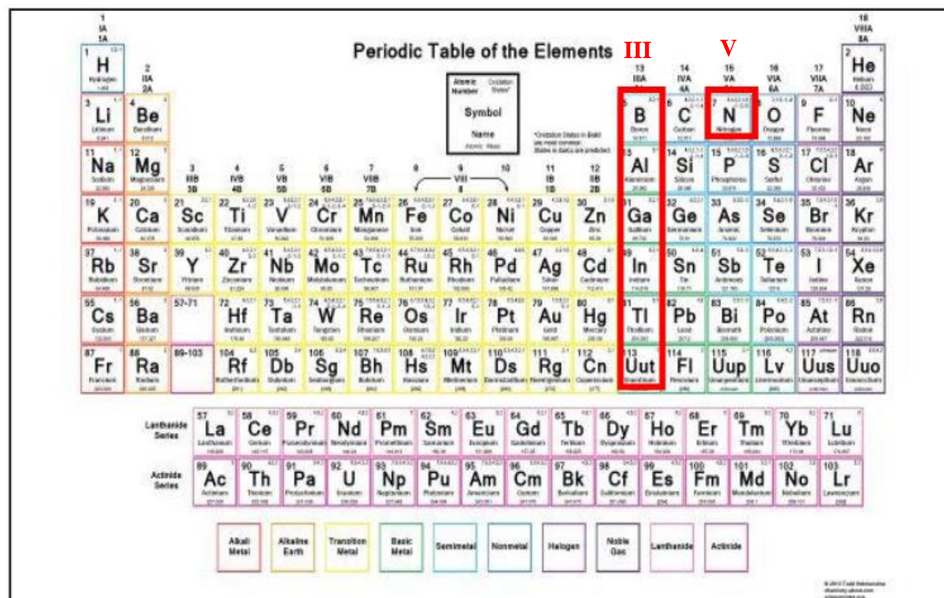

Figure II.1 : particular semiconductor compounds (III-V) indium gallium-nitride (InGaN)[5]

II.3 InGaN material properties

III-Nitrides can crystallize according to two crystalline structures, one with a hexagonal lattice (wurtzite) and the other with a cubic lattice (zinc blende). The most commonly used form is the wurtzite-type lattice due to its advantageous physical properties and ease of growth compared to the other structure. III-V semiconductors are of great interest due to their properties:

- They are robust
- They have high thermal conductivity
- Their melting point is high
- They have a direct band gap

II.3.1 Optical and Optoelectronics Properties

III element nitrides (GaN, AIN, InN and their alloys) are semiconductors with remarkable properties. The most important is undoubtedly the small band gap of InN at 0.7 eV [6]. This extends the spectral coverage of nitrides, now ranging from far ultraviolet with AIN (6.2 eV, or 200 nm) [7], to mid-infrared with InN (0.7 eV, or 1770 nm), through near ultraviolet with GaN (3.39 eV, or 365 nm) [8], and visible with the InGaN or AllnN alloys. The bandgap energies of ternary alloys of type $A_xB_{1-x}N$ can be described by the following equation [9]:

$$E_g^{A_xB_{1-x}N} = E_g^{AN}x + E_g^{BN}(1-x) + b^{A,B}x(1-x) \qquad (II.1)$$

where $b^{A,B}$ is the non-linearity (bowing) term representing the deviation from the Vegard's law. It is equal to 1eV for AlGaN, 1.4eV for InGaN, and 2.5eV for InAlN [9].

- Note that other physical quantities such as piezoelectric and elastic coefficients also follow the same formula except for the bowing term.

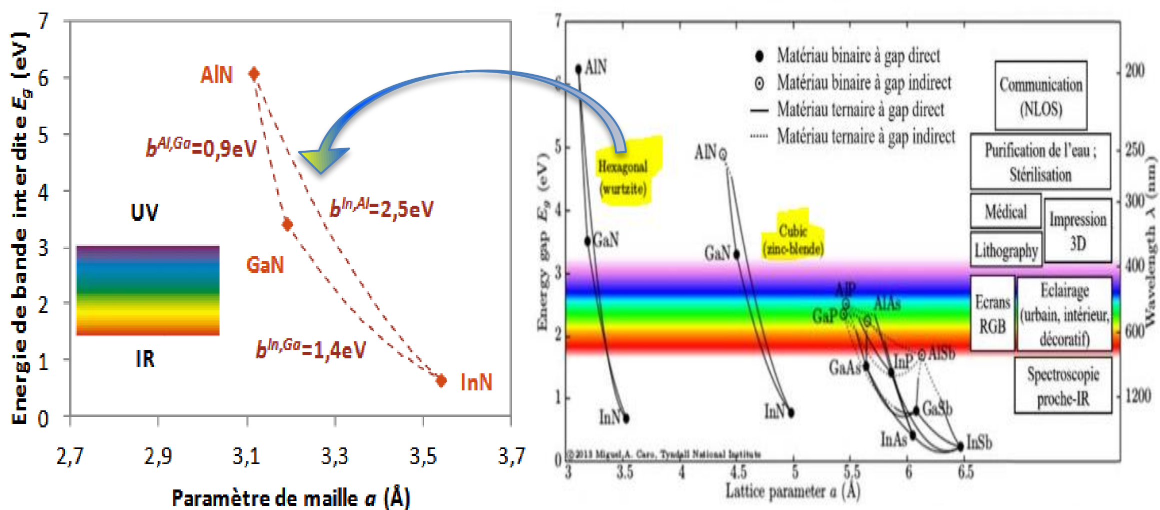

Figure II.2 : Band gap and the corresponding wavelength as a function of the lattice hexagonal and Cobic [10][11].

The solar spectrum AM_x impact InGaN gap :

The solar spectrum, specifically AM_x, significantly impacts the band gap of InGaN materials, allowing them to cover a wide range of the solar spectrum from UV to IR regions[12]. InGaN alloys exhibit band gaps ranging from 0.7eV to 3.4eV, making them suitable for absorbing a large portion of sunlight[13]. By adjusting the indium (In) concentration in InGaN, the band gap can be modulated to maximize solar spectrum absorption, with InGaN reaching band gaps from 3.42 to 0.7eV [14]. This tunability enables the optimization of InGaN-based solar cells, with simulations showing that the In composition plays a critical role in determining the short circuit current density, open circuit voltage, fill factor, and conversion efficiency of InGaN solar cells . Additionally, the research highlights the potential of InGaN thin films with larger band gaps to match the solar spectrum effectively, paving the way for the design of more efficient multi-junction solar cells .

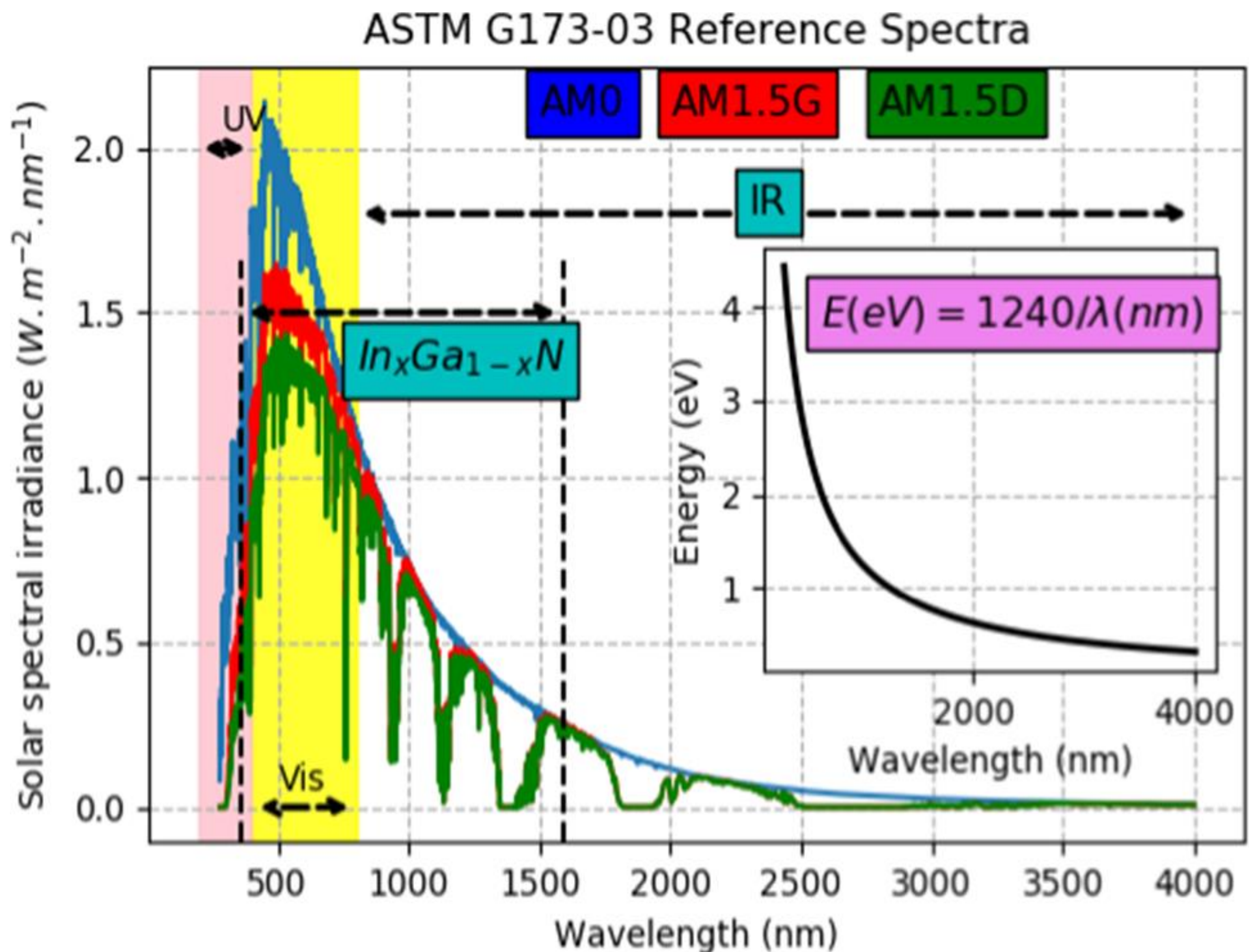

Figure II.3 : Correspondence between the solar spectrum AM_x and the $In_{(x)}Ga_{(1-x)}N$ gap [15].

The resulting absorption coefficient spectra as well as the wavelength-dependent refractive indices of GaN and $In_xGa_{1-x}N$ films used in the simulations are presented in **Figure II.4** [16] :

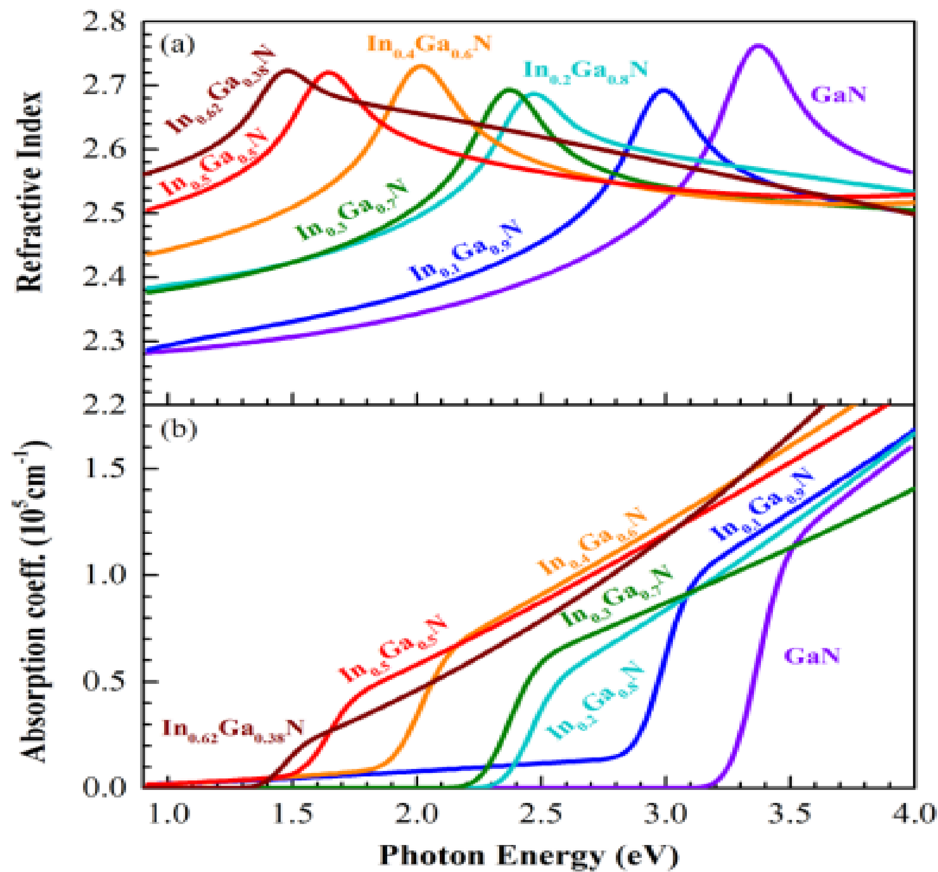

Figure II.4 : (a) Refractive index dispersion relations and (b) absorption coefficient spectra of GaN substrate and $In_xGa_{1-x}N$ films used in the simulations, as extracted from the ellispometric data analysis.[16].

II.3.2 Structural properties of group-III nitrides

II.3.2.1 Zinc Blende (GaN and InN structural parameters)

Zinc blende is the cubic crystals structure shown by zinc sulfide (ZnS). The structure has a diamond-like network. It is a thermodynamically more favoured structure than the other form of zinc sulfide. However, it can change its structure upon changing the temperature. For instance, zinc blende can become wurtzite if we change the temperature.
We can characterize the zinc blende as a cubic close-packed (CCP) and a facecentred

cubic structure. Also, this structure is denser than the wurtzite structure. However, when the temperature increases, the density tends to decrease; therefore, a conversion can take place from zinc blende to wurtzite. Besides, in this structure, the cations (zinc ions) occupy one of the two types of tetrahedral holes present in the structure, and it has four asymmetric units in its unit cell[16][17][18].

II.3.2.2 Wurtzite (GaN and InN structural parameters)

Wurtzite is the hexagonal crystal structure shown by zinc sulfide (ZnS). We call this crystal structure hexagonal close packing structure (HCP). We can characterize it by 12 ions in the corners of each unit cell, which creates a hexagonal prism structure.
However, this structure has low thermodynamic stability; thus, it slowly converts into a zinc blende structure. Also, this structure has the cations (zinc ions) occupying one of the two types of tetrahedral holes present in the structure, but it has two asymmetric units in its unit cell.

Table II.1: GaN and InN structural parameters[18].

lattice of InGaN	wurtzite (Hexagonal)			Zinc Blende(Cubic)
	a(A°)	c(A°)	U(A°)	a(A°)
GaN	3.189	5.185	0.377	4.47
InN	3.54	5.7	0.378	4.96

Nitride-based materials such as GaN, AlN and InN are widely used for optoelectronic applications. These materials can exist in wurtzite, zinc blende and rocksalt crystalline structures. In this chapter, we will focus only on the wurtzite structure properties because it is the most thermodynamically stable configuration that is usually grown by MOCVD (and in this thesis). Schematic of the wurtzite structure is presented in **Figure II. 5** [17][18].

$$\begin{cases} a\ A_xB_{1-x}N = x*a(AN) + (1-x)*a(BN) \\ c\ A_xB_{1-x}N = x*c(A) + (1-x)*c(BN) \end{cases} \quad (II.2)$$

$$\begin{cases} a\ In_xGa_{1-x}N = x*a(InN) + (1-x)*a(GaN) \\ c\ In_xGa_{1-x}N = x*c(In) + (1-x)*c(GaN) \end{cases} \quad (II.3)$$

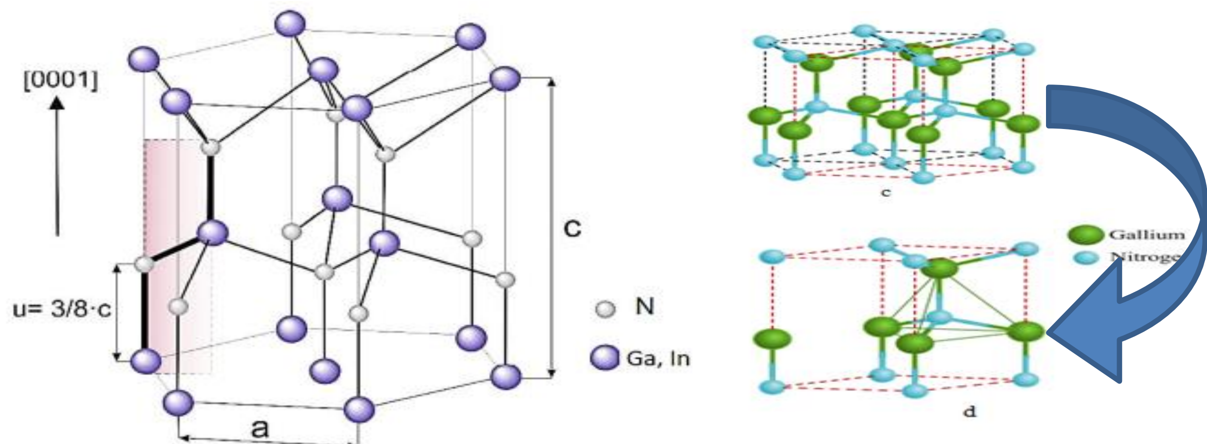

Figure II. 5: Schematic wurtzite lattice of InGaN material and ((c) Crystal structure of wurtzite. (d) Unit cell of the wurtzite structure. [17][18].

Table II.2: Difference Between Zinc Blende and Wurtzite[18].

	Zinc Blende	Wurtzite
Crystal System	Cubic	Hexagonal
Density	High	Low
Asymmetric Units	Has 4 asymmetric units	Has 2 asymmetric units
Stability	Thermodynamically more stable	Thermodynamically less stable

II.3.3 Effect of polarization

The presence of a spontaneous and piezoelectric polarization field is one of the original physical properties of III-N semiconductor compounds with a wurtzite structure, grown by epitaxy along the <0001> direction, which has consequences for electronic applications. The significance of total polarization in nitride compounds is of great interest compared to other III-V compound semiconductors such as GaAs[19].

II.3.3.1 Spontaneous Polarization

Considering the electronegativity possessed by nitrogen in relation to other elements of group V such as gallium and indium, it enables nitrogen to attract electrons more strongly in the Ga-N bond. The electron cloud will no longer be symmetrical, and the barycenter of the electric charges will no longer be located at the center of the two atoms (Ga, N). Such a bond is said to be polarized because it acts as if it has a positive pole and a negative pole. The gallium atom associated with the four neighboring nitrogen atoms forms dipoles illustrated in figure I-5 as follows [19]:

$$\sum_{i=1}^{i=4} \overrightarrow{P_i} = \overrightarrow{P_{sp}} \qquad (II.4)$$

There is the appearance of a succession of dipoles oriented in the <0001> direction and the creation of an electric field in the opposite direction to this polarization, the material thus has a polarization along the c-axis. At zero stress, there exists a spontaneous polarization Psp, as mentioned in Table I.2 [19].

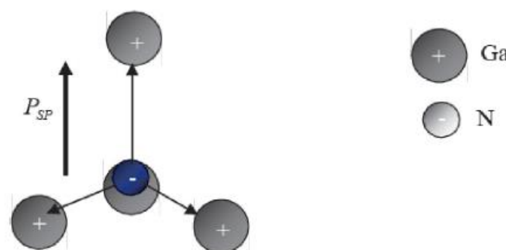

Figure II. 6: polarisation spontanée dans le GaN [19]

The crystalline structure of GaN has a symmetry along the c axis, resulting in the polarization gradient $\nabla\vec{p}=-\sigma=0$ and zero volume charge density. The numerical value of the spontaneous polarization of GaN, as well as some III-N elements, is reported in **Tableau II-3**

Tableau II-3 : Principales propriétés des III-N, à température ambiante (300K). [20]

Wurtzite	a (Å)	c (Å)	P_{sp} (C/m²)
GaN	3,189	5,185	-0,029
AlN	3,112	4,982	-0,081
InN	3,538	5,703	-0,032

A linear law representing the evolution of the spontaneous polarization of the $In_mGa_{1-m}N$ compound as a function of the aluminum content m can be established based on the values of the spontaneous polarization of InN and GaN[20] [22].

Psp(m)=(-0.052m-0.029) C/m².

$$\boxed{P_{sp}(In_xGa_{1-x}N)=x*P_{sp}(InN)+(1-x)*P_{sp}(GaN)-b*x*(1-x).}\quad Unité\ C/m^2 \qquad (II.5)$$

$$b=2P_{sp}(InN)+2P_{sp}(GaN)-4P_{sp}(In_{0.5}Ga_{0.5}N) \qquad (II.6)$$

II.3.3.2 Piezoelectric Polarization

Piezoelectricity is the ability of certain materials to produce an electric dipole proportional to the mechanical stress (tension or compression) that deforms them. **Figure II. 7** compares the properties of different semiconductors, including GaN, applying pressure to the nitride crystals, forcing the structure to accommodate the constraints by varying its lattice parameters, namely a0 and c0. This results in a variation of polarization that is not due to the variation of spontaneous polarization, since it always exists in the crystal and does not depend on any external effect, but rather to another type that will be called piezoelectric polarization. The value of this polarization will be calculated from the following formula $(II.7)$ [21] :

$$P_{pz}=\left(\frac{a(0)-a(m)}{a(m)}\right).\left(e_{31}(m)-\frac{e_{33}(m)C_{13}(m)}{C_{33}(m)}\right)\quad Unité\ C/m^2 \qquad (II.7)$$

With:
e_{31} and e_{33} : the piezoelectric constants.
C_{13} and C_{33} : the elastic constants.
a(0) and a(m) : the equilibrium and under constraint lateral lattice constants.

Tableau II-4 : Elastic and piezoelectric coefficients of the main III element nitrides compared to GaN. [20]

Wurtzite	C_{11} (GPa)	C_{13} (GPa)	C_{33} (GPa)	e_{31} (C/m^2)	e_{33} (C/m^2)
GaN	367	103	405	-0,49	0,73
AlN	396	108	373	-0,6	1,46
InN	223	92	224	-0,57	0,97

It should be noted that the coefficients e_{33}, C_{13}, and C_{33} are always positive, whereas e31 is negative: the term (e_1-e_{33} (C_{13}/C_{33}) will therefore be negative, resulting in the fact that for a biaxial tensile deformation of the crystal (GaN layers subjected to an extensive stress a>ao), the piezoelectric polarization is negative like the spontaneous polarization (**Figure II. 7**.a), and for a compression deformation, the piezoelectric polarization is positive contrary to the spontaneous polarization (**Figure II. 7**.b) [22].Contrainte en tension compression

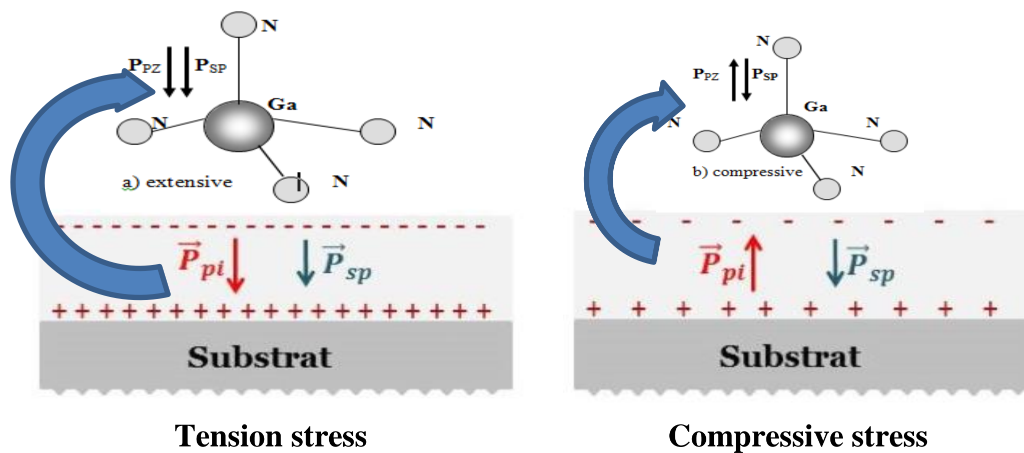

Figure II. 7: Piezoelectric polarization in GaN[22]

$$\vec{P}_{pz} = \begin{pmatrix} 0 & 0 & 0 & 0 & e_{15} & 0 \\ 0 & 0 & 0 & e_{15} & 0 & 0 \\ e_{31} & e_{31} & e_{33} & 0 & 0 & 0 \end{pmatrix} \times \begin{pmatrix} \varepsilon_{xx} \\ \varepsilon_{yy} \\ \varepsilon_{zz} \\ \varepsilon_{yz} \\ \varepsilon_{xz} \\ \varepsilon_{xy} \end{pmatrix}$$

$$\Leftrightarrow \left\{ \begin{array}{l} P_{pz} = e_{31}(\varepsilon_{xx} + \varepsilon_{yy}) + e_{33}\varepsilon_{zz} \\ \varepsilon_{xx} = \varepsilon_{yy} = (a(x) - a_0)/a_0. \\ \varepsilon_{zz} = (c(x) - c_0)/c_0 \end{array} \right. \Leftrightarrow \boxed{P_{pz} = 2\frac{(a(x) - a_0)}{a_0}\left(e_{31} - e_{33}\frac{c_{13}}{c_{33}}\right)} \qquad (II.8)$$ [19][21]

II.3.4 Thermal properties

The parameters for defining thermal properties are:

- **Thermal Dilation**: Any material subjected to a temperature change is deformed: this is the phenomenon of thermal dilation. This has to be taken into account when studying the properties of semiconductors at different temperatures, it was calculated by Krukowski et al [23], a $5.59.10^{-6}.K^{-1}$ for axis a and $4.47.10^{-6}.K^{-1}$ to axis c.
- **Debye temperature**: It characterizes the maximum value of vibration energies, it was calculated by Kim et al [24]. And another predicting it between 620 and 690 K.
- **Thermal conductivity**: Thermal conductivity is the kinetic property that is determined by the contributions of the degrees of electronic freedom: rotation and vibration. In semiconductors, due to low electron densities and conduction holes, the main contribution to heat transport comes from phonons. In a pure crystal, thermal conductivity is determined only by the process of diffusion of phonons. In a real crystal, it is also determined by the punctual defects. Of all thermal properties, thermal conductivity is most affected by structural defects, the value obtained by porowski et al [II.25], and 1.7 W.cm-1K-1 for impunity concentration of 10^{18} cm^{-3}.

II.3.5 Electronic properties

The many mechanical, thermodynamic, optical, electronic, structural, thermal and electrical properties of the GaN make this semiconductor an attractive element in several areas of use. In this paragraph, we will cite a set of properties that we find useful for our further study.

II.3.5.1 Band Gap

The GaN, like most III-V materials, has a direct banned broadband. The bandwidth was estimated at 3.4 eV at room temperature **Figure II. 8** [26]

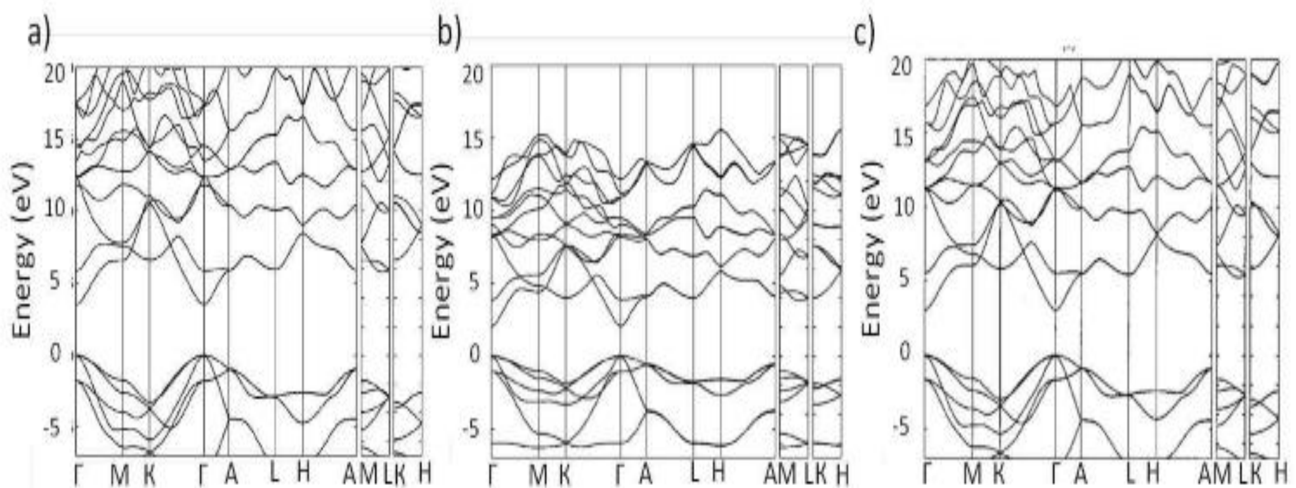

Figure II. 8 : Band structure of wurtzite phase a) GaN; b) InN and c) InGaN[26]

II.3.5.2Carrier mobility

Compared to GaAs and Si, SiC and GaN materials have lower electronic mobility: 800 and 1000 $cm^2 \cdot V^{-1} \cdot s^{-1}$, respectively. Nevertheless, the ability of III-nitrite materials to create a two-dimensional electron gas (2DEG) makes GaN very interesting for high-frequency and high-voltage applications. Indeed, HEMTs use heterogeneity to contain carriers in a potential well and create a two-dimensional channel without any need for GaN doping. In this way, the diffusion effects of the mobility of a doped material such as diffusion by ionized impurities are eliminated and mobility is significantly increased. This allows a HEMT AlGaN/GaN to have a mobility greater than 1200 $cm^2 \cdot V^{-1} \cdot s^{-1}$.

II-3-5-3 Dielectric rigidity

The field of a material is the maximum electrical field it can withstand. Is its value proportional to Eg 3/2, or Eg is the energy of gap [II.27]. It is measured at 3.106V/cm at 300K°. The GaN has a higher clutch range than the Si and Sic, making the round the most suitable for high voltage applications.

Tableau II-5 : Presents the electronic and thermal properties of several well-known semiconductors in comparison with GaNProperties at 300 K. [11]

Properties at 300 K	SI	GaAs	InP	4H-SiC	GaN	ALN	Diamant
Band Energy interdit E_g (eV)	1.12	1.43	1.35	3.25	3.43	6.0	5.45
Champ of claquage F_d (MV/cm)	0.3	0.4	0.45	3	3	12	10
Electron Saturation Rate V_s(*10^7cm/s)	1	1	1	2	1.75	1.5	2.7
Mobility of electrons $\mu_e\left(\times 10^{12} cm^2/Vs\right)$	1500	0.85	0.46	800	0.5	300	1800
Electron Density per Surface Unit $n_s\left(\times 10^{12} cm^{-2}\right)$	.	0.2	3	.	.	.	.
Thermal conductivity $\theta_\chi\left(w/cm.k\right)$	1.5	0.5	0.7	4.9	1.5	2	22

II.4 State-of-the-art of InGaN-based solar cells :

The proposal to use InGaN alloys for solar cell application has been done in 2003 by Wu et al. But the first announcement about a InGaN-based device has been published only two years later. Different structure designs were verified to optimize photovoltaic properties of InGaN solar cells. Generally, all proposed structures can be divided on two main groups that are discussed in this sub-section: homojunctions and heterojunctions.

II.4.1 Homojunctions

A homojunction is a type of semiconductor junction where both sides of the junction are made of the same material. In other words, it is a junction formed between two regions of the same semiconductor material but with different doping levels. This type of junction is commonly used in semiconductor devices such as diodes and transistors. The homojunction allows for the easy formation of a pn-junction, which is important for the operation of many semiconductor devices[28].
examples of semiconductor devices that utilize homojunctions:

Bipolar Junction Transistors (BJTs): In a BJT, the emitter-base and base-collector junctions are often homojunctions. These junctions are crucial for the operation of the BJT as they control the flow of current in the device.

Diodes: Many types of diodes, such as p-n junction diodes, Schottky diodes, and tunnel diodes, utilize homojunctions at their core for rectification and signal processing purposes.

Photodiodes: Photodiodes are semiconductor devices that convert light into electrical current. They often consist of a homojunction that generates electron-hole pairs when exposed to light.

Solar Cells: Solar cells, also known as photovoltaic cells, convert sunlight into electricity. Most solar cells are made using homojunctions or heterojunctions to improve the efficiency of converting light into electrical energy.

Integrated Circuits (ICs): ICs consist of interconnected semiconductor components, including transistors and diodes, that are often built using homojunction technology at their core.

These are just a few examples of semiconductor devices that make use of homojunctions. Homojunctions play a vital role in the functionality and performance of various semiconductor devices in modern electronics.

The performance of p-InGaN/P-InGaN/n-InGaN homojunctions can be significantly affected by the introduction of a P-InGaN layer. Here are some ways in which the P-InGaN layer can impact the performance:

1. Improved hole injection: The P-InGaN layer can facilitate efficient injection of holes into the active region of the device, which can enhance the overall carrier distribution and improve device performance.

2. Reduction of polarization effects: The introduction of a P-InGaN layer can help reduce the effects of built-in electric fields due to polarization mismatch at the heterointerfaces, which can improve the device's efficiency and operational stability.

3. Enhanced carrier confinement: The P-InGaN layer can help confine carriers within the active region of the device, leading to improved recombination efficiency .
Certainly! Here are some examples of semiconductor devices that utilize homojunctions[28].
.

II.4.2 Heterojunctions or Multi-junction cells

Multi-junction cells, particularly those based on III-V compound materials, offer a promising avenue for achieving high-efficiency solar cells beyond the limitations of single-junction cells approaching the Shockley-Queisser limit . By stacking semiconductor materials with different bandgaps, multi-junction cells can efficiently absorb various portions of the solar spectrum, leading to impressive conversion efficiencies. These cells have demonstrated record efficiencies of up to 47.1% under concentration, showcasing their potential for high power generation per unit cost . Additionally, advancements in multi-junction cell technologies, such as integrating nanoantenna arrays to concentrate electromagnetic radiation and improve current generation, further enhance the efficiency and performance of these cells . Overall, multi-junction cells represent a significant advancement in photovoltaic technology, offering a pathway towards cleaner and more efficient energy production[29].

Semiconductor power devices like InGaN and GaN exhibit essential material characteristics crucial for power electronics applications. GaN, a wide bandgap semiconductor, possesses high electron saturation velocity, a large critical field, and excellent thermal stability, making it ideal for high-power microwave frequencies [29]. GaN devices benefit from a two-dimensional electron gas (2DEG) generated by spontaneous and piezoelectric polarization effects in GaN heterostructures, leading to high sheet charge density essential for high power handling capabilities . In contrast, InGaN, a III-V compound semiconductor, offers large bandwidth, high thermal conductivity, and fast electron saturation rates, making it suitable for high-frequency and high-power electronic devices . The integration of these materials in power converters is crucial for enhancing performance beyond the limitations of traditional Silicon-based switches [30].

II.4.3 Generation of solar cells

. Photovoltaic cells can be categorized by four main generations: first, second, third, and fourth generation. The details of each are discussed in the next section[31]

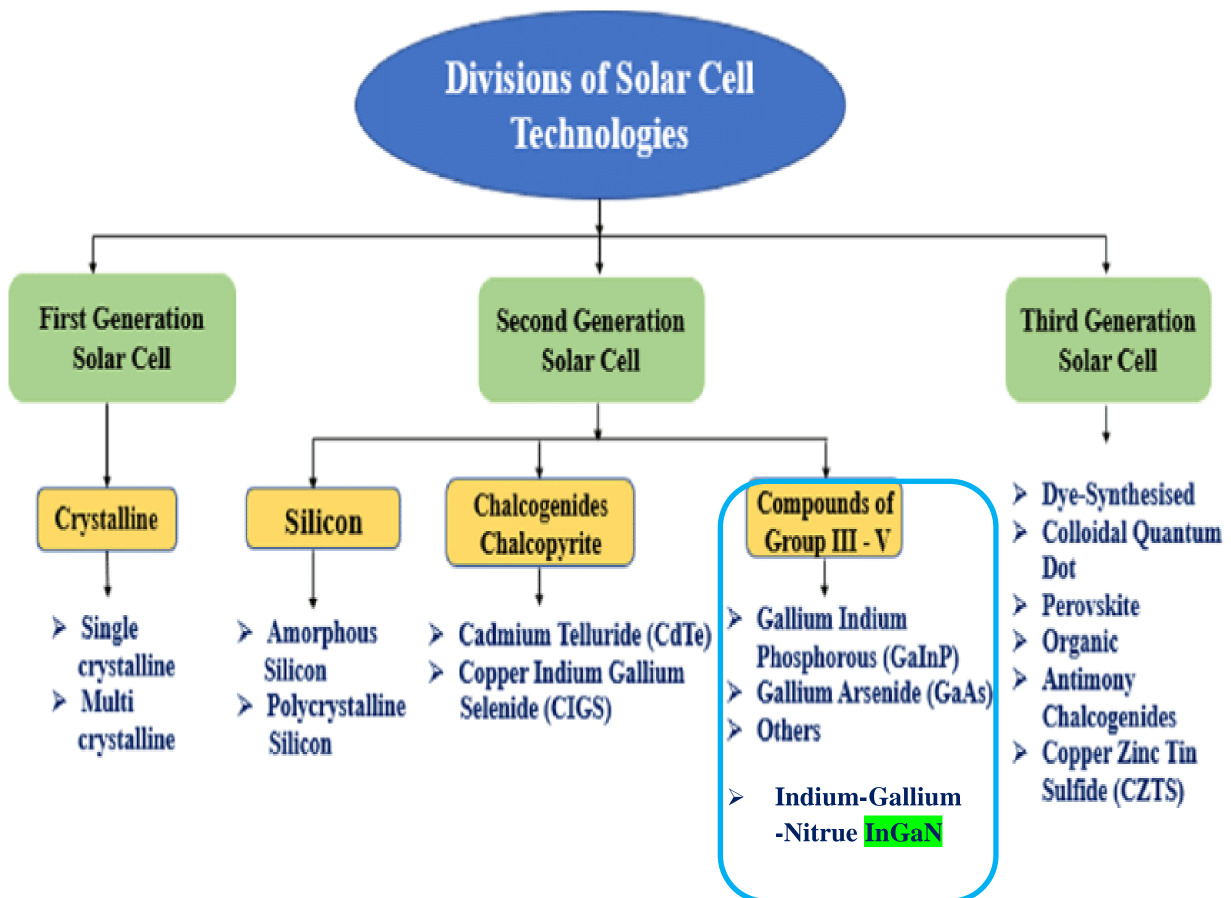

Figure II. 9 : Generation of solar cells InGaN[31]

II.4.4 Advantages, challenges, and strategies of InGaN-based solar cells

II.4.4.1 Advantages of InGaN-based Solar Cells[32].

1. **Wide Bandgap:** Indium Gallium Nitride (InGaN) has a wide bandgap, which allows for the absorption of a large portion of the solar spectrum, including the ultraviolet and visible regions.

2. **High Absorption Coefficient:** InGaN materials have a high absorption coefficient, enabling efficient absorption of sunlight with a relatively thin absorber layer.

3. **Tunability:** The bandgap of InGaN can be tuned by adjusting the indium composition, allowing for optimization of the absorption spectrum for solar energy conversion.

4. **High Carrier Mobility:** InGaN materials exhibit high carrier mobility, enabling efficient charge transport within the solar cell structure.

5. Temperature Stability: InGaN-based solar cells can exhibit good temperature stability, maintaining performance under varying environmental conditions.

II.4.4.2 Challenges of InGaN-based Solar Cells

1. **Heterostructure Growth:** Growing high-quality InGaN heterostructures with precise control over composition and defect density is challenging, affecting the performance and reliability of the solar cells.

2. **Carrier Recombination**: InGaN materials are prone to carrier recombination processes, reducing the efficiency of charge extraction and affecting overall device performance.

3. **Material Compatibility**: Integrating InGaN with other materials in the solar cell structure can pose challenges due to differences in lattice constants and thermal expansion coefficients.

4. **Surface Morphology**: Achieving smooth and defect-free surfaces in InGaN layers is crucial for device performance, but it can be challenging during the growth process[32]..

II.4.4.3 Strategies for Enhancing InGaN-based Solar Cells

1. **Optimized Growth Techniques**: Implementing advanced growth techniques such as molecular beam epitaxy (MBE) or metal-organic chemical vapor deposition (MOCVD) can improve the quality of InGaN layers and heterostructures.

2. **Surface Passivation**: Employing surface passivation techniques to reduce surface recombination and improve the overall quality of InGaN-based solar cells.

3. **Incorporation of Nanostructures**: Integration of nanostructures like quantum dots or nanowires in InGaN solar cells can enhance light absorption and charge carrier extraction.

4. **Band Engineering**: Tailoring the band structure of InGaN-based solar cells through alloy composition engineering and bandgap grading to improve carrier collection and reduce recombination losses.

5. **Improved Contact Layers**: Designing efficient transparent conductive oxide (TCO) and metal contact layers to enhance light transmission and improve charge carrier extraction efficiency.

By addressing these challenges and implementing strategic approaches to enhance the performance of InGaN-based solar cells, researchers aim to harness the unique advantages of InGaN materials for efficient and cost-effective solar energy conversion applications[32] **Figure II. 10.**.

Figure II. 10 : Advantages, challenges, and strategies of InGaN-based solar cells [32].

II.5 conclusion

In this second chapter, we present a study of the structural and electrical properties of indium gallium nitride (InGaN). InGaN is an ideal candidate for the manufacture of high-performance photovoltaic solar cells, particularly for high-temperature applications. We have also presented its equivalent circuit and the state of the art of InGaN-based PV cells shows that this material has significant advantages for the realization of high-efficiency solar cells.

The following chapter III will focus on the simulation of single-junction PN and PPN structures, with the influence of p-InGaN layer thickness and doping concentrations on the photovoltaic parameters of InGaN-based solar cells.

REFERENCES

[1] **El-Huni, Walid, et al.** "High-efficiency indium gallium nitride/Si tandem photovoltaic solar cells modeling using indium gallium nitride semibulk material: monolithic integration versus 4-terminal tandem cells." Progress in Photovoltaics: Research and Applications 24.11 (2016): 1436-1447.

[2] **Wu, J., et al.** "Superior radiation resistance of In 1− x Ga x N alloys: Full-solar-spectrum photovoltaic material system." Journal of Applied Physics 94.10 (2003): 6477-6482.

[3] **BOUDAOUD chahrazad**, thèse doctorat en sciences spécialité: energies renouvelables sur le thème cellules solaires tandem à base d'ingan, pour haut rendement : modélisation et simulation des performances 13/ 03/ 2021 à universite abou-bekr belkaid - tlemcen

[4] **Mostefaoui, M. A**. Contribution à l'amélioration des performances des cellules solaires à base de InGaN (Doctoral dissertation).

[5] **OMAR SOUILAH, THESE DE DOCTORAT (2020-2021),** Contribution à la modélisation d'une cellulephotovoltaïque multijonction à la base de InGaN

[6] **Alessandro, Caria., M., Nicoletto., Carlo, De, Santi., Matteo, Buffolo., Xu, Chu, Huang., Houqiang, Fu., Hong, Chen., Yuji, Zhao., Gaudenzio, Meneghesso., Enrico, Zanoni., Matteo, Meneghini. (2022).** Quantum efficiency of InGaN–GaN multi-quantum well solar cells: Experimental characterization and modeling. Journal of Applied Physics, doi: 10.1063/5.0076833

[7] **F., Bouzid., Fortunato, Pezzimenti., Lakhdar, Dehimi. (2020).** Modelling and performance analysis of a GaN-based n/p junction betavoltaic cell. Nuclear Instruments & Methods in Physics Research Section A-accelerators Spectrometers Detectors and Associated Equipment, doi: 10.1016/J.NIMA.**2020**.164103

[8] **Marc Burgelman Koen Decock, Alex Niemegeers, Johan Verschraegen, Stefaan Degrave** Version: 23 january 2018 .SCAPS manual

[9] **S. O'Leary, B. Foutz, M. Shur, and L. Eastman**, "The sensitivity of the electron transport within bulk wurtzite indium nitride to variations in the crystal temperature, the doping concentration, and the non-parabolicity coefficient: an updated Monte Carlo analysis," Journal of Materials Science: Materials in Electronics, vol. 21, pp. 218-230, 2010.

[10] **Yacine MAROUF**, Magister en Electronique **2013** Modélisation des cellules solaires en InGaN en utilisant Atlas Silvaco

[11] **N. Grandjean** « Composants optiques à base de GaN », CNRS-CRHEA, Sophia Antipolis, 2002.

[12] Ting, Wang., Guankong, Mo., Hongli, Zhao., Juan, Yao., Zhuoliang, Zou., Yuechun, Fu., Xiaoming, Shen., Huan, He. **(2021).** Growth of Amorphous InGaN Films on Si for Potential Photovoltaic Application. Journal of Electrical Engineering & Technology, doi: 10.1007/S42835-021-00939-7

[13] **(2022). Simulation Result of InGaN for Solar Cell Application. doi: 10.1149/osf.io/kb726**

[14] **Dennai, Benmoussa., Ben, Slimane, Hassane., Helmaoui, Abderrachid. (2013). Simulation of In 0.52 Ga 0.48 N solar cell using AMPS-1D. doi: 10.1109/IRSEC.2013.6529713**

[15] **Pearton, S.J.; Ren, F.; Tadjer, M.; Kim, J. Perspective**: Ga2O3 for ultra-high power rectifiers and MOSFETS. J. Appl. Phys. 2018, 124, 220901. [Google Scholar] [CrossRef] [Green Version]

[16] **Kazazis, S. A., Papadomanolaki, E., & Iliopoulos, E**. (2017). Polarization-Engineered InGaN/GaN Heterojunctions for Photovoltaic Applications.

[17] V. Prasad, Electrical properties of n-GaN based MOS type schottky junctions, Sri Venkateswara university, 2021.

[18] **ANDER UDABE , IGOR BARAIA-ETXABURU , AND DAVID GARRIDO DIEZ**Electronics and Computer Science Department, University of Mondragon, Arrasate, 20500 Mondragon, SpainReceived 25 **April 2023**, accepted 13 May 2023, date of publication 17 May 2023, date of current version **24 May 2023**. DIO 10.1109/ACCESS.2023.3277200

[19] **N. VELLAS**, «Etudes Expérimentales de Transistors HFET de La Filière De nitrure Galium Verser Des Applications De Puissance hyperfréquences », Thèse de doctorat le 18 Décembre soutenue 2003, Université de lille

[20] **N. Grandjean** « Composants optiques à base de GaN », CNRS-CRHEA, Sophia Antipolis, 2002.

[21] S. O'Leary, B. Foutz, M. Shur, and L. Eastman, "The sensitivity of the electron transport within bulk wurtzite indium nitride to variations in the crystal temperature, the doping concentration, and the non-parabolicity coefficient: an updated Monte Carlo analysis," Journal of Materials Science: Materials in Electronics, vol. 21, pp. 218-230, 2010.

[22] **Abdoulwahab ADAINE, DOCTEUR** DE L'UNIVERSITE DE LORRAINE, 2018 préparée au sein du, Laboratoire Matériaux, Optiques, Photonique et Systémes - EA 4423, Université de Lorraine et CentraleSupélec, (Optimisation numérique de cellules solaires a trés haut rendementa base d'InGaN)

[23] **S. Krukowski, M. Leszczynski and S. Porowski** « Thermal properties of the group III Nitrides », **publication INSPEC**, Datareview series n°23 (1998), p. 21-28.

[24] **K. Kim, R. L. Lambrecht and B. Segall** « Elastic constants and related properties of tetrahedrally

bonded BN, AlN, GaN and InN », Phys. Rev. B, Vol. 53 (1996), p. 1631016326.

[25] **S. Porowski and I. Grzegory** « Thermodynamical properties of III–V nitrides and crystal growth of GaN at high N2 pressure », J. Cryst. Growth, 1-2, Vol. 178 (1997), p. 174-188.

[26] **Goano, M., Bellotti, E., Ghillino, E., Ghione, G., & Brennan, K. F. (2000).** Band structure nonlocal pseudopotential calculation of the III-nitride wurtzite phase materials system. Part I. Binary compounds GaN, AlN, and InN. Journal of Applied Physics, 88(11), 6467–6475**.** https://doi.org/10.1063/1.1309046

[27] **D., Parajuli., Deb, Kumar, Shah., Devendra, Kc., Subhash, Kumar., Mi, Na, Park., B., Pant. (2022).** Influence of Doping Concentration and Thickness of Regions on the Performance of InGaN Single Junction-Based Solar Cells: A Simulation Approach. Electrochem, doi: 10.3390/electrochem3030028

[28] **Subba Ramaiah Kodigala,**Chapter 1 - Introduction,Editor(s): Subba Ramaiah Kodigala,Thin Films and Nanostructures,Academic Press,Volume 35,2010,Pages 1-19,ISS1543-506,ISBN 9780123736970,https://doi.org/10.1016/B978-0-12-373697-0.00001-8. (https://www.sciencedirect.com/science/article/pii/B9780123736970000018)

[29] **Arie, Adriaensen**. **(2023)**. Basic characteristics of GaN devices. doi: 10.1016/b978-0-12-821204-2.00002-7

[30] **João, P., de, Melo, Cunha., Ricardo, A., Marques, Lameirinhas., João, Paulo, N., Torres. (2022).** Multi-Junction Solar Cells and Nanoantennas. Nanomaterials, doi: 10.3390/nano12183173

[II.29] **Masafumi, Yamaguchi., Frank, Dimroth., Nicholas, J., Ekins-Daukes., Nobuaki, Kojima., Yoshio, Ohshita. (2022).** Overview and loss analysis of III–V single-junction and multi-junction solar cells. EPJ Photovoltaics, doi: 10.1051/epjpv/2022020

[30] **D., Parajuli., Viplav, Bhandari., Devendra, K.C.., Ajita, Thapaliya., Amrit, Subedi., Amrit, Dhakal., Sandip, Dangi., Rabina, Koirala., Manish, Bhatta. (2023).** Numerical Approach of Single-Junction InGaN Solar Cell Affected by Carrier Lifetime and Temperature. doi: 10.3126/pdmdj.v5i1.52309

[31] **Karthikeyan Vijayan, S.P. Vijayachamundeeswari, Kalainathan Sivaperuman, Nazmul Ahsan, Thirumalaisamy Logu, Yoshitaka Okada,**A review on advancements, challenges, and prospective of copper and non-copper based thin-film solar cells using facile spray pyrolysistechnique, Solar Energy,Volume 234**, 2022,** Pages 81-102, ISSN 0038-092X, https://doi.org/10.1016/j.solener.2022.01.070. (https://www.sciencedirect.com/science/article/pii/S0038092X22000810)

[32] **Zhao, Y., Xu, M., Huang, X., Lebeau, J., Li, T., Wang, D., Fu, H., Fu, K., Wang, X., Lin, J., & Jiang, H. (2022).** Toward High Efficiency at High Temperatures: Recent Progress and Prospects on InGaN-Based Solar Cells. In Department of Electrical and Computer Engineering, Rice University, Houston, TX 77005, USA. https://www.sciencedirect.com/science/article/pii/S2468606922002878

Chapitre III

Simulation of a Single Junction p-InGaN/n-InGaN (Results and Discussion)

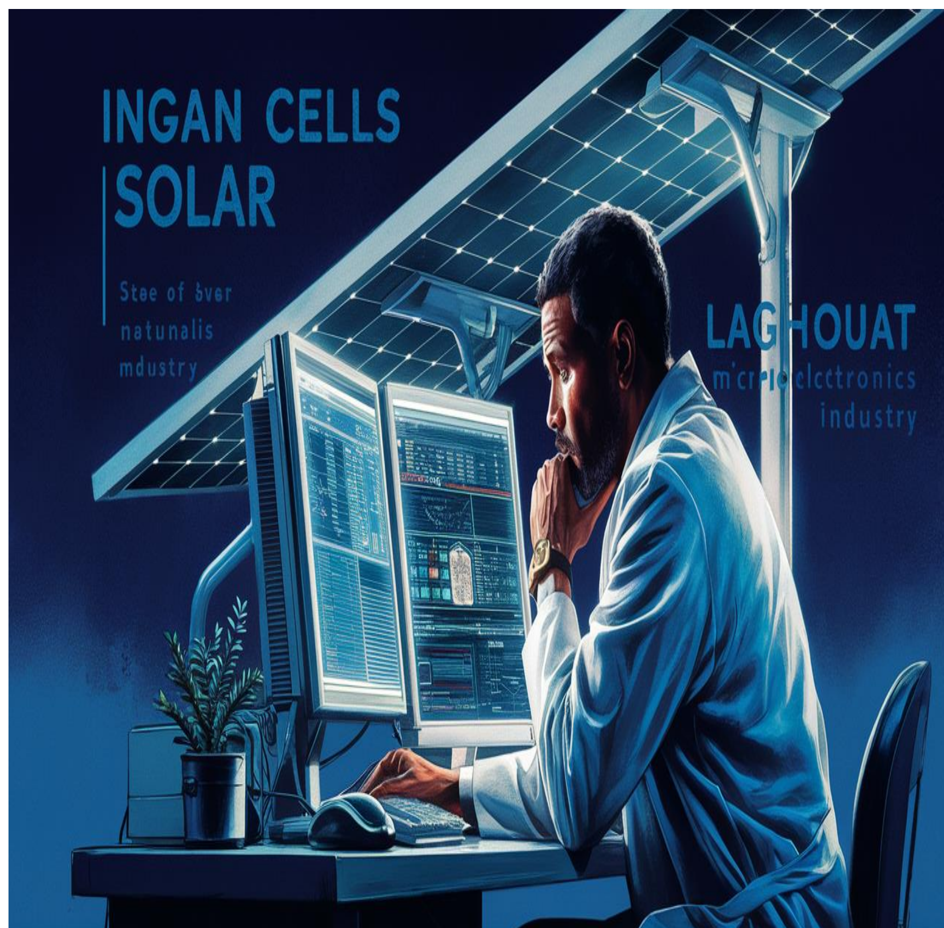

III.1 Introduction

This chapter consists of two main parts, the first part gives a detailed description of the Solar Cell Capacitance Simulator (SCAPS-1D) which is used to simulate the solar cell performances based on p-InGaN/n-InGaN Single Junction. The second part describes the PN and PPN junction solar cells structures , some physical parameters such as thickness and doping concentration concerning both junction used in this study. This part also presents and discusses some results obtained using the Scaps 1D program.

III.2 Description of the SCAPS 1D Simulator [1]

In order to simulate and control all the parameters of a photovoltaic device using SCAPS software, we need to go through three main windows:

- Execution window « action panel » ;

- Device design and problem definition window « Definition panel » ;

- Results window.

a). Main menu « Action panel »

After launching the software and opening the run window (Figure III.1), you can modify the following parameters: temperature, series and parallel resistance, and illumination parameters. At any time, you can access the other two windows, the device design window and the results window, as shown in the figures below.

b) Structure selection

When you click on the « SET PROBLEM » button on the action panel, the « SOLAR DEFFINITION « panel appears. This allows you to create or modify solar cell structures and save or load them from other files (Figure III. 2).

There are dedicated panels for the basic actions:

1. Run SCAPS:

1. Run SCAPS .
2. Define the problem, thus the geometry, the materials, all properties of your solar cell
3. Indicate the circumstances in which you want to do the simulation, i.e. specify the working point
4. Indicate what you will calculate, i.e. which measurement you will simulate.
5. Start the calculation(s)
6. Display the simulated curves.

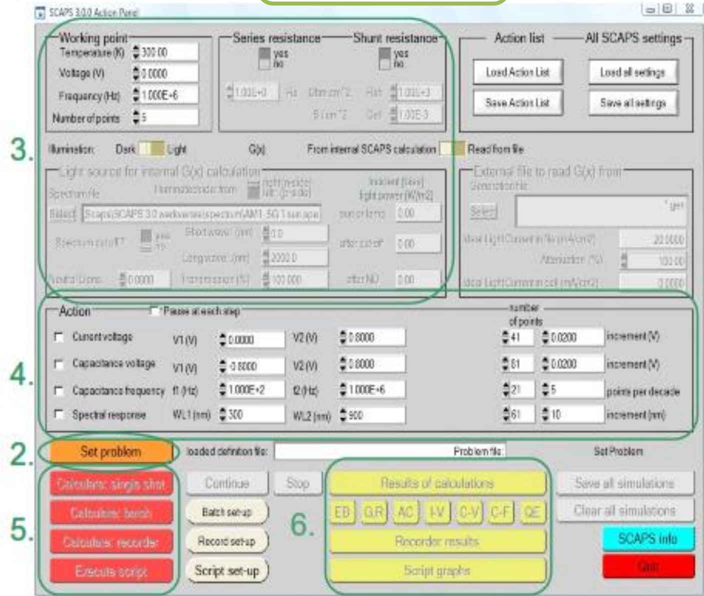

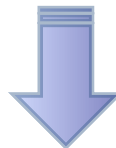

1. Run SCAPS :

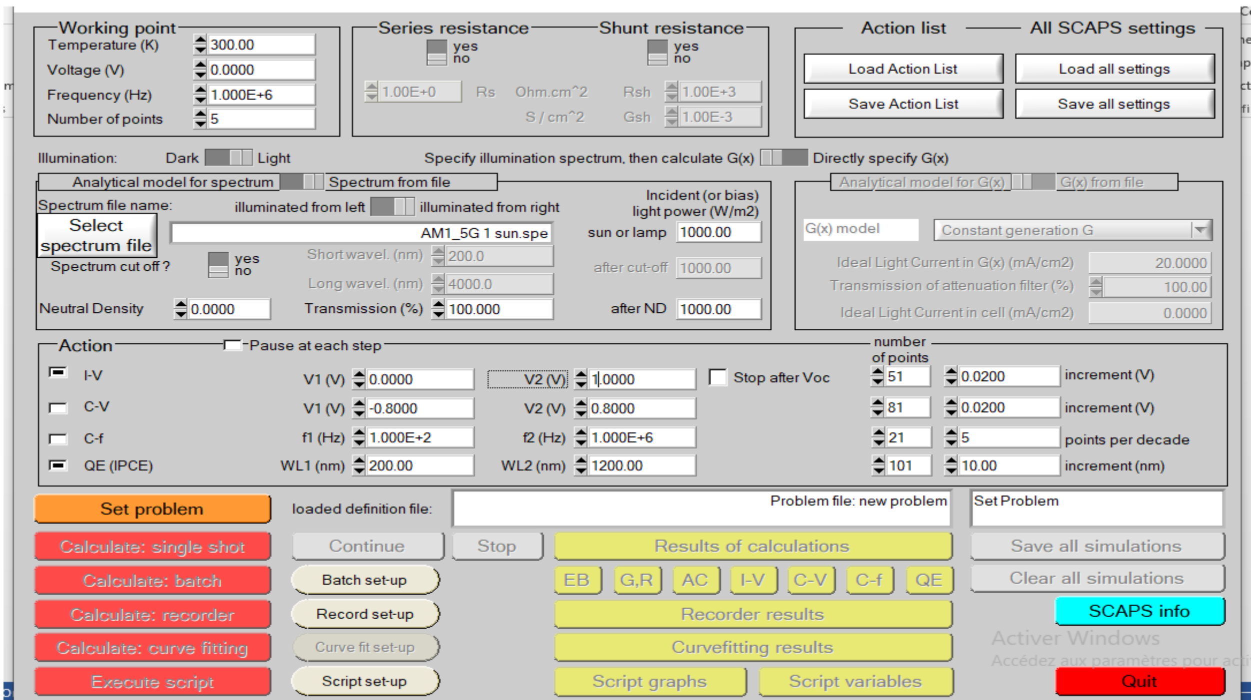

Figure III.1: SCAPS startup panel, the action or main panel

2. Define the problem, thus the geometry, the materials, all properties of your solar cell

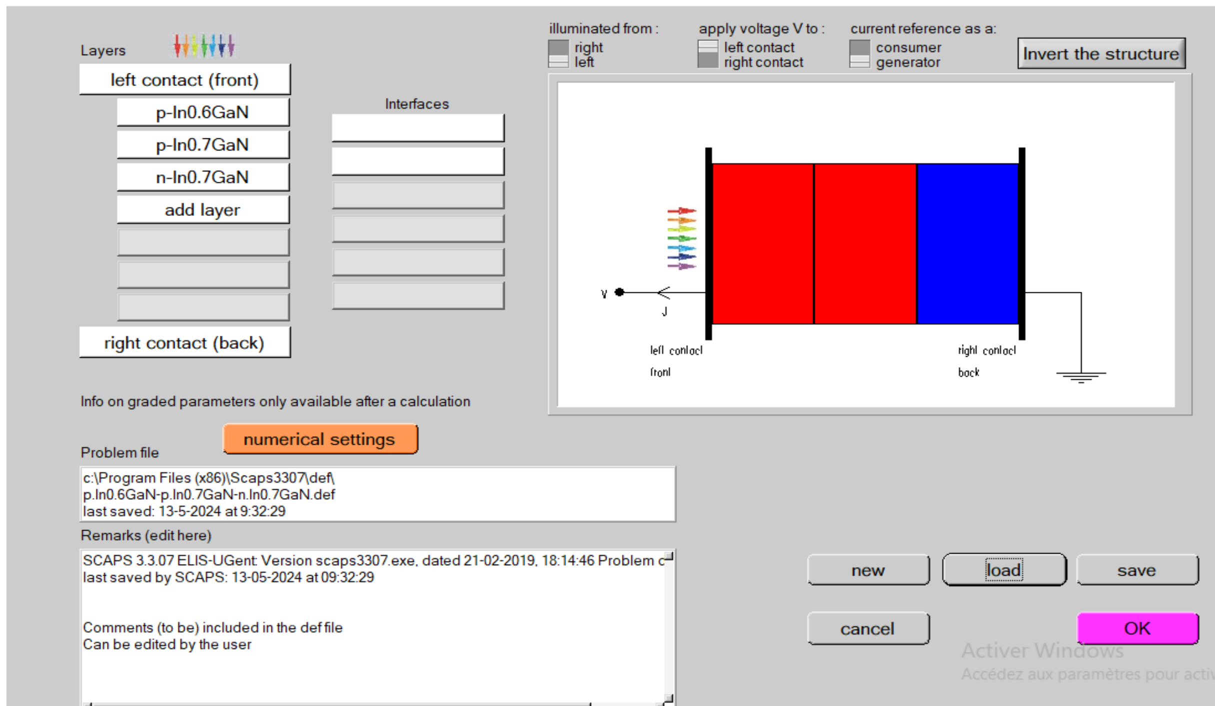

Figure III.2: Definition of a solar cell structure.

c). Layer properties

The window shown in Figure. III.3 contains several parameters such as gap energy, electrical permittivity, affinity, doping and doping type. It should be noted that the user can directly use standard values in the software's data files.

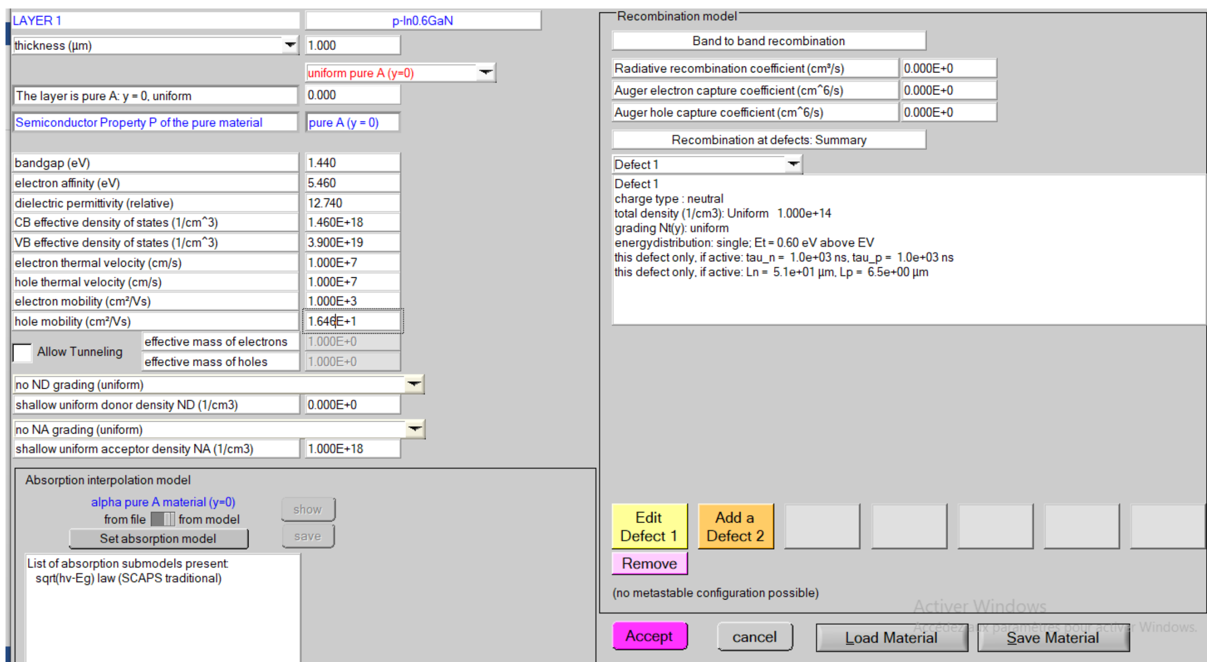

Figure III.3: Parameters of a p-$In_{0.60}Ga_{0.40}N$ cell layer.

d). Simulation results « Characteristic I(V) »

Run the « Calculate » simulation, note the simulation results (J_{sc} ,V_{oc} ,FF, η) in the « I-V panel » window, the I-V characteristic....These results can be displayed and copied as a table by pressing « show » (figure III.4).

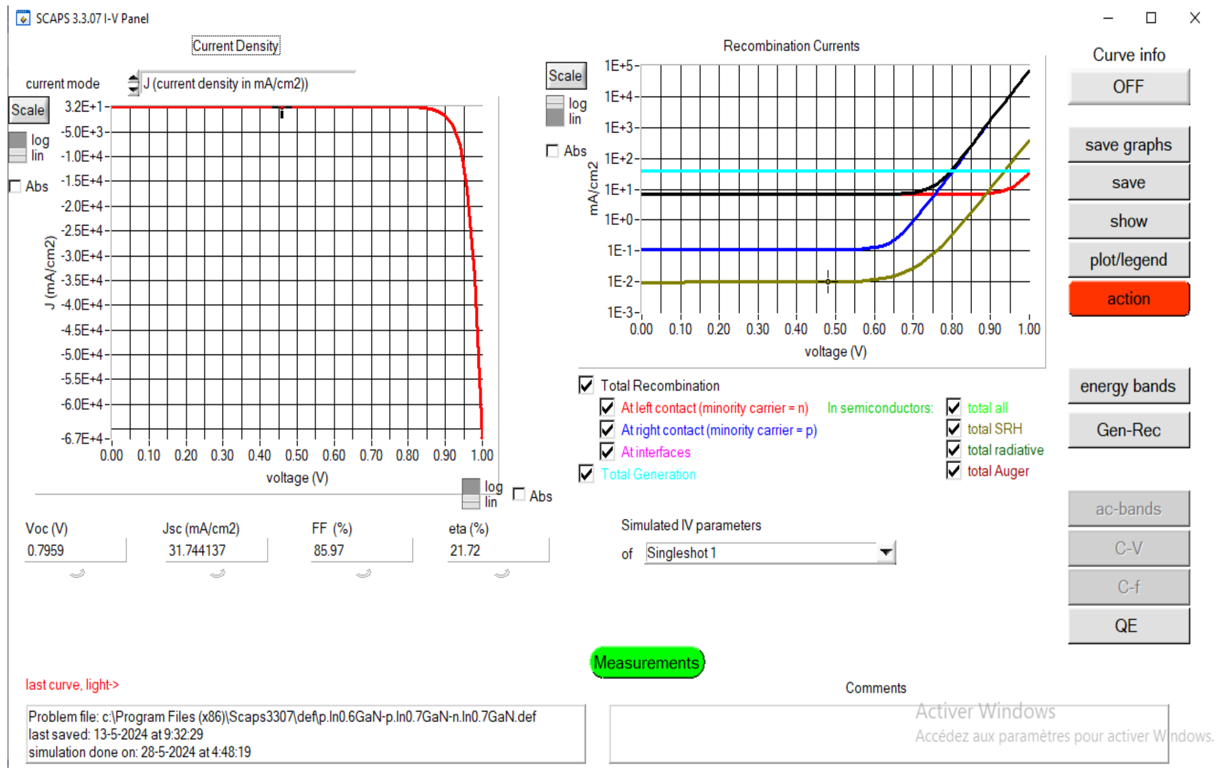

Figure III.4: Display panel for I-V curves

III.3 Structure of a PN and PPN-junction

The structure chosen for our study is an InGaN-based solar cell, one having a PN structure : p-$In_{0.70}Ga_{0.30}N$/ n-$In_{0.70}Ga_{0.30}N$ single junction and the other is PPN cell: p-$In_{0.60}Ga_{0.40}N$/ p-$In_{0.70}Ga_{0.30}N$/ n-$In_{0.70}Ga_{0.30}N$, as schematized in figure III.5. Where the top layer is quasi-transparent, to allow radiation absorption in the p region.

In order to obtain a high efficiency, we will use an indium concentration of 60% and 70%. The PPN-InGaN solar cell was created with indium composition ranging from 60% to 70% (x = 0.6–0.7) because most reports in the literature suggested that the best efficiency can be achieved using these indium compositions [2,3]. For comparison, a PN-junction $In_{0.70}Ga_{0.30}N$ solar cell was also simulated (Figure III.5).

The In_xGa_{1-x} N material system is a ternary system where it's electrical and optical parameters are determined by the composition ratio of In and Ga. The $In_xGa_{1-x}N$ absorption coefficient [4], $\alpha(E)$, is a function of energy and band gap as a function of indium composition can be expressed, respectively [5]:

$$\alpha(E)=\alpha_0\sqrt{\frac{E-E_g(x)}{E_g(x)}} \qquad (III.1)$$

$$E_g\left(In_xGa_{1-x}N\right)=x*E_g(InN)+x(1-x)*E_g(GaN)-b*x*(1-x) \qquad (III.2)$$

where $Eg(x)$ is the band gap of $In_xGa_{1-x}N$, E is the energy of photons and α0 for GaN is approximately 2×10^5 cm^{-1}. The α_0 of the $In_xGa_{1-x}N$ is assumed to be the same as that of GaN. Eg (InN) is equal to 0.7eV, Eg (GaN) is equal to 3.4eV and b is the bowing parameter, which account for the non-linear fit of band gap energies, and is equal to 1.43eV [6].

To obtain the electron mobility in the alloy, we used the concentration-dependent formula below [7].

$$\mu_i(N)=\mu_{\min,i}+\frac{\mu_{\max,i}-\mu_{\min,i}}{1+\left(N/N_{g,i}\right)^{y_i}} \qquad (III.3)$$

i represents electrons or holes, N and Ng represent the doping concentration and critical doping of the material respectively, and y is a constant.

In order to calculate the mobility of the material, we have grouped together in the table below the various values taken from the literature for the different parameters of GaN and InN [1].

Table III.1: Difference Parameters Between GaN and InN [1,2].

Parameters	*GaN*	*InN*
$\mu_{min,e}$ $(cm^2/V.s)$	55	30
$\mu_{max,e}$ $(cm^2/V.s)$	1000	1100
y_e [s d]	1	1
$N_{g,e}$ (cm^{-3})	2.10^{17}	8.10^{18}
$\mu_{min,h}$ $(cm^2/V.s)$	3	3
$\mu_{max,h}$ $(cm^2/V.s)$	170	340
y_h [s d]	2	2
$N_{g,h}$ (cm^{-3})	3.10^{17}	3.10^{17}

All the InxGa1-xN parameters used for the simulation are listed below

- Relative permittivity [8 , 9]:

$$\varepsilon\left(In_xGa_{1-x}N\right)=x*\varepsilon\left(InN\right)+\left(1-x\right)*\varepsilon\left(GaN\right)=14.6*x+10.4*(1-x) \qquad (III.4)$$

- No. of state in conduction band [8,9]:

$$N_C\left(In_xGa_{1-x}N\right)=x*N_C\left(InN\right)+\left(1-x\right)*N_C\left(GaN\right)=\left(0.9*x+2.3*\left(1-x\right)\right)*10^{18}cm^{-3} \qquad (III.5)$$

- No. of state in valence band [8,9]:

$$N_V\left(In_xGa_{1-x}N\right)=x*N_V\left(InN\right)+\left(1-x\right)*N_V\left(GaN\right)=\left(5.3*x+1.8*\left(1-x\right)\right)*10^{19}cm^{-3} \qquad (III.6)$$

- Electron affinity [8,9]:

$$\chi=\chi\left(GaN\right)+0.7\left(3.4-Eg\right)=4.1+0.7\left(3.4-Eg\right)\left(eV\right) \qquad (III.7)$$

III.3.1 Solar cell structure

Figure III.5 depicts the schematic structure of the p- $In_{0.65}Ga_{0.35}N$ /n- $In_{0.65}Ga_{0.35}N$ PN single-junction solar cell and p-$In_{0.60}Ga_{0.40}N$/ p-$In_{0.70}Ga_{0.30}N$/ n-$In_{0.70}Ga_{0.30}N$ PPN junction under investigation. In our structures, dp and dn of the PN junction and dp_1,dp_2 and dn2 of the PPN junction represents the thicknesses, respectively. The solar cells receive sun radiation AM 1.5G lighting with an irradiation intensity of 1000 W/m^2.

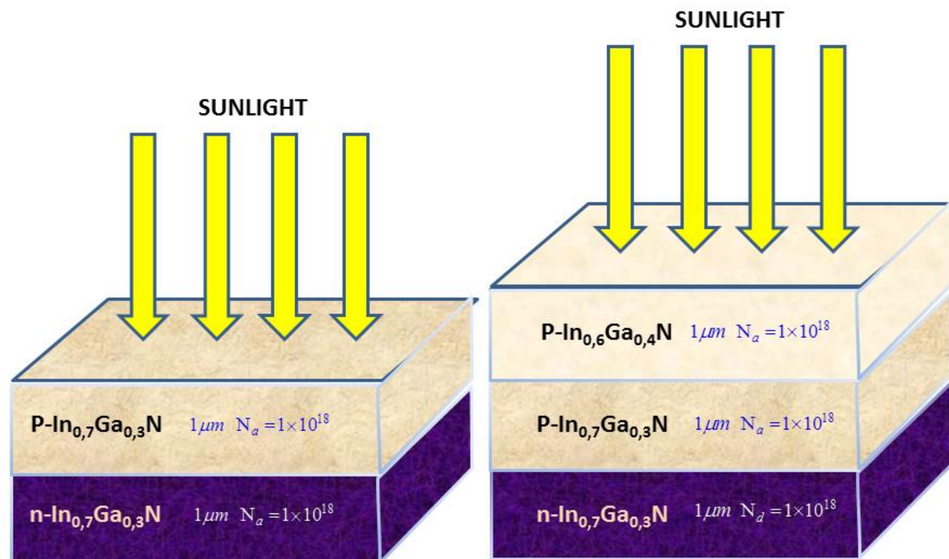

Figure. III.5 Structure of a PN-junction (left) and a PPN-junction (right) InGaN solar cell.

The physical and geometric parameters of each layer of InGaN are given in the Table1 below [10]:

Table III.2 : Simulation parameters for the InGaN materials in the PN and PPN junction InGaN solar cells. [10]

Parameters	**Value**	
	$In_{0.7}Ga_{0.30}N$	**$In_{0.6}Ga_{0.40}N$**
Bandgap, Eg (eV)	1.21	1.44
Electron affinity, χ (eV)	5.2	5.46
Relative permittivity,ε	13.38	12.74
Effective density state of the conduction band Nc (cm^{-3})	1.32×10^{18}	1.46×10^{18}
Effective density state of the valence band Nv (cm^{-3})	4.25×10^{19}	3.90×10^{19}
Carrier concentration (cm^{-3}) for n and p layers	1×10^{18}	1×10^{18}
Capture cross section electrons (cm^{2})	1.0×10^{-15}	1.0×10^{-15}
Capture cross section holes (cm^{2})	1.0×10^{-15}	1.0×10^{-15}
Defect density (cm^{-3})	1.0×10^{-14}	1.0×10^{-14}

III.3.2 The bandgap strucure of PN and PPN junction InGaN solar cells

The PPN solar cell is composed of a thin p-InGaN layer with a high indium composition on top of a PN junction InGaN solar cells. The addition of a thin top p-InGaN layer creates a graded energy bandgap.

Figure III.6 (a), (b) shows that the PPN structure performs better than the PN structure because it includes an additional layer of p-$In_{0.6}Ga_{0.4}N$ with a slightly larger bandgap. In addition, the extra layer of p-InGaN has increased the number of holes in the solar cell and caused the Fermi level to shift towards the conduction band. The generation of holes and electrons in the PN and PPN junction solar cells is shown in Figure III.6 (black and white circles represent electrons and holes respectively). The PPN structure had a wider band gap and could absorb more light than the PN structure[10].

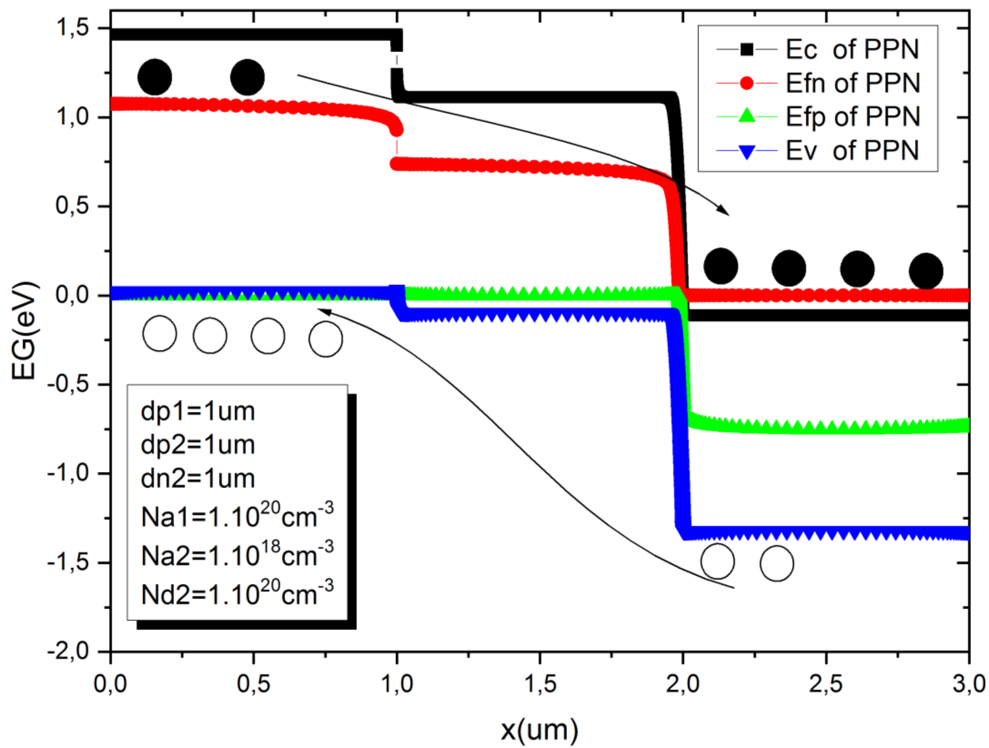

Figure III. 6 (a) Diagram of band energy levels of the PPN structure

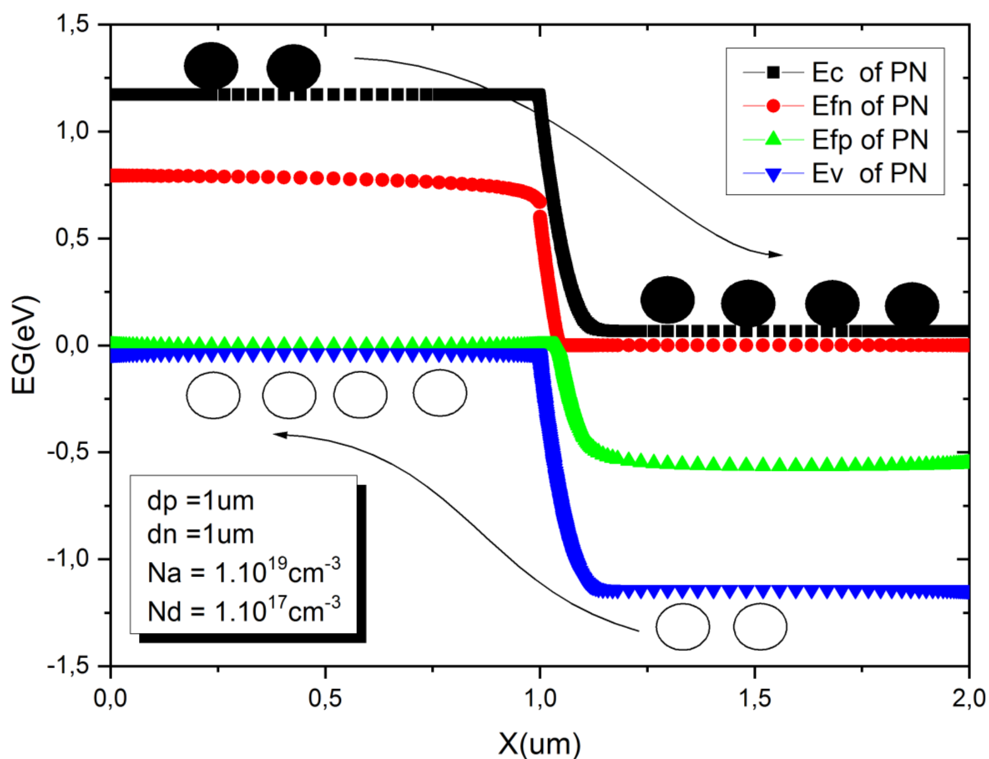

Figure III. 6 (b) Diagram of band energy levels of the PN structure

III.3.3 Structure of PN junction p-$In_{0.7}Ga_{0.3}N$/ n-$In_{0.7}Ga_{0.3}N$

III.3.3.1 Influence of the thickness in the p-$In_{0.70}Ga_{0.30}N$ and n-$In_{0.70}Ga_{0.30}N$ regions.

The effects of the thickness layers in the p-$In_{0.70}Ga_{0.30}N$ and n-$In_{0.70}Ga_{0.30}N$ regions on the photovoltaics parameters sush as V_{oc}, J_{sc}, FF, and η of the PN junction solar cells were investigated.

a- Influence of the thickness in top p-$In_{0.7}Ga_{0.3}N$ region (dp)

The thickness of top layer p-$In_{0.7}Ga_{0.3}N$ (dp) was varied from 0.01 µm to 1.0 µm while maintaining the thickness of bottom layer n-$In_{0.7}Ga_{0.3}N$ at 1.0 µm and carrier density Na and Nd at 10^{18} cm^{-3}. The results are provided in Table 1 and Figure. III.7.(a),(b),(c) and (d).

Table *III.3* : Influence of the thickness of top p-InGaN region (dp)

dn = 1um, Na = 1.10^{18} cm^{-3} , Nd = 1.10^{18} cm^{-3}

dp (um)	0.01	0.05	0.1	0.3	0.5	0.8	1
Jsc(mA/cm^2)	34.767575	35.393179	35.883707	35.591176	34.078541	31.514610	29.895391
Voc (V)	0.7607	0.7614	0.7621	0.7633	0.7634	0.7632	0.7629
FF (%)	84.83	85.04	85.09	85.18	85.22	85.25	85.26
η (%)	22.44	22.92	23.27	23.14	22.17	20.50	19.44

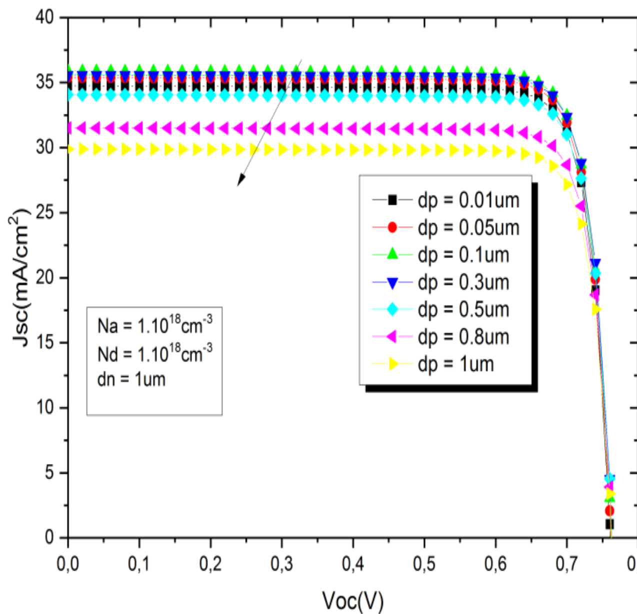

Fig.III.7 (a) IV curves of the PN-junction InGaN solar cell structure.

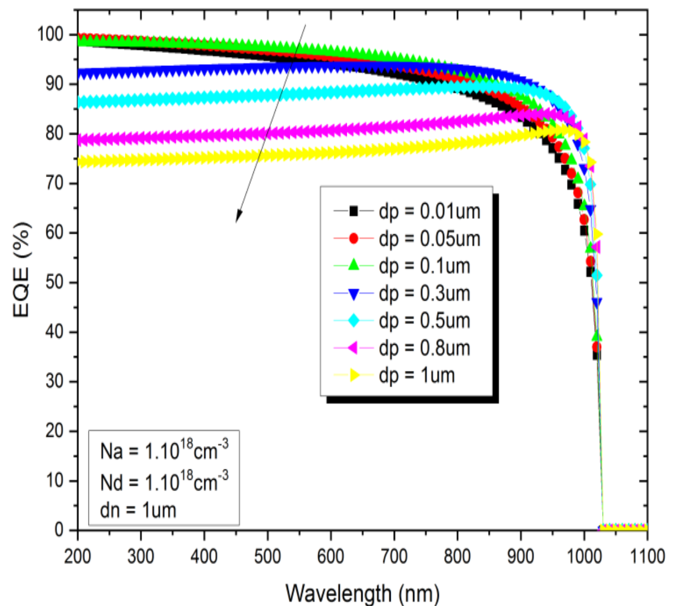

Fig.III.7 (b) Quantum efficiency curves of the PN-junction InGaN solar cell structure.

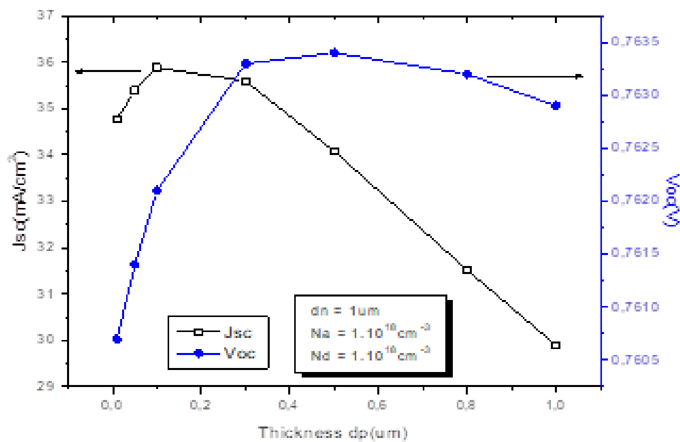

Fig III.7 (c) Effect of thickness of top layer on Jsc and Voc

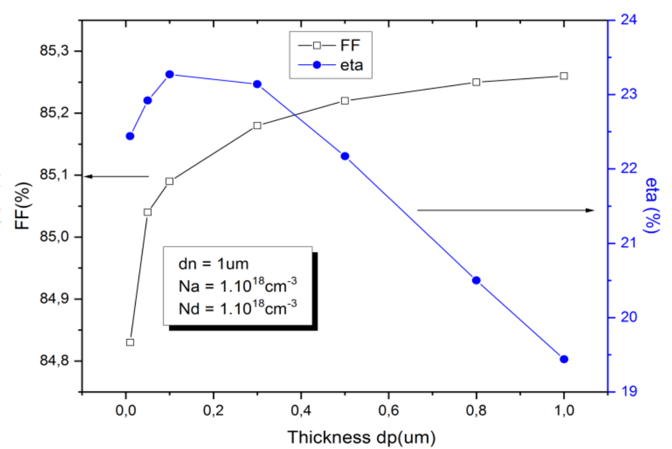

Fig III.7 (d) Effect of thickness of top layer on FF and eta

Figure III.7 (a) depicts the J(V) characteristics of p- $In_{0.7}Ga_{0.30}N$ /n- $In_{0.7}Ga_{0.30}N$ single junction solar cells of varying p- $In_{0.7}Ga_{0.30}N$ thicknesses (dp). We can see that the p-$In_{0.65}Ga_{0.35}N$ layer thikness of 10 nm has the highest Jsc (35.88 mA/cm^2) and Jsc decrease with increasing p- $In_{0.7}Ga_{0.30}N$ layer thikness. On the other hand Voc increases slowly of few mV from 0.7607 to 0.7634 V at 500 nm and drop at 0.7629V

when p-$In_{0.7}Ga_{0.30}N$ layer thikness is of 1000 nm. Although a thicker p- $In_{0.7}Ga_{0.30}N$ layer improves absorption and creates more carriers, a longer drift length makes it more difficult for photogenerated carriers to reach the p contact. J_{SC} reduces slightly [11,12].

The quantum efficiency of p-$In_{0.7}Ga_{0.30}N$ /n-$In_{0.7}Ga_{0.30}N$ single junction solar cells under AM1.5 is displayed in Figure III.7 (b). was around 98% with dp of 0.1um to 75% with dp of 1um, throughout a broad spectral range (200–600 nm), and it progressively decreased at longer wavelengths. These findings demonstrate the efficiency of the suggested single-junction solar cell construction and the near total conversion of all absorbed photons into charge carriers [11,12].

Figure.III.7 (c) represents both the variation of short-circuit density current Jsc and open circuit voltage (Voc), as function of the p-$In_{0.7}Ga_{0.30}N$ layer thikness (dp) ranging from 0.01 µm to 1 µm. As we can see, the short circuit density current Jsc is decreasing linearly with increasing p-$In_{0.7}Ga_{0.30}N$ layer thikness (dp) [11,12]

Figure.III.7 (d) shows the effects of the p-$In_{0.7}Ga_{0.30}N$ layers' thickness on the Efficiency (η) and FF. It can be seen that the Efficiency (η) and FF are more sensitive to the thickness variation of p-$In_{0.7}Ga_{0.30}N$. In this range, it can be noticed that the η of the p-$In_{0.7}Ga_{0.30}N$ solar cells reduces with increasing p-$In_{0.7}Ga_{0.30}N$ thickness, while the FF increase slowly with

increasing p-$In_{0.7}Ga_{0.30}N$ thickness. It's clear that the p-$In_{0.7}Ga_{0.30}N$ layer thikness of 0.1 µm gives maximum efficiency of about **23.27%** and fill factor FF starts to increase slowly beyond this value of p-$In_{0.7}Ga_{0.30}N$ layer thikness.

b-Influence of the thickness in bottom n-In0.7Ga0.3N region (dn)

The thickness of bottom layer n-In0.7Ga0.3N (dn) was varied from 0.01 µm to 1.0 µm while maintaining the thickness of top layer p-In0.7Ga0.3N at 1.0 µm and carrier density Na and Nd at 1018 cm-3. The results are provided in table 2 and Figure. III.8.(a-d).

Table III.4 : Influence of the thickness of bottom n-InGaN region (dn)

	dp = 1um, Na = 1.10^{18} cm^{-3} , Nd = 1.10^{18} cm^{-3}						
dn (um)	0.01	0.05	0.1	0.3	0.5	0.8	1
Jsc(mA/cm^2)	29.507892	29.528137	29.585752	29.726687	29.801548	29.866861	29.895391
Voc (V)	0.7496	0.7500	0.7516	0.7561	0.7591	0.7617	0.7629
FF (%)	84.97	85.12	85.14	85.18	85.19	85.23	85.26
η (%)	18.79	18.85	18.93	19.14	19.27	19.39	19.44

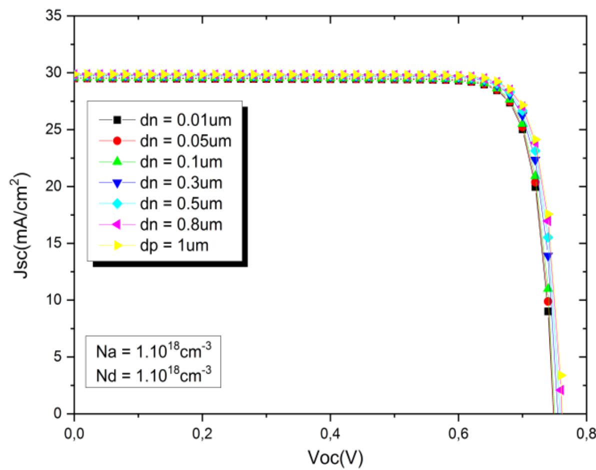

Fig.III.8 (a) IV curves of the PN-junction InGaN solar cell structure.

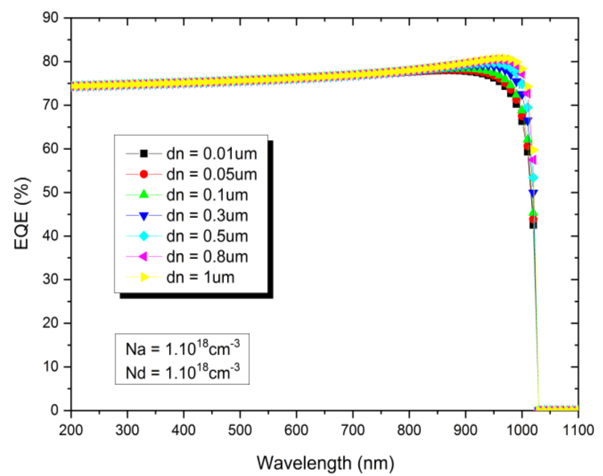

Fig.III.8 (b) Quantum efficiency curves of the PN-junction InGaN solar cell structure.

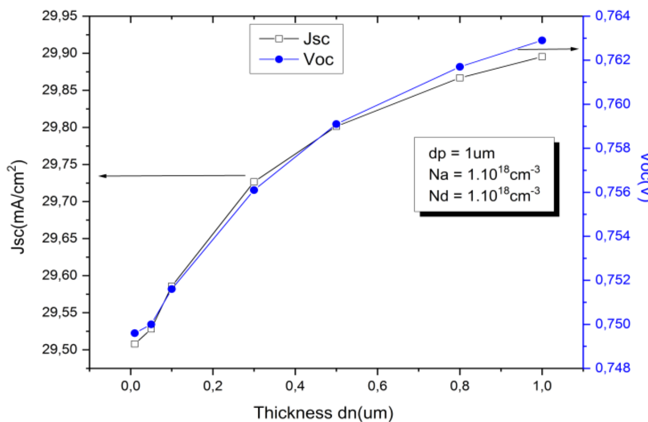

Fig III.8 (c) Effect of thickness of bottom layer on Jsc and Voc

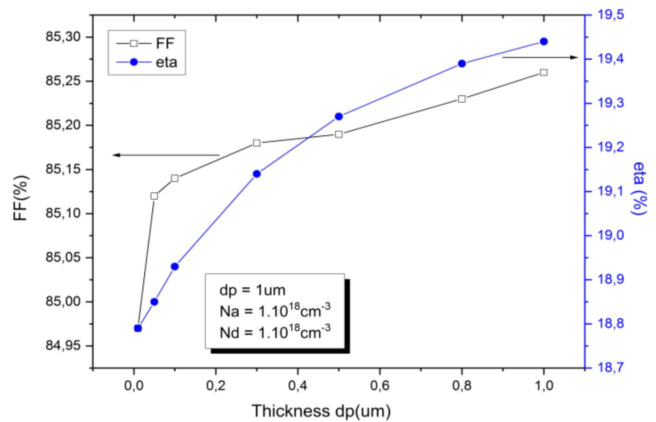

Fig III.8 (d) Effect of thickness of bottom layer on FF and eta

In figure III.8 we can see that the thickness of the bottom n-InGaN (dn) layer in the PN jonction did not have any notable effects on Voc and FF (Fig.III.8 (a) and [b]) but had a remarkable effect on Jsc and η (Fig. III.8 (c) and (d)).

III.3.3.2 Influence of the doping concentration in the p-In0.70Ga0.30N and n-In0.70Ga0.30N regions.

The effects of the doping concentration in the p-$In_{0.70}Ga_{0.30}N$ and n-$In_{0.70}Ga_{0.30}N$ regions on the photovoltaics parameters sush as *Voc*, *Jsc*, FF, and *η* of the PN junction solar cells were investigated.

a- Influence of the doping concentration in the top p-$In_{0.70}Ga_{0.30}N$ region

The doping concentration of the top layer p-$In_{0.7}Ga_{0.3}N$ (Na) was varied from 1.10^{15} to 1.10^{20} cm^{-3} while maintaining the thickness of top (dp) and bottom (dn) layer at 0.01 and 1.0 µm respectivelly and carrier density Nd of the bottom layer at 10^{18} cm^{-3}. The results are provided in table 3 and Figure. III.9.(a),(b).

Table III.5 : Influence of the doping concentration in the top p-InGaN region

	dp = 0.01um, dn = 1um, Nd = 1.10^{18} cm^{-3}					
Na (cm^{-3})	1.10^{15}	1.10^{16}	1.10^{17}	1.10^{18}	1.10^{19}	1.10^{20}
Jsc(mA/cm^2)	34.686092	34.707217	34.729528	34.767576	34.875249	34.911269
Voc (V)	0.5882	0.6478	0.7068	0.7607	0.7905	0.7973
FF (%)	82.02	83.15	84.10	84.83	85.26	85.29
η (%)	16.74	18.69	20.64	22.44	23.51	23.74

In the PN structure, as the doping concentration of top layer increased from 10^{15} cm^{-3} to 10^{20} cm^{-3}, *Voc* gradually increased from 0.5882 V to 0.7973 V . *Jsc* and FF

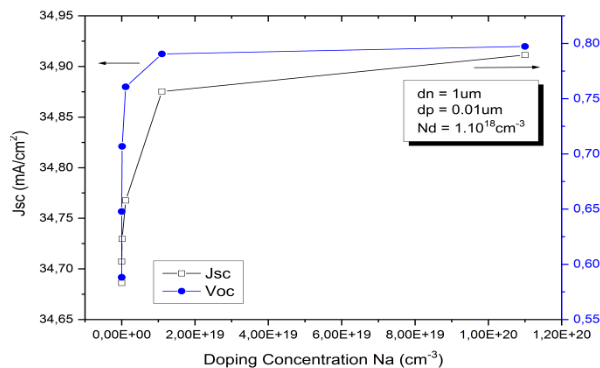

Fig III.9 (a) Effect of the doping concentration of top layer on Jsc and Voc

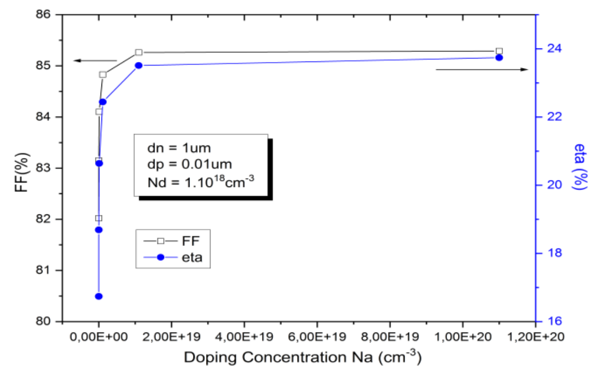

Fig III.9 (b) Effect of the doping concentration of top layer on FF and eta

Remained constant and eta increase (Figure. III.9.(a),(b)).

The doping concentration of the top layer p-$In_{0.7}Ga_{0.3}N$ (Na) was varied from 1.10^{15} to 1.10^{20} cm^{-3} while maintaining the thickness of top (dp) and bottom (dn) layer at 0.01 and 1.0 µm respectivelly and carrier density Nd of the bottom layer at 10^{20} cm^{-3}. The results are provided in Table 6.

Table III.6 : Influence of the doping concentration in top layer (dp = 0.01 um, dn = 1um, Na = 1.10^{20} cm^{-3})

	dp = 0.01um, dn = 1um, Nd = 1.10^{20} cm^{-3}					
Na (cm^{-3})	1.10^{15}	1.10^{16}	1.10^{17}	1.10^{18}	1.10^{19}	1.10^{20}
Jsc(mA/cm^2)	34.140502	34.142734	34.144964	34.146764	34.161853	34.198341
Voc (V)	0.5880	0.6477	0.7073	0.7668	0.8259	0.8800
FF (%)	82.50	83.67	84.68	85.52	86.31	86.91
η (%)	16.56	18.50	20.45	22.39	24.35	26.16

The doping concentration of the top layer p-$In_{0.7}Ga_{0.3}N$ (Na) was varied from 1.10^{15} to 1.10^{20} cm^{-3} while maintaining the thickness of top (dp) and bottom (dn) layer at 1.0 µm and carrier density Nd of the bottom layer at 10^{20} cm^{-3}.The results are provided in Table 7.

Table III.7 : Influence of the doping concentration in top layer (dp = 1 um, dn = 1um, Nd = 1.10^{20} cm^{-3})

	dp = 1um, dn = 1um, Nd = 1.10^{20} cm^{-3}					
Na (cm^{-3})	1.10^{15}	1.10^{16}	1.10^{17}	1.10^{18}	1.10^{19}	1.10^{20}
Jsc(mA/cm^2)	38.189579	30.718637	30.718637	29.998063	29.763546	29.687995
Voc (V)	0.5925	0.6524	0.7120	0.7715	0.8302	0.8823
FF (%)	77.20	80.33	83.70	85.33	86.34	87.00
η (%)	17.47	17.31	18.31	19.75	21.34	22.79

b- Influence of the doping concentration in the bottom n-$In_{0.7}Ga_{0.3}N$ region

The doping concentration of the bottom layer n-$In_{0.7}Ga_{0.3}N$ (Nd) was varied from 1.10^{15} to 1.10^{20} cm^{-3} while maintaining the thickness of top (dp) and bottom (dn) layer at 0.01 and 1.0

µm respectivelly and carrier density Na of the bottom layer at 10^{18} cm^{-3}. The results are provided in table 8 and Figure. III.10.(a),(b).

Table III.8 : Influence of the doping concentration in the bottom n-InGaN region

	dp = 1um, dn = 0.01um, Na = 1.10^{18} cm^{-3}					
Nd (cm^{-3})	1.10^{15}	1.10^{16}	1.10^{17}	1.10^{18}	1.10^{19}	1.10^{20}
Jsc(mA/cm^2)	29.470475	29.480007	29.490156	29.507892	29.560180	29.582094
Voc (V)	0.5843	0.6438	0.7020	0.7496	0.7680	0.7709
FF (%)	82.18	83.34	84.29	84.97	85.30	85.32
η (%)	14.15	15.82	17.45	18.79	19.36	19.46

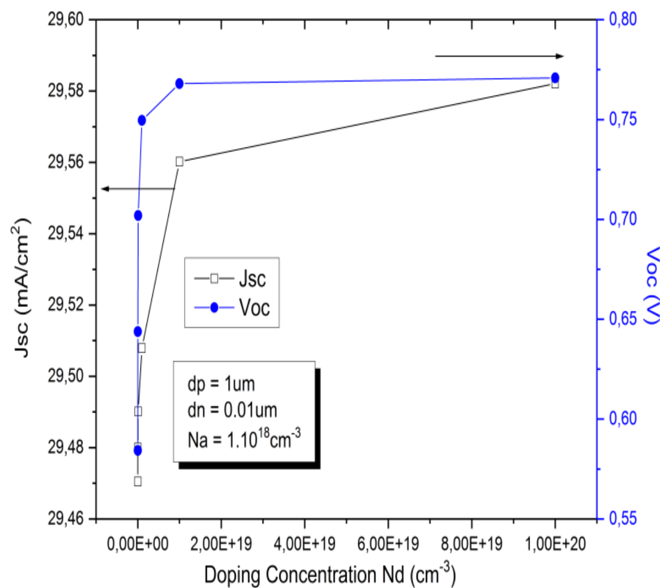

Fig III.10 (a) Effect of the doping concentration of bottom layer on Jsc and Voc

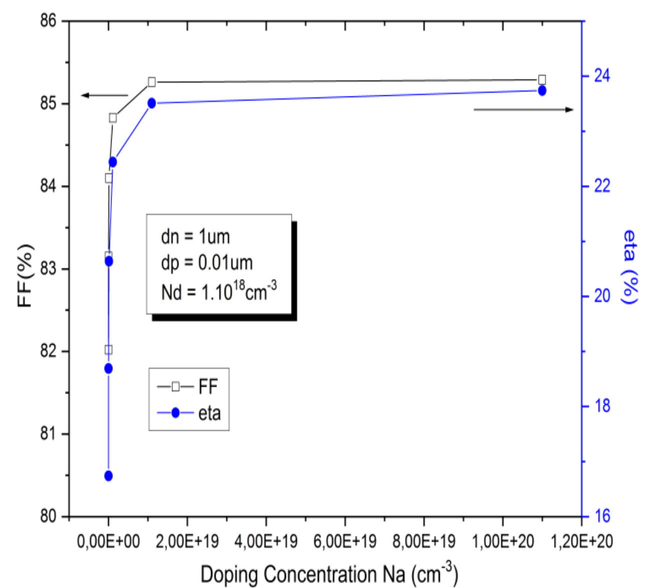

Fig III.10 (b) Effect of the doping concentration of bottom layer on FF and eta

The change in the doping concentration of the bottom layer in the PN jonction from 10^{15} cm^{-3} to 10^{20} cm^{-3} resulted in little change in η (Fig. III.10 (b)).However eta (η) increased from 14.15% to 19.46%.

The doping concentration of the bottom layer n-In0.7Ga0.3N (Nd) was varied from 1.1015 to 1.1020 cm-3 while maintaining the thickness of top (dp) and bottom (dn) layer at 1 and 0.01 µm respectivelly and carrier density Na of the bottom layer at 1020 cm-3. The results are provided in table III. 9.

Table III.9 : Influence of the doping concentration in the bottom n-InGaN of PN junction (dn =0.01um)

	dp = 1um, dn = 0.01um, Na = 1.10^{20} cm^{-3}					
Nd (cm^{-3})	1.10^{15}	1.10^{16}	1.10^{17}	1.10^{18}	1.10^{19}	1.10^{20}
Jsc(mA/cm^2)	29.231984	29.235254	29.238405	29.243078	29.255813	29.270796
Voc (V)	0.5842	0.6438	0.7035	0.7630	0.8213	0.8684
FF (%)	82.34	83.52	84.54	85.42	86.24	86.88
η (%)	14.06	15.72	17.39	19.06	20.72	22.08

The doping concentration of the bottom layer n-$In_{0.7}Ga_{0.3}N$ (Nd) was varied from 1.10^{15} to 1.10^{20} cm^{-3} while maintaining the thickness of top (dp) and bottom (dn) layer at 1 µm and carrier density Na of the bottom layer at 10^{20} cm^{-3}. The results are provided in Table III.10.

Table III.10 : Influence of the doping concentration in the bottom n-InGaN of PN junction (dn = 1um)

	dp = 1um, dn = 1um, Na = 1.10^{20} cm^{-3}					
Nd (cm^{-3})	1.10^{15}	1.10^{16}	1.10^{17}	1.10^{18}	1.10^{19}	1.10^{20}
Jsc(mA/cm^2)	29.702907	29.661760	29.620538	29.624532	29.675050	29.687996
Voc (V)	0.6036	0.6712	0.7333	0.7932	0.8483	0.8823
FF (%)	82.22	0.8395	85.06	85.89	86.60	87.00
η (%)	14.74	16.71	18.47	20.18	21.80	22.79

III.3.4 Structure of PPN junction p-$In_{0.6}Ga_{0.4}N$/p-$In_{0.7}Ga_{0.3}N$/n-$In_{0.7}Ga_{0.3}N$

III.3.4.1 Influence of the thickness in PPN junction

The effects of the thickness layers in the p-$In_{0.6}Ga_{0.4}N$/p-$In_{0.7}Ga_{0.3}N$/n-$In_{0.7}Ga_{0.3}N$ regions on the photovoltaics parameters sush as *Voc*, *Jsc*, *FF*, and η of the PN junction solar cells were investigated.

III.3.4.1.1 Influence of the thickness of top p-$In_{0.6}Ga_{0.4}N$ region (dp_1)

The tickness of the top layer p-$In_{0.6}Ga_{0.4}N$ (dp_1) was varied from 0.01 to 1um while maintaining the thickness of middle (dp_2) and bottom (dn_2) layer at 1.0 µm and carrier density

Na_1 of the top, Na_2 of the middle and Nd_2 of the bottom layer at 10^{18} cm^{-3}. The results are provided in table 11 and Figure. III.11.(a-d).

Table III.11 : Influence of the thickness layer in the top p-InGaN of PPN junction

	dp_2 = 1um, dn_2 = 1um, $Na_1 = 1.10^{18}$ cm^{-3}, $Na_2 = 1.10^{18}$ cm^{-3}, $Nd_2 = 1.10^{18}$ cm^{-3}						
dp_1 (um)	0.01	0.05	0.1	0.3	0.5	0.8	1
Jsc(mA/cm²)	38.576743	38.490464	38.281416	36.915974	35.333319	33.089020	31.744137
Voc (V)	0.8019	0.8018	0.8016	0.8002	0.7989	0.7970	0.7959
FF (%)	85.93	85.94	85.94	85.98	85.98	85.97	85.97
η (%)	26.58	26.52	26.37	25.40	24.27	22.67	21.72

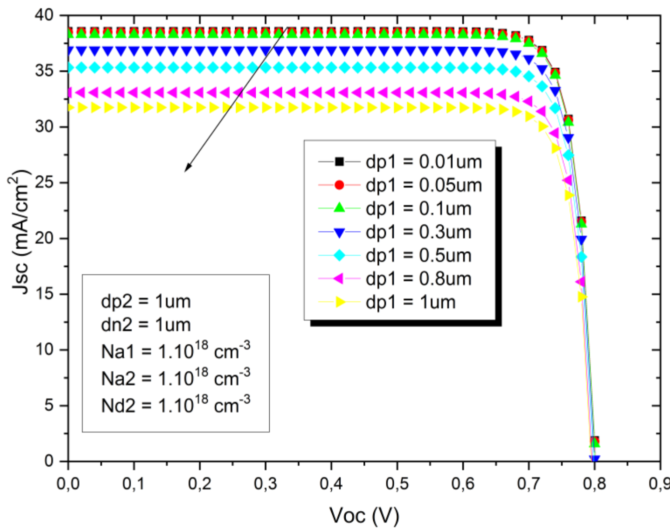

Fig.III.11 (a) IV curves of the PPN-junction InGaN solar cell structure.

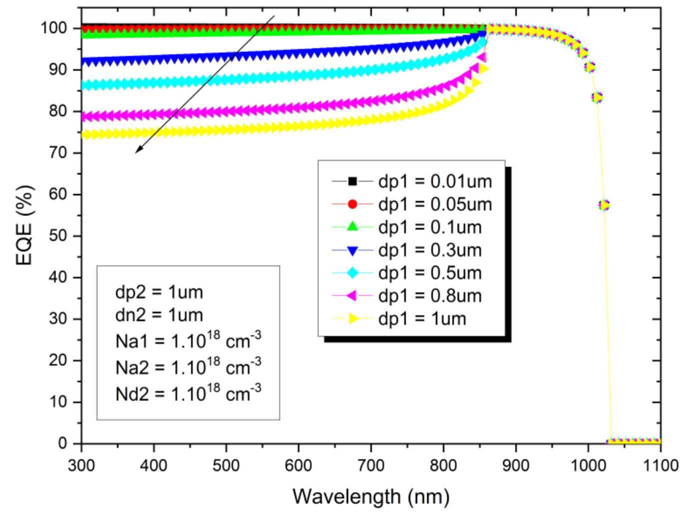

Fig.III.11 (b) Quantum efficiency curves of the PPN-junction InGaN solar cell structure.

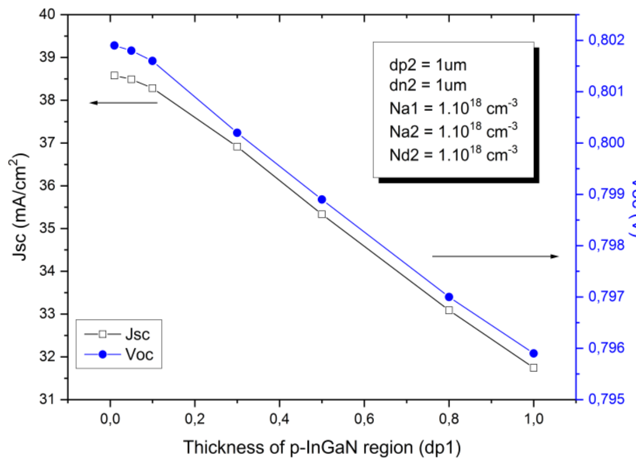

Fig III.11 (c) Effect of the thickness of top (dp_1) layer on Jsc and Voc

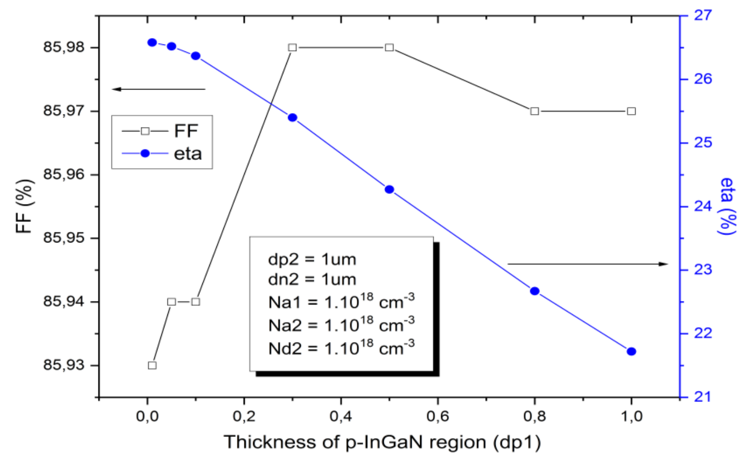

Fig III.11 (d) Effect of the thickness of top (dp_1) layer on FF and eta.

The variations in quantum efficiency as a function of incident wavelength for solar cell is shown in Fig.III.11.(b). The PPN structure achieved a higher quantum efficiency than the PN structure because the thin p-In0.6Ga0.4N layer had an energy bandgap of approximately 1.44 eV (840 nm), which fell within the highest power in the AM0 and AM1.5 spectra (800 nm–900 nm). Moreover, the thin p-In0.6Ga0.4N layer caused the absorption edge to shift toward higher energy photons [10].

III.3.4.1.2 Influence of the thickness of the middle p-$In_{0.7}Ga_{0.3}N$ region (dp_2)

The tickness of the middle layer p-$In_{0.7}Ga_{0.3}N$ (dp_2) was varied from 1.10^{15} to 1.10^{20} cm^{-3} while maintaining the thickness of top (dp_1) and bottom (dn_2) layer at 1.0 µm and carrier density Na_1 of the top, Na_2 of the middle and Nd_2 of the bottom layer at 10^{18} cm^{-3}. The results are provided in table 12 and Figure. III.12.(a),(b).

Table III.12 : Influence of the thickness layer in the middle p-InGaN of PPN junction

	dp_1 = 1um, dn_2 = 1um, $Na_1 = 1.10^{18}$ cm^{-3}, $Na_2 = 1.10^{18}$ cm^{-3} , $Nd_2 = 1.10^{18}$ cm^{-3}						
dp_2 (um)	0.01	0.05	0.1	0.3	0.5	0.8	1
Jsc(mA/cm^2)	30.094914	30.181155	30.405661	31.028006	31.376548	31.648247	31.744137
Voc (V)	0.7943	0.7945	0.7947	0.7953	0.7956	0.7958	0.7959
FF (%)	85.62	85.84	85.86	85.92	85.94	85.96	85.97
η (%)	20.47	20.58	20.75	21.20	21.45	21.65	21.72

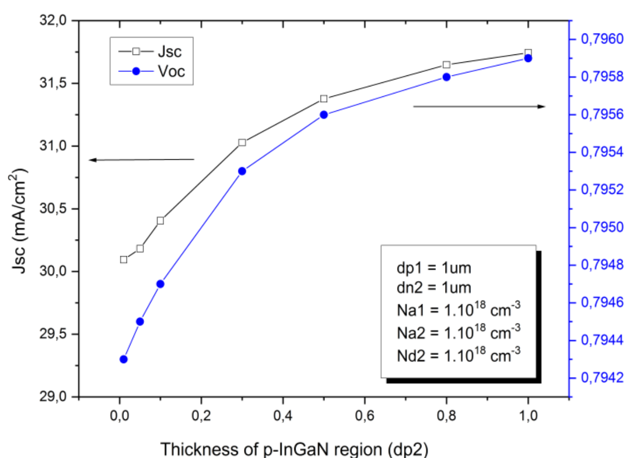

Fig III.12 (a) Effect of the thickness of bottom (dn_2) layer on Jsc and Voc

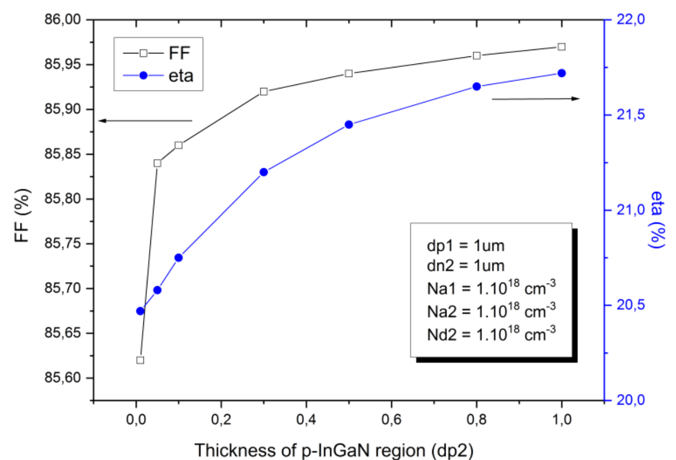

Fig III.12 (b) Effect of the thickness of bottom (dn_2) layer on FF and eta

The bottom p-$In_{0.7}Ga_{0.3}N$ layer (dn_2) of the PPN structures did not contribute to any substantial change in J_{sc} , V_{oc}, FF and η.

III.3.4.2 Influence of the doping concentration in the PPN junction

The effects of the doping concentration in the p-$In_{0.6}Ga_{0.4}N$/p-$In_{0.7}Ga_{0.3}N$/n-$In_{0.7}Ga_{0.3}N$ regions on the photovoltaics parameters sush as V_{oc}, J_{sc}, FF, and η of the PN junction solar cells were investigated.

III.3.4.2.1 Influence of the doping concentration in the top p-$In_{0.60}Ga_{0.40}N$ region (Na_1)

The doping concentration of the top layer p-$In_{0.6}Ga_{0.4}N$ (Na_1) was varied from 1.10^{15} to 1.10^{20} cm^{-3} while maintaining the thickness of top (dp_1), middle (dp_2), and bottom (dn_2) layer at 0.01, 1.0 and 1.0 µm respectivelly and carrier density (Na_2) of the middle and (Nd_2) of the bottom layer at 10^{18} cm^{-3} respectivelly. The results are provided in Table 13 and Figure. III.13.(a),(b).

Table III.13 : Influence of the doping concentration in the top p-InGaN of PPN junction ($Nd2 = 1.10^{18}$ cm-3)

	$dp_1 = 0.01um$, $dp_2 = 1um$, $dn_2 = 1um$, $Na_2 = 1.10^{18}\ cm^{-3}$, $Nd_2 = 1.10^{18}\ cm^{-3}$					
Na_1 (cm^{-3})	1.10^{15}	1.10^{16}	1.10^{17}	1.10^{18}	1.10^{19}	1.10^{20}
Jsc(mA/cm^2)	36.948724	38.348353	38.549770	38.576743	38.579215	38.578846
Voc (V)	0.7914	0.8000	0.8011	0.8012	0.8012	0.8012
FF (%)	85.90	85.98	86.01	86.01	86.01	86.01
η (%)	25.12	26.38	26.56	26.58	26.59	26.59

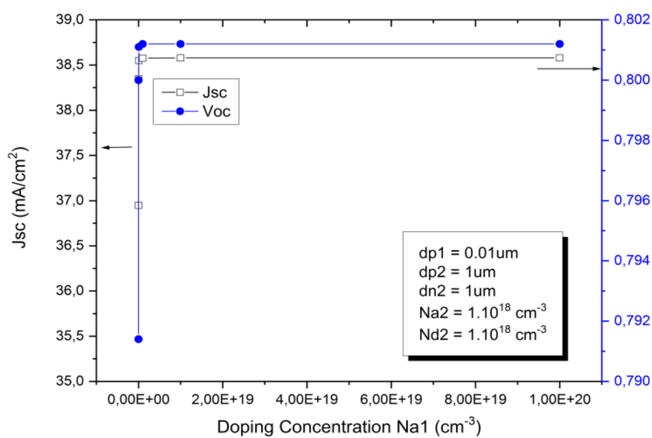

Fig III.13 (a) Effect of the doping concentration of top (dp_1) layer on Jsc and Voc

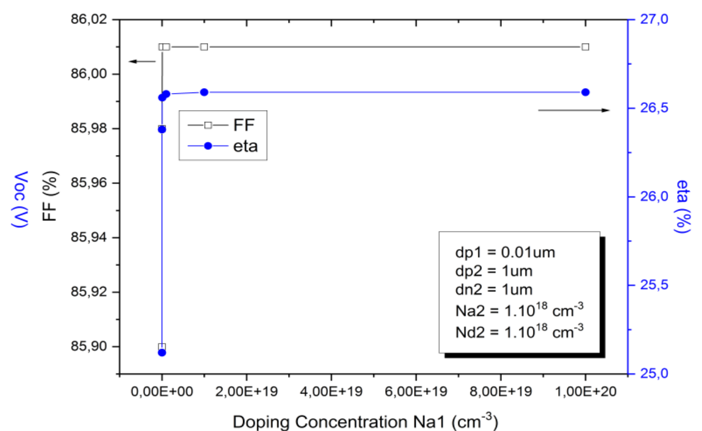

Fig III.13 (b) Effect of the doping concentration of top (dp_1) layer on FF and eta

The doping concentration of the top p-$In_{0.60}Ga_{0.40}N$ layer (Na_1) in the PPN structure did not substantially affect *Jsc* and FF (Fig.III.13 (a) and (b)). However, a noticeable change was observed in *Voc* and *η* (Fig.III.13 (a) and (b)).

Voc: it changed from 0.7914 V to 0.8012 V and *η* from 25.12 % to 26.58 % as the doping concentration of the top p-$In_{0.60}Ga_{0.40}N$ layer (Na_1) varied from 10^{15} cm^{-3} – 10^{18} cm^{-3} .

The doping concentration of the top layer p-$In_{0.6}Ga_{0.4}N$ (Na_1) was varied from 1.10^{15} to 1.10^{20} cm^{-3} while maintaining the thickness of top (dp_1), middle (dp_2), and bottom (dn_2) layer at 0.01, 1.0 and 1.0 µm respectivelly and carrier density (Na_2) of the middle and (Nd_2) of the bottom layer at 10^{18} and $10^{20}cm^{-3}$ respectivelly. The results are provided in (table III.14) .

Table III.14 : Influence of the doping concentration in the top p-InGaN of PPN junction (Nd2 = 1.1020 cm-3)

	$dp_1 = 0.01um, dp_2 = 1um, dn_2 = 1um, Na_2 = 1.10^{18} cm^{-3}, Nd_2 = 1.10^{20} cm^{-3}$					
Na_1 (cm^{-3})	1.10^{15}	1.10^{16}	1.10^{17}	1.10^{18}	1.10^{19}	1.10^{20}
Jsc(mA/cm^2)	36.961833	38.342601	38.541660	38.568384	38.570831	**38.570460**
Voc (V)	0.8244	0.8746	0.9048	0.9115	0.9123	**0.9124**
FF (%)	86.27	86.84	87.06	87.11	87.11	**87.11**
η (%)	26.29	29.12	30.36	30.62	30.65	**30.65**

III.3.5 Conparaison between PN and PPN junction of InGaN solar cell [10,12] :

Optimized InGaN solar cells with PN and PPN junctions were compared. The best layer thickness and carrier density, determined in the previous sections, were chosen (Table. 15). With these optimized parameters, PN- and PPN-junction InGaN solar cells were simulated.

Table III.15 : Comparaison of an optimized values of the photovoltaics parameters between the PPN and the PN structures[10,12].

	Optimized Values			
	PN		PPN	
	$dp = 1um, dn = 1um,$ $Na = 1.10^{20} cm^{-3}, Nd = 1.10^{20} cm^{-3}$		$dp_1 = 0.01um, dp_2 = 1um, dn_2 = 1um,$ $Na_1 = 1.10^{20} cm^{-3}, Na_2 = 1.10^{18} cm^{-3},$ $Nd_2 = 1.10^{20} cm^{-3}$	
	Our work	[Manzoor et al]	**Our work**	[Manzoor et al]
Jsc(mA/cm^2)	**29.687996**	32.20	**38.570460**	38.14
Voc(V)	**0.8823**	0.77	**0.9124**	0.91
FF(%)	**87.00**	85.36	**87.11**	87.13
η(%)	**22.79**	21.39	**30.65**	30.23

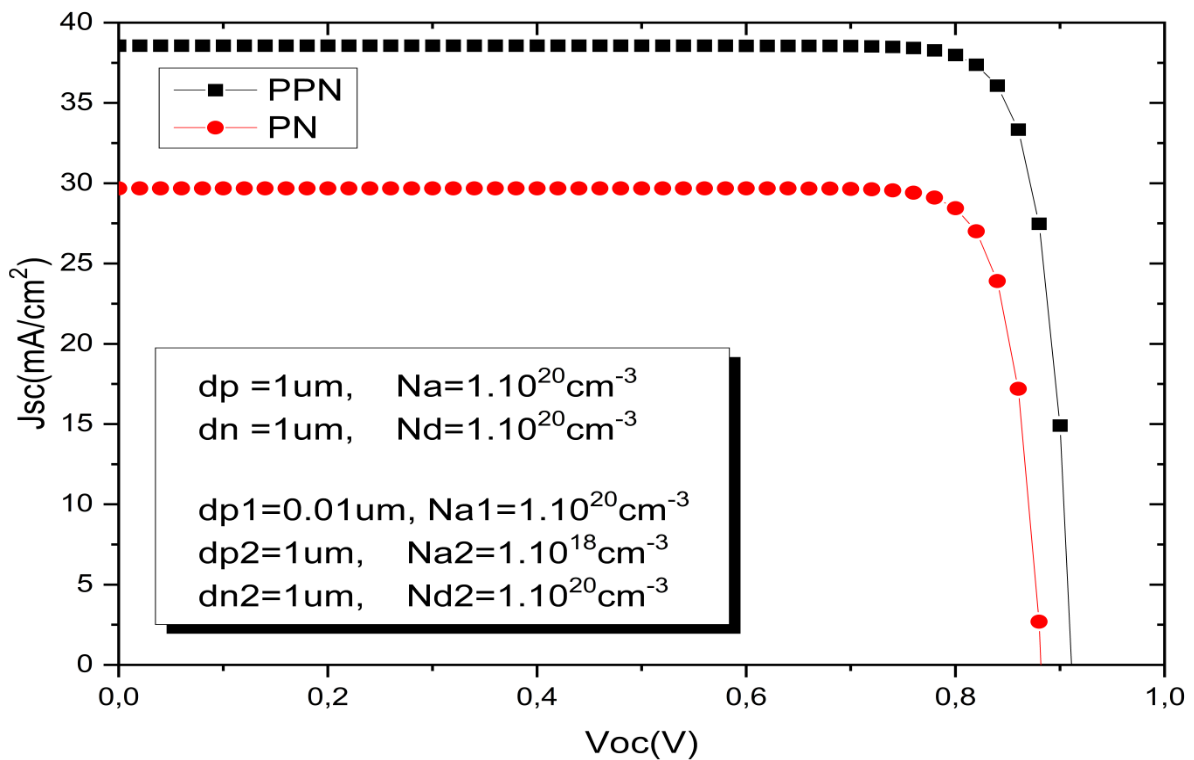

Figure III.14 .Coparaison of IV curves between PPN-junction and PN-junction of InGaN solar cell structures.

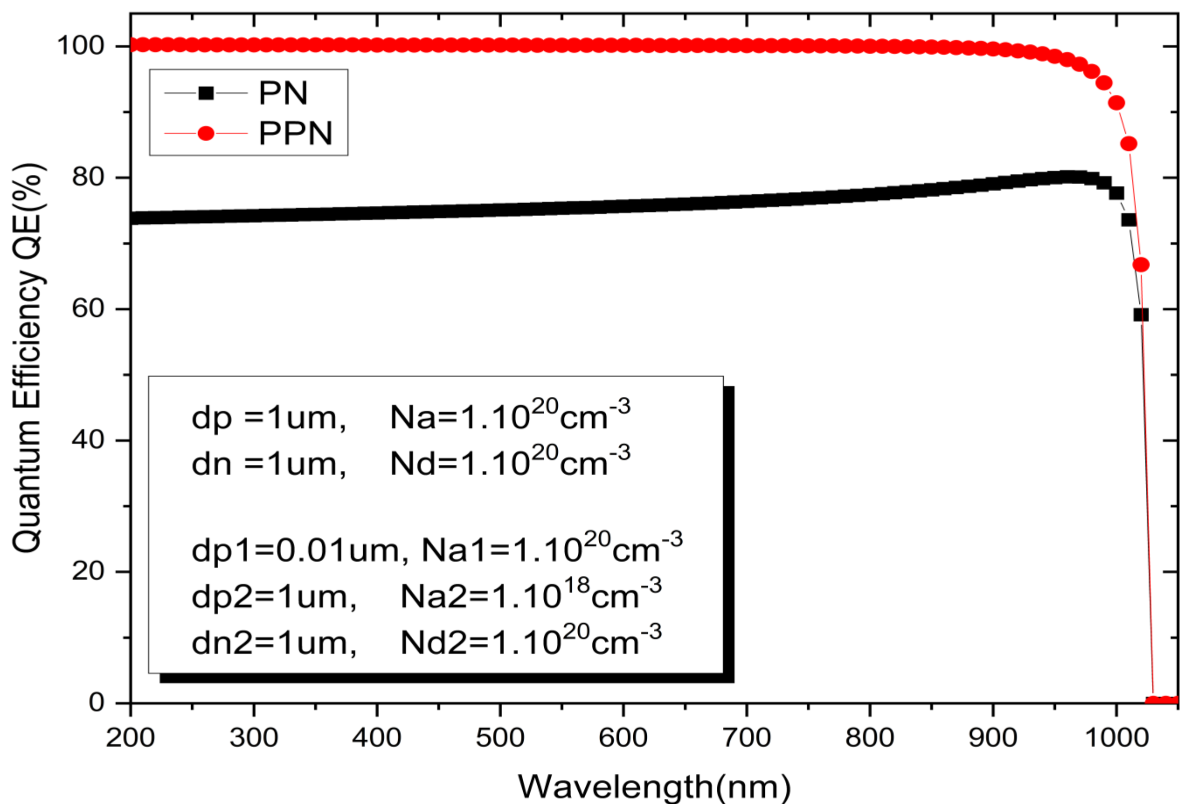

Figure III.15 Comparaison of quantum efficiency curve between PPN-junction and PN-junction of InGaN solar cells structures.

Adding a p-InGaN layer as thin as 0.01 µm on the top of the PN-junction solar cell substantially improved the conversion efficiency of the solar cell from 22.79% (PN) to 30.65% (PPN).

According to the simulated results, the optimized values of the photovoltaics parameters such as the open circuit voltage (*Voc*), current density (*Jsc*), fill factor (FF), and conversion efficiency (η) for the PN solar cell were 0.8823 V, 29.687996 mA/cm^2, 87.00 %, and 22.79 %, respectively, whereas those for the PPN solar cell were 0.9124 V, 38.570460 mA/cm^2, 87.11 %, and 30.65 %, respectively.

The PPN jonction achieved a higher quantum efficiency than the PN jonction.

For the PPN-junction InGaN solar cell, the quantum efficiency was approximately 99% over a wide spectral region (from 200 nm to 1000 nm). By contrast, the quantum efficiency of the PN-junction InGaN solar cell was gradually reduced at 75% at 200 nm and increase to 80% at 1000 nm. These results implied that the proposed three-layer solar cell structure is very efficient where all the absorbed photons are almost fully converted to charge carriers.

Conclusion :

In this third chapter, the optimized PN- and PPN-junction InGaN solar cells were compared. According to the simulated results, the optimized values of the photovoltaics parameters such as the open circuit voltage (*Voc*), current density (*Jsc*), fill factor (FF), and conversion efficiency (η) for the PN solar cell were 0.8823 V, 29.687996 mA/cm^2, 817.00 %, and 22.79 %, respectively, whereas those for the PPN solar cell were 0.9124 V, 38.570460 mA/cm^2, 87.11 %, and 30.65 %, respectively.

The PPN structure achieved a higher quantum efficiency than the PN structure because the thin p-$In_{0.6}Ga_{0.4}N$ layer had an energy bandgap of approximately 1.44 eV (840 nm), which fell within the highest power in the AM0 and AM1.5 spectra (800 nm–900 nm). Moreover, the thin p-$In_{0.6}Ga_{0.4}N$ layer caused the absorption edge to shift toward higher energy photons.

The results demonstrated that the thin p-InGaN layer on the top of the PN-junction solar cell dramatically improved its performance. The PPN structure performed better than the PN structure because it had an additional p-$In_{0.6}Ga_{0.4}N$ layer with a slightly larger energy bandgap.

REFERENCES

[1]	**Marc Burgelman Koen Decock, Alex Niemegeers, Johan Verschraegen, Stefaan Degrave** Version: 23 january 2018 . « SCAPS manual »
[2]	**Y. Marouf, L. Dehimi, F. Pezzimenti,** Simulation study for the current matching optimization in In0.48Ga0.52N/In0.74Ga0.26N dual junction solar cells, Superlattice. Microst. 130 (2019) 377–389, **https://doi.org/10.1016/j. spmi.2019.05.004**.
[3]	**I.U.I. Chowdhury, J. Sarker, A.S.M.Z. Shifat, R.A. Shuvro, A.F. Mitul,** Performance analysis of high efficiency InxGa1□ xN/GaN intermediate band quantum dot solar cells, Results Phys 9 (2018) 432–439, **https://doi.org/10.1016/j.rinp.2018.03.003**.
[4]	**Vurgaftman, I., Meyer, J.R**.: Band parameters for nitrogen-containing semiconductors. J. Appl. Phys. 94,3675–3696 (2003)
[5]	**Feng, S.W., Lai, C.M., Chen, C.H., Sun, W.C.:** Theoretical simulation of the effect of the indium content, thickness and defect density of the i-layer on the performance of PIN InGaN single homojunction solar cells. J. Appl. Phys. 108, 093118 (2010)
[6]	**Wu, J., Walukiewicz, W., Yu, K.M., Ager, J.W., Haller, E.E., Lu, H., Schaff, W.J.:** Small band gap bowing in InGaN alloy. Appl. Phys. Lett. 80, 4741–4743 (2002).
[7]	**D. M. Caughey, and R. E. Thomas**" Carrier mobilities in silicon empirocallY realted to doping and field" proceeding of the IEEE, vol. 55, pp. 2192-2193 , 1967.
[8]	**Levinshtein, M.E., Rumyantsev, S.L., Shur, M.S**.: Properties of Advanced Semiconductor Materials. Willey, Chichester (2001).
[9]	**Li, N.:** Simulation and Analysis of GaN-Based Photoelectronics Devices. Dissertation (in Chinese). Institute of semiconductors, Chinese Academy of Sciences, Beijing (2005)
[10]	**Manzoor, H. U., et al.** "High conversion and quantum efficiency indium-rich p-InGaN/p-InGaN/n-InGaN solar cell." Physica B: Condensed Matter 622 (2021): 413339.
[11]	**M. Moustafa, T. Alzoubi**, Numerical simulation of single junction InGaN solar cell by SCAPS, Key Eng. Mater. 821 (2019). **https://dx.doi.org/10.4028/www.scientifi** c.net/KEM.821.407. KEM:407–13.
[12]	**A. Bellakhdar, M. Birane, N. Selmane, A. Cheknane and A. Telia**, "Investigation of photovoltaic characteristics performance of p-InGaN/n-InGaN single junction solar cells using SCAPS 1D," 2023 1st International Conference on Renewable Solutions for Ecosystems: Towards a Sustainable Energy Transition (ICRSEtoSET), Djelfa, Algeria, **2023**, pp. 1-4, **doi: 10.1109/ICRSEtoSET56772.2023.10525344.**

GENERAL CONCLUSION

This work involves studying and simulating solar cells with PN (p-In 0.7 Ga 0.3 N/n- In 0.7 Ga 0.3 N) and PPN (p-In 0.6 Ga 0.4 N/p-In 0.7 Ga 0.3 N/n-In 0.7 Ga 0.3 N) In order to identify which of the two solar cells absorbs the maximum solar radiation and also delivers the maximum electrical energy, we have also studied the influence of the thickness of the P and N InGaN layers, as well as the doping concentration of these layers, on the photovoltaic parameters of this solar cell. This simulation work is carried out using the SCAPS 1D software designed for solar cell simulation.

In this case, the optimized PN- and PPN-junction InGaN solar cells were compared. According to the simulated results, the optimized values of the photovoltaics parameters such as the open circuit voltage (Voc), current density (Jsc), fill factor (FF), and conversion efficiency (η) for the PN solar cell were 0.8823 V, 29.687996 mA/cm 2 , 87.00 %, and 22.79 %, respectively, whereas those for the PPN solar cell were 0.9124 V, 38.570460 mA/cm 2 , 87.11 %, and 30.65 %, respectively.

The PPN structure achieved a higher quantum efficiency than the PN structure because the thin p-In 0.6 Ga 0.4 N layer had an energy bandgap of approximately 1.44 eV (840 nm), which fell within the highest power in the AM0 and AM1.5 spectra (800 nm–900 nm). Moreover, the thin p-In 0.6 Ga 0.4 N layer caused the absorption edge to shift toward higher energy photons.

The results demonstrated that the thin p-InGaN layer on the top of the PN-junction solar cell dramatically improved its performance. The PPN structure performed better than the PN structure because it had an additional p-In 0.6 Ga 0.4 N layer with a slightly larger energy bandgap.

الملخص

الهدف من هذه الأطروحة هو دراسة ومحاكاة خليتين شمسيتين على مادة InGaN .

PPN (p-$In_{0.6}Ga_{0.4}N$/p-$In_{0.7}Ga_{0.3}N$/n-$In_{0.7}Ga_{0.3}N$) و **PN** (p-$In_{0.7}Ga_{0.3}N$/n-$In_{0.7}Ga_{0.3}N$)

والتنبؤ بأي من الخليتين تتمتع بأفضل امتصاص للضوء من خلال دراسة تأثير سمك طبقاتN-InGaN و P، وكذلك تركيز المنشطات لهذه الطبقات، على الوسائط الكهروضوئية لهذه الخلايا الشمسية, تم تنفيذ أعمال المحاكاة هذه باستخدام برنامج SCAPS 1D المصمم لمحاكاة الخلايا الشمسية.

وفقًا لنتائج المحاكاة، تُظهر القيم المثلى للوسائط الكهروضوئية أن بنية PPN(30.65%) حققت كفاءة كمية أعلى من بنية PN (22.79%) لأن الطبقة الرقيقة من p-$In_{0.6}Ga_{0.4}N$ لديها فجوة في نطاق الطاقة تبلغ حوالي 1.44 فولت (840 نانومتر). وبالإضافة إلى ذلك، أدت الطبقة الرقيقة من p-$In_{0.6}Ga_{0.4}N$ إلى تحول حافة الامتصاص نحو فوتونات الطاقة الأعلى كما انه يحتوي فجوة نطاق أكبر قليلا.

الكلمات المفتاحية: InGaN، PN، PPN، SCAPS 1D، الوسائط الكهروضوئية، الخلايا الشمسية.

ABSTRACT

The aim of this thesis is to study and simulate two solar cells on InGaN.
PPN(p-$In_{0.6}Ga_{0.4}N$/p-$In_{0.7}Ga_{0.3}N$/n-$In_{0.7}Ga_{0.3}N$) and **PN** (p-$In_{0.7}Ga_{0.3}N$/n-$In_{0.7}Ga_{0.3}N$)
By studying the effect of the thickness of the N-InGaN and P layers, as well as the doping concentration in these layers, on the photovoltaic media of these solar cells, these simulations were carried out using SCAPS 1D software designed for solar cell simulation.
According to the simulation results, the optimal PV media values show that the PPN structure (30.65%) achieved higher quantum efficiency than the PN structure (22.79%) because the p-In0.6Ga0.4N thin film has an energy band gap of about 1.44 V (840 nm). In addition, the thin layer of p-In0.6Ga0.4N shifted the absorption edge towards higher energy photons and has a slightly larger band gap.
Keywords: InGaN, PN, PPN, 1D SCAPS, photovoltaic media, solar cells.

RÉSUMÉ

Le but de cette thèse est d'étudier et de simuler deux cellules solaires sur InGaN.
PPN(p-In0.6Ga0.4N/p-In0.7Ga0.3N/n-In0.7Ga0.3N) et PN (p-In0.7Ga0.3N/n-In0.7Ga0.3N)
En étudiant l'effet de l'épaisseur des couches N-InGaN et P, ainsi que la concentration dopage dans ces couches, sur les milieux photovoltaïques de ces cellules solaires, ces simulations ont été réalisées à l'aide du logiciel SCAPS 1D conçu pour la simulation de cellules solaires.
Selon les résultats de la simulation, les valeurs optimales des milieux photovoltaïques montrent que la structure PPN (30,65 %) a atteint un rendement quantique plus élevé que la structure PN (22,79 %) parce que le film mince p-In0,6Ga0,4N a une bande interdite d'environ 1,44 V (840 nm). En outre, la couche mince de p-In0,6Ga0,4N a déplacé le bord d'absorption vers des photons d'énergie plus élevée et a une bande interdite légèrement plus grande.

Mots-clés : InGaN, PN, PPN, 1D SCAPS, milieux photovoltaïques, cellules solaires.